2016

Characterization of Skin Immune Reactions Induced by the Contact Sensitizer Diphencyprone in Healthy Volunteers and Metastatic Melanoma Patients

Nicholas Gulati

CHARACTERIZATION OF SKIN IMMUNE REACTIONS INDUCED BY THE CONTACT SENSITIZER DIPHENCYPRONE IN HEALTHY VOLUNTEERS AND METASTATIC MELANOMA PATIENTS

A Thesis Presented to the Faculty of

The Rockefeller University

in Partial Fulfillment of the Requirements for

the degree of Doctor of Philosophy

by

Nicholas Gulati

June 2016

CHARACTERIZATION OF SKIN IMMUNE REACTIONS INDUCED BY THE CONTACT SENSITIZER DIPHENCYPRONE IN HEALTHY VOLUNTEERS AND METASTATIC MELANOMA PATIENTS

Nicholas Gulati, Ph.D.

The Rockefeller University 2016

Melanoma is a life-threatening malignant disease, of which the standard of care treatment is rapidly becoming immunologically driven, due to favorable recent clinical trials using immune checkpoint inhibitors. Diphencyprone (DPCP), a topically applied contact sensitizer, has been used with an 84% success rate to treat cutaneous melanoma metastases, but the immune mechanisms underlying its efficacy are largely unknown. This thesis characterizes skin immune reactions induced by DPCP, both in healthy volunteers and patients with metastatic melanoma.

In healthy volunteers, DPCP led to upgregulation of many immune molecules that may be anti-neoplastic effectors, including IFNγ, IL-24, and IL-9. We also examined the potential roles of miRNAs in skin reactions to DPCP, as they may be involved in its therapeutic applications, but are largely unstudied in skin biology and immunology. Furthermore, we used comprehensive T cell receptor sequencing to show that the immune reactions induced by DPCP are polyclonal, and therefore suggests that the induced inflammation is not due to a single antigen. Also, different individuals expanded different T cell clones in

response to the same application of DPCP, which could mean that DPCP is conjugating with unique proteins in each person. This may have relevance to the action of DPCP in melanoma patients, as each treated patient may expand a unique repertoire of T cells specific to antigens found only in that patient. In sum, this work with healthy volunteers formed a basis for investigating specific immune elements that may be induced in melanoma lesions that are treated with DPCP, as well as the baseline immune competence of cancer patients. It also led to insights regarding the regulation of immune responses, and provides a useful comparison point to inflammatory skin diseases such as psoriasis.

Our clinical trial with metastatic melanoma patients allowed us to more directly study the immunologic mechanisms underlying the efficacy of DPCP to treat skin metastases. Six patients enrolled in the study, and although each had a unique treatment course, 5 demonstrated at least partial melanoma regression in response to DPCP treatment. In these patients, we observed a shift towards Th1 polarization with the repeated DPCP applications required for treatment efficacy. This shift is likely relevant to melanoma treatment, as Th1 cells have established roles in anti-melanoma responses. To further support this, one of our patients who had both a regressing and non-regressing metastasis in response to DPCP, had increased expression of Th1-defining molecules in the former. A different patient, who received DPCP with checkpoint inhibitor therapy, provided proof of concept that these two immunotherapeutics can act synergistically. Overall, this work provides varied insights into cutaneous immune responses, and how they can be successfully employed in the context of skin cancer therapy.

Dedicated to my father, Subhash Chander Gulati, M.D., Ph.D., an incredible scientist, physician, and overall person, whose influence continues to be felt long after his untimely departure from this world

ACKNOWLEDGMENTS

This thesis would not have been possible without the support of a wide variety of people throughout my life. The words on these pages only express a small fraction of the gratitude I feel for them.

First and foremost, I must give thanks to my family for its continuous and unwavering support: my father Subhash, my mother Catherine, my sister Angeli, my brother Tony, and my sister-in-law Caroline. My amazing, impressive extended family, including but not limited to: Harbans Lal Gulati (Papaji), Kailash Gulati (Mummiji), Emil Phillips (Papa), Rosemary Phillips (Grandma), Adarsh Gulati (Chachaji), Nidhi Gulati (Chachiji), Priya Gulati, Akash Gulati, Joginder Nath, Charlotte Nath, Pravene Nath, Brian Nath, Madan Gopal, Susan Gopal, Ajay Gopal, Ravi Gopal, Nisha Gopal, UB Phillips, Barbara Pope, Jack Phillips, Ruth Wall Phillips, Janet Kornfeld, Yen Perez, Greg Phillips, Emil Phillips, Cara Phillips, Sandy Phillips-Jackson, Liz Phillips, Kathie Pi Mutchler, Lynn Faye, Jamie Phillips, Justin Phillips, Casey Phillips, Jack Phillips, Sam Macri, Jean Macri, and Adeline Harpootlian. Although I will not even attempt to list them here, I also want to thank all of my friends from different stages of my life, who helped me become the person that I am today, and kept this journey constantly fun and exciting.

This thesis was more directly made possible by my incredible mentor, James G. Krueger, M.D., Ph.D. I have learned and continue to learn so many valuable lessons from him, not only regarding how to do science well, but also how to be an effective yet compassionate leader, a caring physician, and much more. I am eternally indebted to my wonderful colleagues in the Krueger lab, both past and present: (in no particular order) Hiroshi Mitsui, Claire Q.F. Wang, Patricia Gilleaudeau, Mary Sullivan-Whalen, Mayte Suárez-Fariñas, Judilyn Fuentes-Duculan, Polina Bulkina, Sandy Coats, Juana Gonzalez, Joel Correa da Rosa, Sandra Garcet, David Adrian Ewald, Jamie Harden, Leanne Johnson-Huang, Dan Gareau, Saakshi Khattri, Xuan Li, Yeriel Estrada, Benji Ungar, Dana Malajian, Susan Zheng, Jennifer Belasco, Hui Xu, Shinji Noda, Hanako Ohmatsu, Maria Vittoria Cannizzaro, Nancy Dattola, Andrea Chiricozzi, Kathleen Bonifacio, Norma Kunjravia, Inna Cueto, Artemis Khatcherian, Irma Cardinale, Toyoko Kikuchi, Tinky Nograles, Tali Czarnowicki, Jaehwan Kim, Daniel Kim, Patrick Brunner, Ali Jabbari, Hitokazu Esaki, Nikhil Dhingra, Valerie Yanofsky, Francesca Ortenzio, Shali Zhang, Milene Kennedy Crispin, Dan Belkin, Miriam Herschman, Xiangyu Peng, Kate Pierson, Tim Lentini, Luke Hyder, Hideki Fujita, Julia Gittler, Julia Pettersen, Daniel Humme, Kejal R. Shah, and Marianne Løvendorf.

Outside of the Krueger lab, there are many individuals and departments at The Rockefeller University who were instrumental to the completion of this work: Donna Brassil, Johanne Andersen, Emil Gotschlich, Dale Miller, Rita Devine,

Barry Coller, Rhonda Kost, Michelle Romanick, the Clinical Research Support Office, the Institutional Review Board, the Center for Clinical and Translational Science, the Genomics Resource Center, the Bio-Imaging Resource Center, the Translational Technology Core Laboratory, the Dean's Office, and the nurses/staff of The Rockefeller University Hospital.

I had the great fortune of receiving additional mentorship from and performing collaborative work with many outstanding physicians and scientists throughout the world, including: Emma Guttman-Yassky, Michelle A. Lowes, Thomas Kupper, Niroshana Anandasabapathy, Arne Akbar, Milica Vukmanovic-Stejic, Neil Renwick, Thomas Tuschl, Kemal M. Akat, John R. Zibert, David E. Hamm, William R. Levis, N. Scott McNutt, Felix Kiecker, Avner Shemer, and Diane Felsen.

I continue to feel grateful and honored to be part of the Weill Cornell/Rockefeller/Sloan Kettering Tri-Institutional MD-PhD Program. Special thanks to Olaf Andersen, Mark Pecker, Jochen Buck, Ruth Gotian, Renee Horton, Elaine Velez, Kenneth Javier, Hanna Silvast, and Caroline Fulford for running an incredible program, and for so effectively guiding its many students through the various challenges of MD-PhD training. Furthermore, the generous financial support provided by the program (made possible by a Medical Scientist Training Program grant from the National Institute of General Medical Sciences of the NIH under award number T32GM07739), cannot be ignored. I would also like to

acknowledge additional funding I have received from the Society for Investigative Dermatology, Adaptive Biotechnologies, and The Rockefeller University Center for Clinical and Translational Science. The research in this thesis was further supported by Hapten Pharmaceuticals and RXi Pharmaceuticals.

I must not forget past research mentors, without whom I would not have even started on the path to a Ph.D. degree: Richard Axel, Meena Jhanwar-Uniyal, and Robert Clancy.

This thesis of course would not be possible without the guidance of my Faculty Advisory Committee: Charles Rice (Chair), Robert Darnell, James Young, Sarah Schlesinger, and John A. Carucci (External Examiner).

As with all human subject research, special recognition must be given to the volunteers, who elect to donate their time and expose themselves to risk for the advancement of science. I would also like to thank our collaborators at Sloan Kettering for their essential role in informing potential subjects about our research study at The Rockefeller University: Jedd D. Wolchok, Charlotte E. Ariyan, Mary Sue Brady, Margaret K. Callahan, Paul B. Chapman, Daniel G. Coit, Allan C. Halpern, and Michael A. Postow.

Table of Contents

LIST OF FIGURES

LIST OF TABLES

CHAPTER 1: INTRODUCTION

Malignant Melanoma

Melanoma is a life-threatening malignant disease arising from melanocytes, the resident pigment-producing cells of the epidermis. The lifetime risk of developing this disease has been increasing since the 1930s (Rigel et al. 2005). In 2015, 73,870 cases of invasive cutaneous melanoma are expected to be newly diagnosed, resulting in an estimated 9,940 deaths (SEER Cancer Statistics Review). Although melanoma constitutes only 4 to 11 percent of all skin cancers, it is responsible for over 75 percent of skin cancer deaths (Netscher et al. 2011), thus highlighting the extreme health burden caused by this disease.

Of paramount clinical consequence are melanoma lesions that metastasize to other organs, including the skin itself. In primary lesions, the depth of invasion, or the distance from the superficial epidermal granular cell layer to the deepest intradermal tumor cells, known as the Breslow thickness, correlates with the probability of metastasis (Breslow 1980). Despite increasing knowledge regarding its molecular mechanisms, metastatic melanoma is often limited in response to treatment (Chudnovsky et al. 2005), and the best predictor of eventual mortality remains depth of invasion as measured on a pathology slide. Improved understanding of the biology of melanoma can be exploited to create targeted drugs and novel therapeutic approaches (Gray-Schopfer et al. 2007).

Although melanomas express many tumor-associated antigens, immune responses against them are often inefficient (Gajewski 2006). Potential mechanisms for this include loss of expression of histocompatibility antigens on tumor cell surfaces, the production of immunosuppressive cytokines, the activation of regulatory T cells, and T cell exhaustion. MLANA-specific T cells isolated from tumor-infiltrated lymph nodes of melanoma patients had impaired IFNγ production and enrichment of the gene set (when compared to MLANA-specific cells from blood) which characterizes exhausted T cells (Baitsch et al. 2011). Although exhausted T cells typify lymphocytes in or adjacent to melanoma lesions, these cells are capable of effector immune responses if negative checkpoints are antagonized or the cells are stimulated by other means.

The inflammatory infiltrates of melanoma have been characterized in several studies, and the presence of tumor-infiltrating lymphocytes improves melanoma prognosis (Clemente et al. 1996). The observed leukocyte infiltration in melanoma may be a side effect of the neoplastic cells stimulating themselves in an autocrine fashion, an innate anti-tumor response, or a combination of both of these along with other prospective explanations. Immunotherapeutic approaches for melanoma, where host lymphocytes are set to kill melanoma cells, is of great interest in part because of the presumably immune-mediated spontaneous melanoma remissions which sporadically occur (McGovern 1975). Also, vitiligo, a disease characterized by patchy depigmentation, is presumed to be due to autoimmune attack on melanocytes (Spritz 2012). This attack appears relatively

specific to melanocytes, as other cell types in the skin are functionally normal, and therefore vitiligo highlights the capacity for the immune system to selectively target melanoyctes. Excellent responses are sometimes obtained with immunotherapy (Hunder et al. 2008), but further work needs to be done to confirm the general applicability of such treatments.

Immune checkpoint blockade, targeting cytotoxic T lymphocyte-associated antigen 4 (CTLA-4) or programmed cell death protein 1 (PD-1), is an emerging therapeutic avenue in a variety of cancer types, but most studied in and FDA approved for malignant melanoma (Postow et al. 2015a). These therapies are antibodies targeted against negative immunologic regulators (checkpoints), effectively allowing for anti-melanoma immune responses to proceed with less interference. Despite many very promising instances of tumor regression, on average only one-third of patients respond to these therapies when given alone, and these failures are thought to have a genetic basis (Snyder et al. 2014). Tumeh *et al*. examined metastatic melanoma patients treated with the PD-1 inhibitor pembrolizumab, and demonstrated that tumor regression with this agent requires pre-existing CD8+ T cells that are negatively regulated by the PD-1/PD-L1 axis (Tumeh et al. 2014). Very recently, the two agents targeting CTLA-4 and PD-1 have been combined, and this dual approach resulted a 61% objective response rate, with a 22% complete response rate (Postow et al. 2015b). Therefore, combination of multiple agents targeting the immune system is a viable therapeutic approach in malignant melanoma.

The melanoma treatment landscape has changed dramatically in the last 5 years, with several agents being approved by the FDA for metastatic melanoma treatment (**Figure 1.1**). These include one agent targeting CTLA-4 (ipilimumab), one inhibiting a kinase (BRAF) commonly mutated in melanoma (vemurafenib), and two targeting PD-1 (pembrolizumab and nivolumab). As a result, patients today have many promising options for treatment that were not available only 5 years ago.

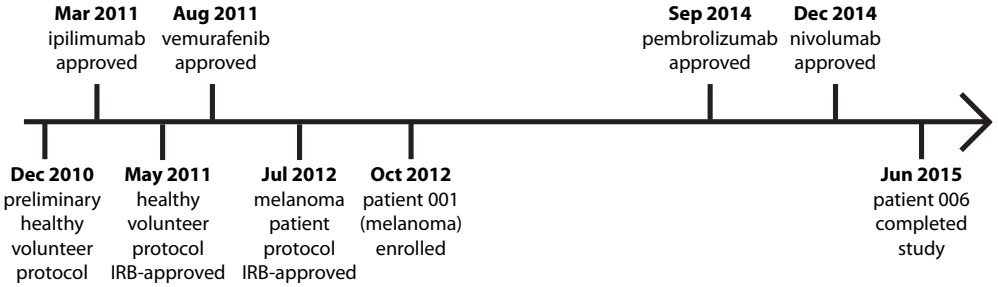

Figure 1.1: Timeline showing FDA approval of new agents for metastatic melanoma treatment. Months when the FDA approved each drug are indicated above the timeline, and below the timeline are key events of the two clinical studies (one in healthy volunteers and one in melanoma patients) that make up this thesis.

Diphencyprone (DPCP)

Another emerging therapeutic approach in melanoma, also in the realm of immunotherapy, is the contact sensitizer diphencyprone (DPCP). This sensitizer has recently been used in an Australian 50-patient case series of cutaneously metastatic melanoma, with 46% of patients having complete clearance of their disease and a further 38% having partial clearance (Damian et al. 2014) (**Figure 1.2**), but is not currently FDA approved for any indication.

Haptens like dinitrochlorobenzene and DPCP induce strong delayed-type hypersensitivity (DTH) recall reactions. Upon first exposure, haptens penetrate the epidermis and then conjugate with endogenous proteins, leading to antigen formation. The antigen is captured by antigen-presenting cells such as Langerhans cells, which mature and migrate to lymph nodes, where they clonally expand T cells specific for the antigen. These clonally expanded cells then circulate, and the individual is sensitized. Upon re-exposure, elicitation or challenge occurs, characterized by skin infiltration of the expanded T cells and resultant clinical inflammation (**Figure 1.3**). Upregulation of an array of inflammatory cytokines occurs during a "peak" challenge response, which ranges from 2-4 days in human skin (Stute *et al*., 1981). Hapten studies performed in mice have shown important roles for both CD4+ helper T cells and CD8+ cytotoxic T cells in the induction of DTH reactions (Saint-Mezard et al. 2005). Although alphabeta-T cells are the effector cells, NKT cells, B-1 cells, and gammadelta-T cells also play important roles in contact sensitivity DTH reactions

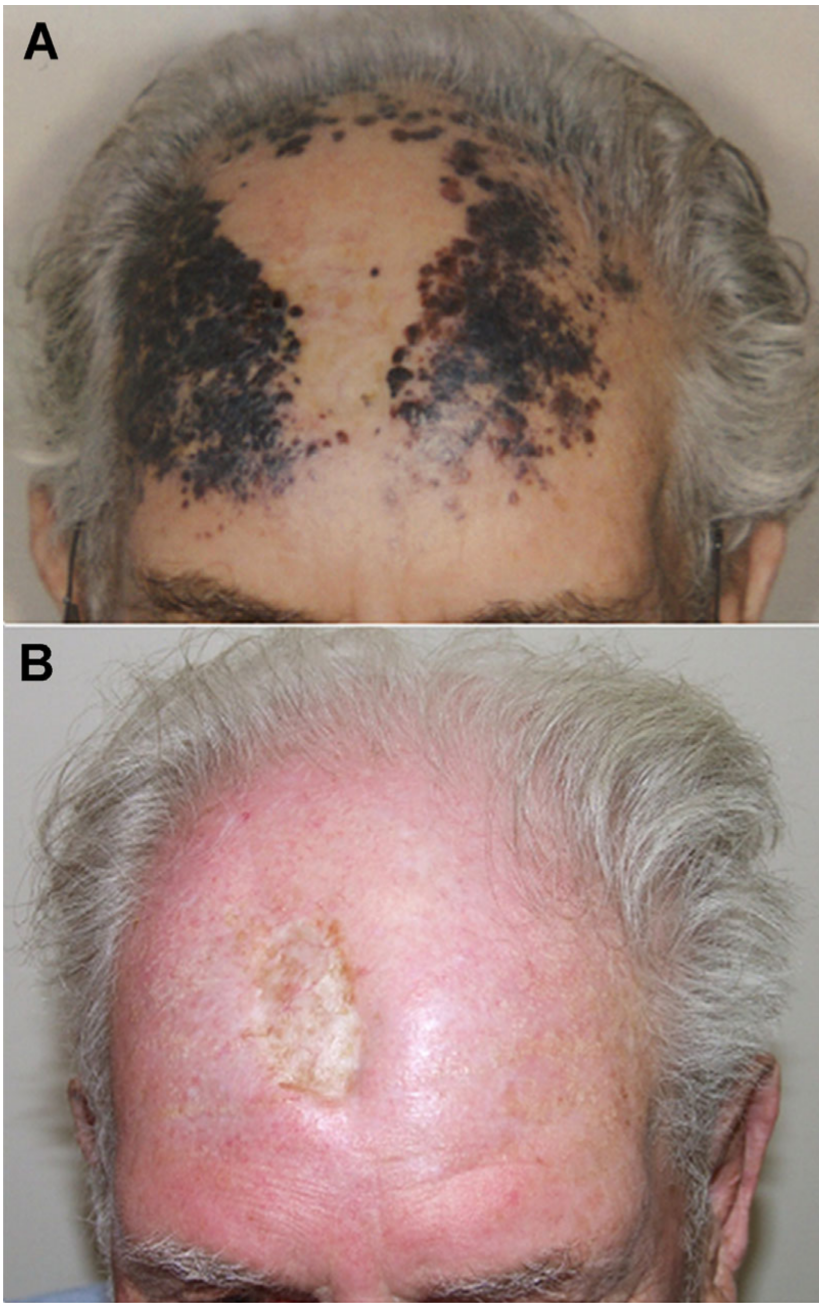

Figure 1.2: Regression of cutaneous melanoma metastases upon DPCP treatment. This 71-year-old man presented with extensive, radiation-resistant recurrent scalp disease (A). All cutaneous melanoma metastases regressed within 4 weeks of starting DPCP (B), and five years later he remains disease free. From (Damian et al. 2014).

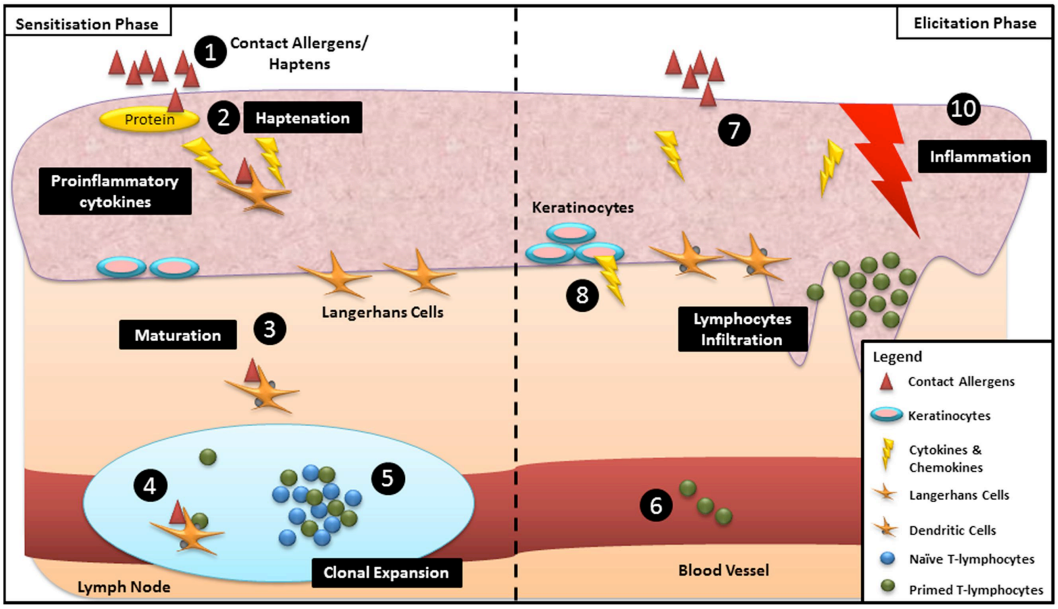

Figure 1.3: Schematic of the sensitization and challenge phases of a DTH reaction. (1) Haptens gain access to the skin through the viable epidermis. (2) Binding of haptens and endogenous skin proteins. (3) Langerhans cells bind to the hapten–protein complex and mature during migration to the lymph node. (4) Langerhans cells present haptenated protein to naïve T cells. (5) Clonal expansion of specific effector and memory T cells. (6) Proliferated T cells disseminate into the blood circulation, resulting in sensitization of an individual. (7) Re-exposure of similar haptens to the same individual. (8) Release of pro-inflammatory cytokines and chemokines by epidermal cells. (9) Infiltration of T cells from blood vessels into the site of contact. (10) Development of clinical inflammation. From (Wong et al. 2015).

(Askenase 2001). Despite these and other murine studies which study haptens as prototypical causes of DTH reactions, the T cell polarization involved has shown conflicting results, with both Th1 and Th2 cells being variably implicated (Black 1999).

In human skin, T cell polarization as well as the cellular and molecular events associated with DTH responses are incompletely understood. This is especially true if one considers that agents like dinitrochlorobenzene and DPCP have been used, somewhat paradoxically, to increase local immune responses for the resolution of warts (Upitis and Krol, 2002) and melanoma metastases (Damian *et al*., 2014), but also to decrease pathogenic immunity for the restoration of hair growth in alopecia areata (Freyschmidt-Paul *et al*., 2003). One might postulate from these various therapeutic applications that cytotoxic effector immune pathways are induced by topical haptens, while activation of negative regulatory pathways also occurs to eventually down-regulate the inflammatory response. Available data from murine models suggest that resolution of cutaneous immune responses to haptens may be strongly dependent on regulatory T cells in the skin (Lehtimäki *et al*., 2012), leading to active mechanisms of immune suppression during the resolution phase of a DTH response. In fact, negative regulatory immune mechanisms may be of more general importance for maintaining skin homeostasis as non-inflammatory in the face of a large population of effector memory T cells that normally reside in the skin (Clark *et al*., 2006). The elimination of regulatory T cells from the skin has the consequence of increasing

skin inflammation due to environmental or chemical allergens in animal models (Freyschmidt *et al*., 2010)(Dudda *et al*., 2008). The absence of negative regulatory mechanisms likely contributes to inflammatory skin diseases like psoriasis, where chronic activation of T cells and dendritic cells, with ongoing production of many inflammatory cytokines, leads to focal plaques of disease that rarely resolve spontaneously. Cellular and molecular events associated with DTH responses to topical and intradermal antigens are much better understood for the sensitization and early elicitation phases (particularly the peak DTH reaction that occurs within 4 days of recall exposure), compared to later phases of the elicitation response when negative regulatory pathways might be dominant (Vocanson et al., 2009). Very little is known about immune cellular elements and expression of negative regulatory immune molecules during this resolution phase in humans.

In this thesis, two clinical studies involving human subjects are presented. First, a study with healthy volunteers was undertaken to examine DTH reactions induced by a single application of DPCP, including the T cell polarization involved and potential anti-neoplastic mechanisms. Second, a treatment protocol with metastatic melanoma patients was completed, this time employing repeated applications of DPCP as was done in the Australian trial (Damian et al. 2014). The goal of this treatment protocol was to examine immune mechanisms associated with melanoma metastasis regression induced by DPCP.

CHAPTER 2: MATERIALS AND METHODS

Study subjects and skin samples – healthy volunteers

Skin biopsies were obtained from 11 volunteers under a protocol approved by The Rockefeller University's Institutional Review Board. Written, informed consent was obtained from all subjects and the study adhered to the Declaration of Helsinki Principles. All volunteers underwent a rigorous screening process, including medical history, physical examination, complete blood count/blood chemistries, and point-of-care HIV test to ensure they were overall healthy and not on any medication which could interfere with immune reactions. Each volunteer was sensitized to 0.4% DPCP (in a topical gel formulation) on his/her right upper arm and 0.04% DPCP on his/her left lower arm. These concentrations were chosen to ensure effective sensitization while minimizing uncomfortable inflammatory reactions on the arms. Previous work has demonstrated that 0.4% but not 0.04% DPCP is consistently able to induce sensitization in immunocompetent individuals (Levis *et al*., 2006). Two weeks later, effective sensitization was confirmed by noting induration at the application sites (all subjects were successfully sensitized) and then two challenge applications of 0.04% DPCP were applied to the subject's left upper thigh. Also at this visit, two placebo applications (identical formulation but without DPCP) were applied to the subject's right upper thigh. Each application of placebo or DPCP gel was 0.2 mL (80 μg for the 0.04% concentration) placed on a 2.5 x 2.5 cm square area bandage which the subject was instructed to leave on for 24 hours before removal and

washing. Three days after these challenge applications, one 6 mm full thickness punch biopsy was taken of a DPCP-treated site and an identical biopsy was taken of a placebo-treated site (day 3 biopsies). Subjects were then observed at 7 and 14 days post-challenge to determine when the DPCP-induced inflammation was resolving, based on clinical scoring of erythema and induration. At that time (14 days post-challenge), another pair of biopsies was taken, but of the two sites not biopsied at 3 days post-challenge (**Figure 2.1**). Six of 11 volunteers were brought back 4-8 months after challenge application for another biopsy of a DPCP-treated site, which clinically no longer exhibited any signs of inflammation. Ultrasound images were acquired using DermaScan C ultrasound scanner (Cortex Technology, Hadsund, Denmark). In these images, dermal inflammation is visualized as a dark zone (brackets) under epidermis and the thickness of this zone correlates with the extent of inflammation/induration (Kelly *et al*., 1998)(Hoffmann et al. 1994a).

Study subjects and skin samples – psoriasis patients

For psoriatic lesional vs. non-lesional skin microarray data, we used the meta-analysis derived (MAD3) transcriptome as previously described (Tian et al. 2012). Psoriatic lesional tissue for qRT-PCR and immunohistochemistry studies were from deidentified residual samples of plaque-type psoriasis vulgaris from previous studies for whom no clinical characteristics are available; a psoriasis area severity index of more than 12 (moderate-to-severe psoriasis vulgaris with >10% body surface area involvement) was required for entry into these trials.

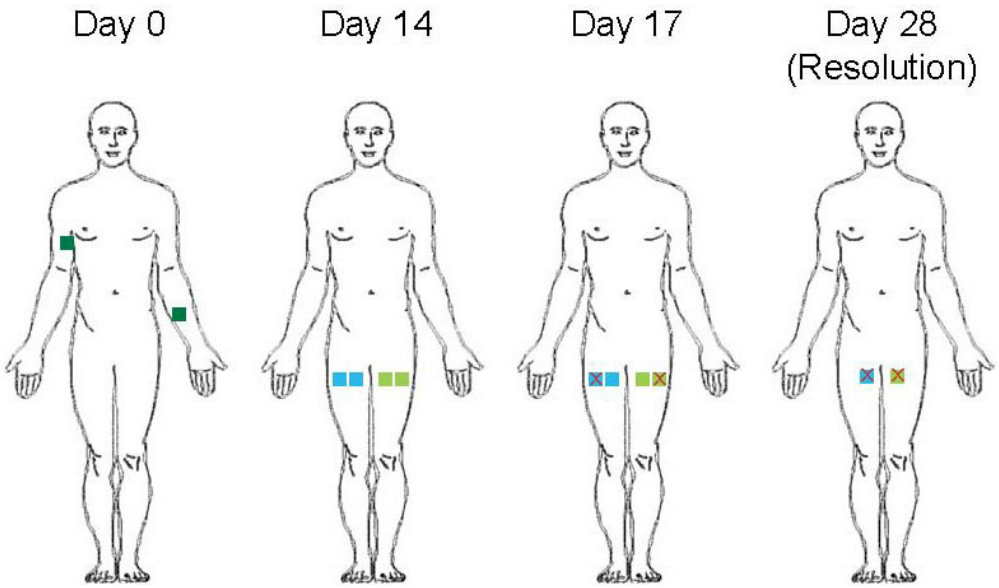

Figure 2.1: Schematic of DPCP sensitization and challenge schedule.

Subjects were sensitized with DPCP at two sites on their arms at Day 0 followed by challenge and placebo applications at Day 14. At Day 17 (3 days post-challenge), one pair of biopsies was taken and a second pair was taken at Day 28 (14 days post-challenge) when the inflammation induced by DPCP was seen to be clinically resolving. Dark green, light green, and blue squares indicate sensitization, challenge, and placebo applications, respectively. A red X is used to represent a biopsy taken.

Study subjects and skin samples – melanoma patients

Skin biopsies were obtained from melanoma patients with cutaneous metastases under a protocol approved by The Rockefeller University's Institutional Review Board. Written, informed consent was obtained and the study adhered to the Declaration of Helsinki Principles. The patients all underwent rigorous screening processes, including medical history, physical examination, and point-of-care HIV test to ensure that they did not have any conditions and were not on any medications which could interfere with immune reactions. While enrolled in our DPCP trial at The Rockefeller University, all patients continued to receive their standard oncologic follow-up and monitoring visits.

Patients were sensitized to 0.4% DPCP (in the same topical gel formulation as used with the healthy volunteers) on one of their cutaneous metastases and their right upper arm, as well as to 0.04% DPCP (also in a topical gel formulation) on their left lower arm. Two weeks later, effective sensitization was confirmed by noting induration at the application sites, and then challenge applications were applied to the subject's cutaneous metastases. Also at this visit, one 0.2 mL application of 0.4% DPCP was applied to one area of non-melanoma skin, and another 0.2 mL application of 0.04% DPCP was applied to a different area of non-melanoma skin. These two applications were completed in order to determine the concentration of DPCP that would induce tolerable inflammation in each patient, so that the appropriate concentration could be used for challenge (treatment) applications. For all patients, one of the inflamed non-melanoma sites challenged

with DPCP was biopsied 3 days later (the classical time of "peak" response to a single application of DPCP). Each application of DPCP (occurring twice weekly) was self-administered by the patient such that all cutaneous metastases were covered with a thin layer of gel (the patient was asked to return the tube containing the DPCP gel at each clinic visit for weighing in order to ensure compliance), and then covered with Tegaderm for at least 2 hours.

All biopsies (6 mm full thickness punch) were bisected: one half was immediately placed in RNAlater RNA Stabilization Reagent (Qiagen, Valencia, CA) for later RNA extraction, and the other half was frozen in optimum cutting temperature (OCT) compound (Thermo Fisher Scientific Inc., Wilmington, DE) for later histological sectioning.

RNA extraction, quantification, and microarray

Total RNA was extracted using the miRNeasy Mini Kit (Qiagen, Valencia, CA) according to the manufacturer's protocol with on-column DNase digestion. The amount of RNA was assessed by NanoDrop 1000 spectrophotometer (Thermo Fisher Scientific Inc., Wilmington, DE). The quality of extracted RNA was examined using Agilent Bioanalyzer 2100 (Agilent Technologies, Palo Alto, CA). RNA was hybridized to HGU133 Plus 2.0 chips (Affymetrix, Santa Clara, CA) to measure relative gene expression.

Statistical analysis of microarray data

Microarray data were analyzed using R/Bioconductor packages (http://www.r-project.org). The Harshlight package (Suárez-Fariñas *et al*., 2005) was used to scan Affymetrix chips for spatial artifacts. Expression values were obtained using the GCRMA algorithm. Genes with low variation and low expression in most samples were filtered out prior to the analysis. Batch effect due to hybridization date was adjusted using ComBat (Johnson *et al*., 2007). Principal Components Analysis (PCA) was used to represent the high dimensionality of the data along the directions of maximal variance. Hypotheses of interest were tested using contrasts in R's *limma* package framework. The *p* values resultant from the moderated paired Student's *t*-tests were adjusted for multiple hypotheses using the Benjamini-Hochberg procedure, which controls for the false discovery rate. Ingenuity Pathway Analysis (www.ingenuity.com) was used to determine canonical pathways significantly linked to various gene sets.

Quantitative RT-PCR

Pre-amplification quantitative RT-PCR technique was used for measuring various genes in total RNA extracted from skin biopsy samples according to the company's instructions. Briefly, 5 ng of total RNA was subjected to first-strand cDNA synthesis using High Capacity cDNA Reverse Transcription kits (Applied Biosystems, Carlsbad, CA). The resulting cDNA was subjected to 14 cycles of pre-amplification using TaqMan PreAmp Master Mix Kit (Applied Biosystems) with desired pooled assay mix. The Gene Amp PCR System 9700 (Applied

Biosystems) was used for the pre-amplification reaction with the following thermal cycler conditions: 10 min at 95^{o}C and 14 cycles of 15 seconds at 95^{o}C followed by 4 min at 60^{o}C. 12.5 µl of pre-amplified cDNA was then used for quantitative RT-PCR reaction using TaqMan Gene Expression Master Mix (Applied Biosystems). The 7900HT Fast Real-Time PCR System was used for PCR reactions, and the thermal cycler conditions were as follows: 2 minutes at 50^{o}C, 5 minutes at 95^{o}C, and 40 cycles of 15 seconds at 95^{o}C followed by 60 seconds at 60^{o}C. Data were analyzed by the Applied Biosystems PRISM 7700 software (Sequence Detection Systems, ver. 1.7) and normalized to human acidic ribosomal protein (hARP) housekeeping gene. All assays were from Applied Biosystems except for RPLP0/hARP, where a custom primer/probe set was used (Forward: CGCTGCTGAACATGCTCAA, Reverse: TGTCGAACACCTGCTGGATG, Probe: 6-FAM-TCCCCCTTCTCCTTTGGGCTGG-TAMRA).

For miRNA studies, individual qRT-PCR assays were used to validate the expression levels of miR-21, -7, -503 and -383 using the TaqMan MicroRNA Reverse Transcription Kit (Applied Biosystems) followed by PCR using TaqMan MicroRNA assays (Applied Biosystems). Samples were analyzed using the 7900HT sequence detection system (Applied Biosystems) according to the manufacturer's directions. The qRT-PCR data were processed using the ΔΔCT method in order to obtain expression fold changes (Schmittgen and Livak 2008), with RNU6B used as the reference gene.

Immunohistochemistry

Frozen sections of skin biopsies were dried at room temperature and then fixed for 2 minutes in acetone. Next, the samples were blocked with 10% normal serum of the species in which the secondary antibody was made and then the samples were incubated overnight at 4^{o}C with the appropriate primary antibody. Biotin-labeled secondary antibodies (Vector Laboratories, Burlingame, CA) were amplified with avidin-biotin complex (Vector Laboratories) and developed with chromogen 3-amino-9-ethylcarbazole (Sigma Aldrich, St. Louis, MO) to produce a red color indicative of positive staining. The number of positive cells per mm was counted manually per field using computer-assisted image analysis (NIH Image 6.1; http://rsb.info.nih.gov/nih-image).

Immunofluorescence

Frozen sections of skin biopsies were dried at room temperature and then fixed with acetone. Next, the samples were blocked with 10% normal goat serum (Vector Laboratories) for 30 minutes. Primary antibody was incubated overnight at 4^{o}C and amplified with the appropriate secondary antibody for 30 minutes. For co-localization, sections were then co-stained overnight with a second antibody, and amplified with the appropriate secondary antibody for 30 minutes. Images were acquired using the appropriate filters of a Zeiss Axioplan 2 wide-field fluorescence microscope (Thornwood, NY) with a Plan Neofluar 20 × 0.7 numerical aperture lens and a Hamamatsu Orca Er-cooled charge-coupled device

camera (Bridgewater, NJ), controlled by METAVUE software (MDS Analytical Technologies, Downington, PA). Images in each figure are presented both as single-color stains (green and red) located above the merged image, so that localization of two markers on similar or different cells can be appreciated. Cells that co-express the two markers in a similar location are yellow in color. A white line denotes the dermoepidermal junction. Dermal collagen fibers gave green autofluorescence, and antibodies conjugated with a fluorochrome often gave background epidermal fluorescence.

miRNA sequencing and statistical analysis

Barcoded small RNA sequencing was performed using a modified version of an established protocol (Hafner et al. 2008). Briefly, 100 ng total RNA from each sample was subjected to 3' and 5' adapter ligation and RT-PCR amplification. The resulting cDNA library was sequenced using Illumina sequencing technology (Illumina, Inc., San Diego, CA). The bioinformatic analysis of the small RNA sequence data was performed as described previously (Farazi et al. 2012). Barcodes were used to mark individual samples so that up to 20 could be processed simultaneously (Hafner et al. 2012).

Sequence data were imported into the R working environment (www.r-project.org) and analysed using the edgeR package from Bioconductor (http://bioconductor.org). edgeR supports differential expression analysis and is based on a negative binomial distribution. It adjusts any differential expression

analysis for varying sequencing depths as represented by differing library sizes (Robinson et al. 2010). Only human miRNAs complying with a threshold of 100 sequence reads per miRNA in a minimum of 50% of the samples within each group were included in the further analysis. Unsupervised principal component analysis (PCA) and Pearson's correlation analysis were applied to explore the association between the samples. False discovery rate < 0.05 was considered as statistically significant.

DNA extraction and T cell receptor (TCR) sequencing

For each biopsy specimen frozen in OCT, 40 sections were cut at 10 micron thickness and then processed for DNA extraction using the QIAamp DNA Mini Kit (Qiagen). DNA samples were shipped on dry ice to Adaptive Biotechnologies (Seattle, WA) for survey level immunosequencing using the immunoSEQ human TCRB assay.

Immunosequencing was performed by first completing multiplex PCR to capture the highly variable CDR3 region. A synthetic immune repertoire was used to iteratively measure and subsequently correct for amplification bias. Then, high-throughput sequencing was done to exclusively target T cell receptor genes. Data analysis was performed by Adaptive Biotechnologies.

CHAPTER 3: HISTOLOGICAL AND GENE EXPRESSION PROFILING OF HEALTHY VOLUNTEER SKIN REACTIONS TO DIPHENCYPRONE

Kinetics of skin inflammation induced by DPCP

Healthy individuals (demographics listed in **Table 3.1**) were sensitized to DPCP and two weeks later received two challenge applications on their left thigh and two placebo applications on their right thigh. Three days after challenge, all subjects exhibited strong clinical inflammation (erythema, induration, and epithelial vesiculation in some cases) only in DPCP-treated sites, whereas placebo-treated sites were indistinguishable from background skin (**Figure 3.1**). The clinical DPCP-induced reaction was clearly diminished by 14 days after the challenge dose. Erythema and induration were quantified using a 0-4 scale derived from the Psoriasis Area Severity Index (PASI). The mean response at day 3 was 5.5 (for sum of erythema and induration) and was reduced to 2.1 by day 14 ($p<10^{-7}$) (**Table 3.1**). Ultrasound measurements further confirmed a decrease in dermal inflammation over time (**Figure 3.1**). Overall, these data support the classical view that 3 days after challenge represents the clinical peak of a DTH response.

Kinetics of cellular and molecular immune response to DPCP in DTH reactions

Biopsies were taken of both DPCP- and placebo-treated sites at day 3 (clinical peak) and at day 14 (resolving inflammation). The first 6 patients also

Table 3.1: Demographics and clinical scoring of inflammatory reactions induced by DPCP in all subjects (n=11)

Subject ID	Gender	Age	Race	Subgroup	day 3[1]	day 14[1]	day 3 score	day 14 score
001	M	55	White	B	4/4 (1.19)	2/1 (0.20)	8	3
006	M	52	Black	A	2/2 (0.30)	0/1 (0.18)	4	1
008	F	42	Asian	B	3/2 (0.66)	1/1 (0.19)	5	2
009	M	58	White	B	2/2 (0.21)	1/0 (0.18)	4	1
012	M	44	White	A	3/2 (0.30)	2/1 (0.10)	5	3
013	F	46	Black	A	3/3 (0.76)	2/1 (0.36)	6	3
014	M	20	Asian	A	3/3 (0.36)	2/0 (0.15)	6	2
015	M	55	Black	B	2/2 (0.21)	1/0 (0.12)	4	1
016	F	29	Black	A	3/1 (0.24)	1/0 (0.18)	4	1
020	M	43	Black	B	3/3 (0.87)	1/1 (0.24)	6	2
021	M	40	Black	B	4/4 (1.51)	2/2 (0.24)	8	4
Average							5.5	2.1

$p = 7.8 \times 10^{-8}$ for DPCP day 3 vs day 14 score comparison (paired two-tailed Student's *t*-test).

[1]Erythema/induration (0-4 scale for each) - scores are sums of these two measures. In parentheses are the quantifications of the extent of inflammation as measured by ultrasound (in mm, see **Figure 3.1**).

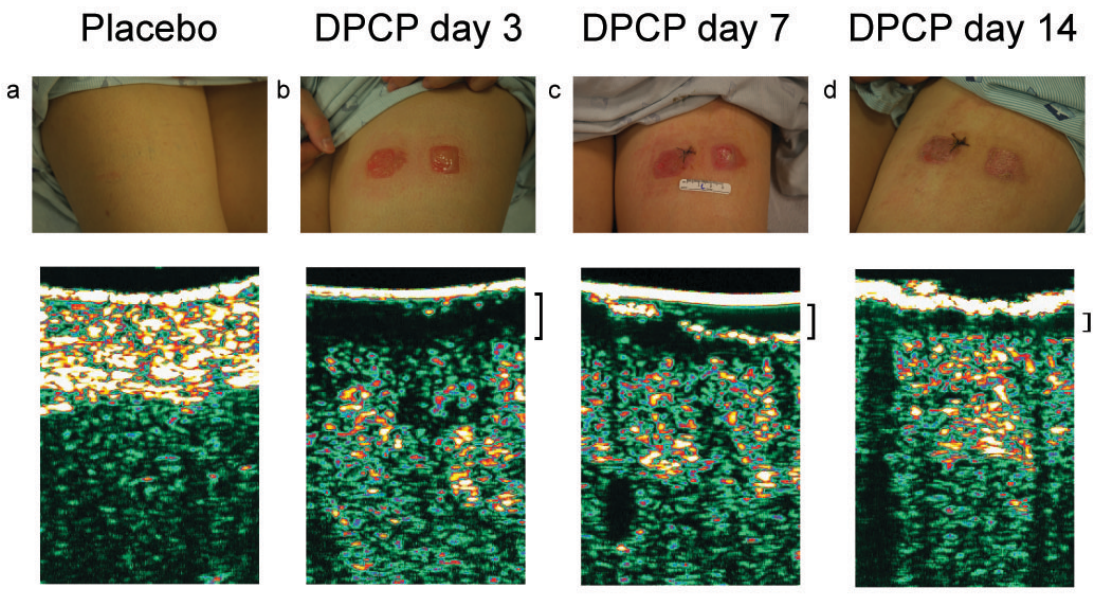

Figure 3.1: Visualization of inflammatory reactions induced by DPCP over time. Clinical photography with ultrasound imaging below of a skin site (a) treated with placebo, (b) 3 days after treatment with DPCP, (c) 7 days after treatment with DPCP, and (d) 14 days after treatment with DPCP. Brackets on ultrasound images indicate extents of inflammatory reactions as reflected by dermal thickness. Shown is a representative subject (subject 008).

underwent skin biopsies of reaction sites 4 to 8 months after DPCP challenge (late biopsy). In the acute response, T cells appeared rapidly at DTH challenge sites with a mean of 1,113 CD3+ T cells/mm of skin. Overall, T cell counts diminished slightly by day 14, with a mean of 946 cells/mm. In late biopsies, T cells were reduced to levels seen in placebo sites (<100/mm). Relative to placebo and generally expected, increases were seen in CD3+ and CD8+ lymphocytes (**Figure 3.2a and b**), as well as in dendritic cell (DC) populations in the day 3 and day 14 biopsies, but two patterns of response were seen with cellular infiltrates as will be discussed in the next section. T cell activation in biopsies was assessed by RT-PCR measures of mRNAs that are associated with specific T cell subsets, e.g., IFNγ defining a Th1 response, IL-13 defining a Th2 response, or IL-17 defining a Th17 response (**Figure 3.2c**). Marked increases in cytokine mRNA levels occurred in day 3 DPCP-treated sites, with changes ranging from 9-fold to >1000-fold ($\log_2$ 3.2 to >10 as graphed in **Figure 3.2c**). The day 14 reactions showed reduced expression of each T cell subset cytokine with the largest declines in IL-9 and IL-13. All cytokine levels normalized in late biopsies (**Figure 3.2c**). The day 3 DPCP response was also associated with a 6-fold increase in forkhead box P3 (Foxp3) mRNA, but this product did not diminish on average in day 14 biopsies. Overall, visible skin inflammation in the DPCP reaction at days 3 and 14 was better correlated with levels of pro-inflammatory cytokine mRNAs than with the number of infiltrating T cells or DCs. The diminishing production of inflammatory cytokine mRNAs at day 14 with persistence of Foxp3 expression suggests the possibility of an altered positive vs. negative regulatory immune

Figure 3.2: Reactions to DPCP include immune activation markers that are present at day 3 but diminish over time. (a, b) Immunohistochemistry for CD3 (a) and CD8 (b) on placebo-treated samples, DPCP day 3 samples, DPCP day 14 samples, and DPCP late samples. Scale bar = 100 μm. (c) RT-PCR analysis for IFNG, IL2, IL2RA, IL13, IL9, IL17A, IL22, and Foxp3. Shown are average normalized expression values for placebo-treated day 3 samples (light blue bars, n=11), placebo-treated day 14 samples (dark blue bars, n=11), DPCP day 3 samples (pink bars, n=11), DPCP day 14 samples (red bars, n=11), and DPCP-treated samples 4-8 months after challenge (late) (brown bars, n=6). Asterisks indicate $p<0.01$ when compared to placebo and error bars represent standard errors of the mean. (d) Principal components analysis (PCA) of microarray data showing all samples as individual dots colored according to sample type. The larger dots are averages for each sample type.

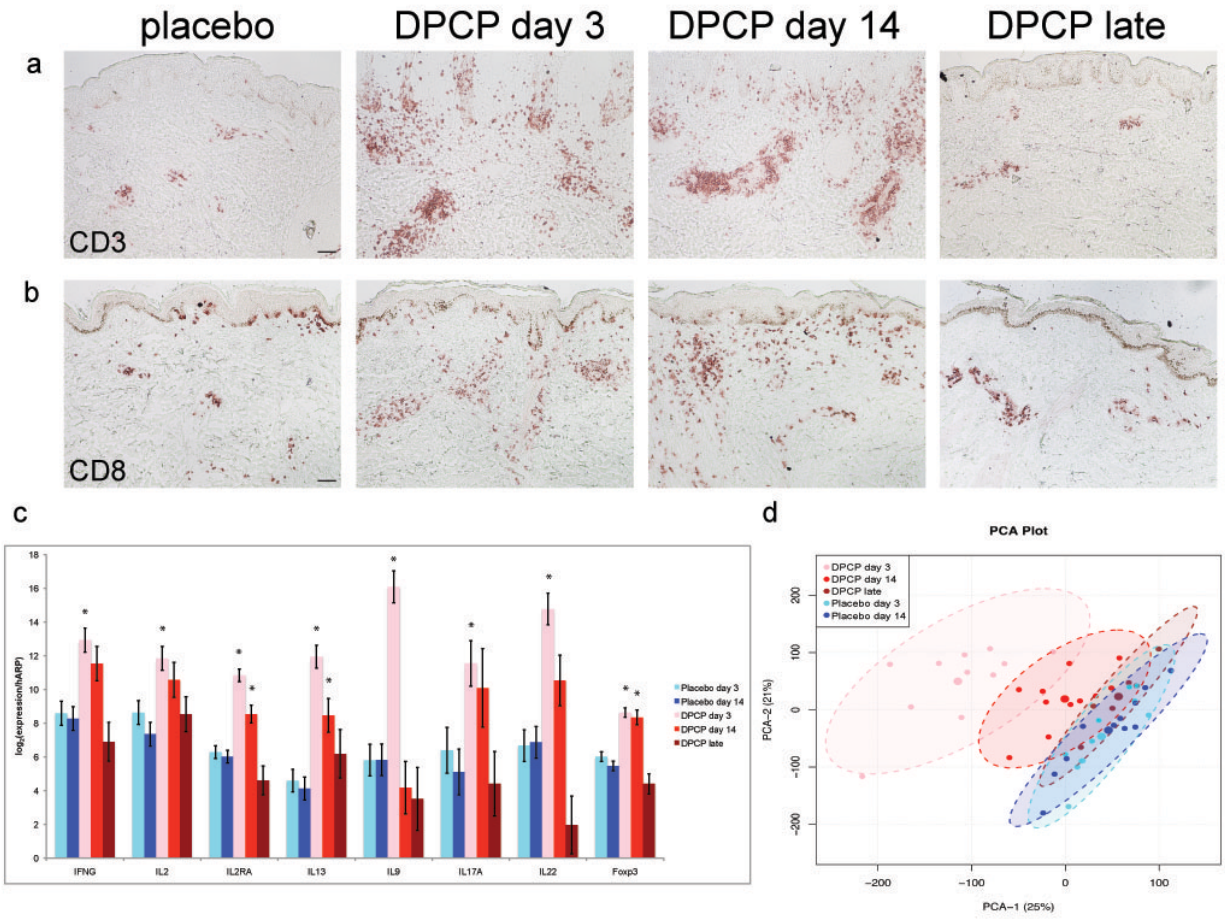
placebo
DPCP day 3
DPCP day 14
DPCP late
a
CD3
b
CD8
c
log2(expression/hARP)
IFNG
IL2
IL2RA
IL13
IL9
IL17A
IL22
Foxp3
Placebo day 3
Placebo day 14
DPCP day 3
DPCP day 14
DPCP late
d
PCA Plot
DPCP day 3
DPCP day 14
DPCP late
Placebo day 3
Placebo day 14
PCA−2 (21%)
PCA−1 (25%)

balance in day 3 vs. day 14 reactions.

Molecular profiling of day 3 and day 14 DPCP responses

To profile the global set of gene expression changes in the DPCP reactions, skin biopsies were hybridized to Affymetrix HGU133 2.0 Plus arrays. A principal components analysis (PCA) of the skin responses is diagrammed in **Figure 3.2d**. Day 3 DPCP reactions were widely separated from placebo responses in the major axis of variation (PCA-1), whereas the day 14 reactions approached the placebo sites and late biopsies overlapped completely with placebo responses. Using cutoffs of false discovery rate<0.05 and fold change>2, the day 3 DTH responses had 3,670 upregulated and 3,884 downregulated probe sets compared to placebo-treated skin. **Tables 3.2 and 3.3** list the top ten up-regulated and down-regulated genes, respectively, in day 3 and day 14 reactions. Since the "top" gene sets are largely different at day 3 vs. day 14, the tables are constructed with a listing of gene expression for both sets of genes at both day 3 and day 14. Among genes with the highest induction at day 3, granzyme B (119-fold increase) and IL-24 (107-fold increase) are molecules with identified roles in tissue rejection or anti-neoplastic control of melanomas or other cancers. Strong expression of CXCL10 (104-fold increase) and CXCL9 (85-fold increase) suggest activation of STAT1-regulated genes by IFNγ production. At day 14, the genes with highest expression at day 3 were strongly down-regulated (on average >10-fold), with IL-24 expression reduced to background levels in placebo-treated skin. In the day 14

Table 3.2: Top 10 up-regulated genes in DPCP day 3 and DPCP day 14 vs placebo samples

Gene	Description	fold change at day 3	fold change at day 14
(a) top up-regulated transcripts at day 3			
SERPINB4	serpin peptidase inhibitor, clade B (ovalbumin), member 4	340.5	10.6
S100A7A	S100 calcium binding protein A7A	170.9	6.1
DEFB4A	defensin, beta 4A	169.5	17.0
MMP1	matrix metallopeptidase 1 (interstitial collagenase)	167.3	4.9
MMP12	matrix metallopeptidase 12 (macrophage elastase)	147.9	8.4
GZMB	granzyme B (granzyme 2, cytotoxic T-lymphocyte-associated serine esterase 1)	118.8	11.2
IL24	interleukin 24	106.8	1.3
CXCL10	chemokine (C-X-C motif) ligand 10	104.2	25.5
S100A9	S100 calcium binding protein A9	97.7	15.7
APOBEC3A	apolipoprotein B mRNA editing enzyme, catalytic polypeptide-like 3A	95.0	1.2

(b) top up-regulated transcripts at day 14			
CXCL9	chemokine (C-X-C motif) ligand 9	84.7	37.3
COL6A6	collagen, type VI, alpha 6	11.0	36.1
CCL18	chemokine (C-C motif) ligand 18 (pulmonary and activation-regulated)	15.0	32.1
CXCL10	chemokine (C-X-C motif) ligand 10	104.2	25.5
SERPINB3	serpin peptidase inhibitor, clade B (ovalbumin), member 3	68.0	23.3
COL6A5	collagen, type VI, alpha 5	15.8	20.1
CD1B	CD1b molecule	10.5	19.6
DEFB4A	defensin, beta 4A	169.5	17.0
S100A9	S100 calcium binding protein A9	97.7	15.7
OASL	2'-5'-oligoadenylate synthetase-like	54.5	12.1
(c) regulatory genes with selective expression in day 14 samples			
ARG1	arginase, liver	0.2	11.6
FLT3	fms-related tyrosine kinase 3	2.5	11.5
XCR1	chemokine (C motif) receptor 1	0.3	6.1

Table 3.3: Top 10 down-regulated genes in DPCP day 3 and DPCP day 14 vs placebo samples

Gene	Description	fold change at day 3	fold change at day 14
(a) top down-regulated transcripts at day 3			
IL37	interleukin 37	-46.0	-2.3
ATP1A2	ATPase, Na+/K+ transporting, alpha 2 polypeptide	-38.3	-3.2
GDF10	growth differentiation factor 10	-36.4	-3.2
SGCG	sarcoglycan, gamma (35kDa dystrophin-associated glycoprotein)	-29.8	-4.4
MYOC	myocilin, trabecular meshwork inducible glucocorticoid response	-29.2	-7.1
VIT	vitrin	-26.8	-2.7
DPP6	dipeptidyl-peptidase 6	-25.6	-3.2
THRSP	thyroid hormone responsive	-24.9	-3.4
DLG2	discs, large homolog 2 (Drosophila)	-23.7	-1.4
FIBIN	fin bud initiation factor homolog (zebrafish)	-23.4	-4.7
(b) top down-regulated transcripts at day 14			
WIF1	WNT inhibitory factor 1	-6.2	-27.1
GALNTL2	UDP-N-acetyl-alpha-D-galactosamine:polypeptide N-	-2.1	-9.9

	acetylgalactosaminyltransferase-like 2		
RBP4	retinol binding protein 4, plasma	-10.8	-8.2
BTC	betacellulin	-19.8	-8.1
LEP	leptin	-7.2	-8.0
TNMD	tenomodulin	-10.2	-7.8
MYOC	myocilin, trabecular meshwork inducible glucocorticoid response	-29.2	-7.1
MUC7	mucin 7, secreted	-5.6	-6.1
IL17D	interleukin 17D	-13.6	-6.1
SPINK1	serine peptidase inhibitor, Kazal type 1	-3.4	-5.9

biopsies, CCL18 was amplified from the day 3 response and CD1b also became more strongly expressed, likely corresponding to increased DCs at this time point.

The only genes common in top up-regulated products between day 3 and day 14 were defensin beta 4, CXCL10, and S100A9. On a more global level, of the 793 up-regulated and 726 down-regulated probesets at day 14, 317 were uniquely expressed at day 14 and not day 3 (**Figure 3.3a**), illustrating that the overall transcriptomic response is distinct between these two time points and that day 14 reactions are not simply an intermediate between day 3 and placebo responses. These unique genes at day 14 included arginase, liver (ARG1), fms-related tyrosine kinase 3 (FLT3), and chemokine, C motif, receptor 1 (XCR1) (**Table 3.2c,** confirmatory immunohistochemistry and immunofluorescence to co-localize with CD11c+ DCs in **Figure 3.3b and c**), all of which may play roles in immune response resolution. In terms of genes that were down-regulated in the DPCP response (**Table 3.3**), we noted that the day 3 and day 14 responses were largely distinct, as with up-regulated genes. The top down-regulated gene at day 3 was IL-37, which is known to negatively regulate inflammatory responses and where ~20-fold increased expression at day 14, relative to day 3, could represent an active regulatory mechanism. A full list of genes that are up-regulated or down-regulated in day 3 and day 14 biopsies is available on request and all microarray data have been deposited in a public database. Granulysin was also highly upregulated (47-fold) and appeared in mononuclear leukocytes in the dermis at days 3 and 14. To localize cells producing granulysin, two color

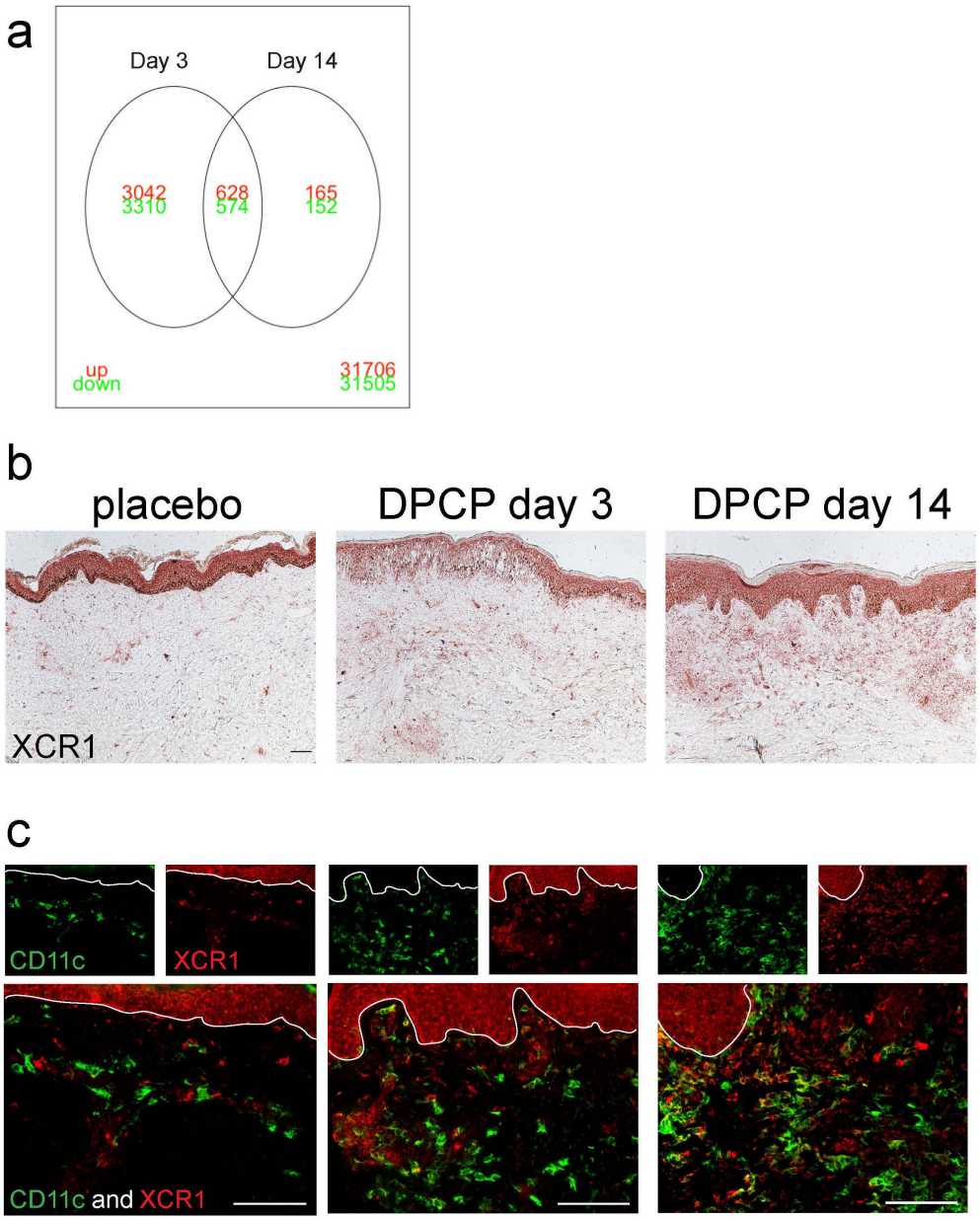

Figure 3.3: DPCP day 14 reactions include many unique genes and XCR1+ DCs not present in day 3 reactions. (a) Venn diagram showing up- and down-regulated probesets (red and green, respectively) in day 3 and day 14 reactions. (b) Immunohistochemistry for XCR1 and (c) immunofluorescence for XCR1 (red)/CD11c (green) on representative placebo-treated (left), DPCP day 3 (middle) and DPCP day 14 (right) samples. Scale bar = 100 μm.

immunofluorescence was performed. The strongest co-localization with granulysin was CD3+ T cells, with some but not all CD8+ cells staining for this cytolytic effector molecule. A few CD11c+ dendritc cells also appeared to produce granulysin (**Figure 3.4**).

Immune infiltrates follow two distinct patterns after a DPCP challenge

In all patients, we measured marked increases in CD3+ T cells and CD11c+ DCs in day 3 "peak" reactions. However, we detected two distinct reaction patterns for the day 14 "resolution" reaction. One pattern seen in 5/11 patients (subgroup A, **Figure 3.5**) showed increasing numbers of T cells and/or DCs in the day 14 biopsies compared to the day 3 reactions, a response that was entirely unexpected (**Figure 3.5c and d**). This subset of patients also showed even larger increases in mature (DC-LAMP+) DCs in day 14 biopsies compared to day 3 biopsies, and this subgroup had the most pronounced dermal infiltrates of Langerin+ cells (**Figure 3.5e and f**). However, the expression of inflammation-associated cytokines and CD25 (IL-2RA) usually decreased in day 14 biopsies compared to day 3 reactions, so we detected a disassociation between cellular immune infiltrates and production of inflammatory cytokines/activation molecules (**Figure 3.5a**). As further evidence for this, both CD3+ and CD11c+ cell counts did not significantly correlate with gene expression levels of any of the following immune activation markers: IFNγ, IL-2, and IL-2RA (**Figure 3.6**). The other response pattern seen in 6/11 patients (subgroup B, **Figure 3.7**) fit the expected response kinetics for a DTH reaction: T cell and DC infiltrates peaked at day 3

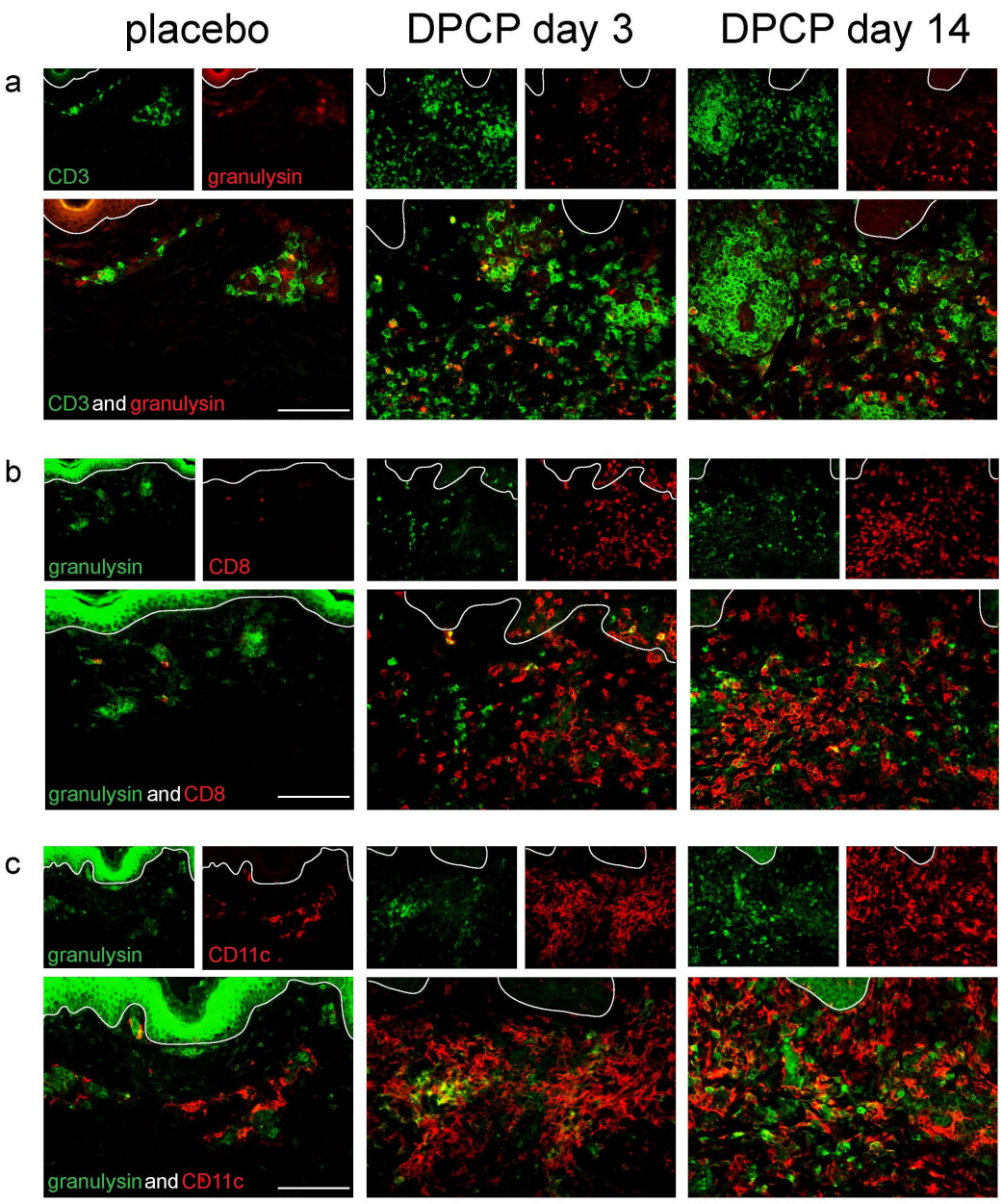

Figure 3.4: Granulysin co-localizes with CD3+ (both CD8+ and CD8-) and CD11c+ cells. Immunofluorescence staining of granulysin with (a) CD3 (green), (b) CD8 (red), and (c) CD11c (red). Left panels are placebo-treated samples, middle panels and DPCP day 3 samples, and right panels are DPCP day 14 samples. Shown is a representative subject (subject 013). Scale bar = 100 μm.

Figure 3.5: RT-PCR and histological analysis of subjects whose CD3+ or CD11c+ infiltrates increase from 3 days to 14 days post-DPCP challenge (subgroup A, n=5). (a) RT-PCR analysis for IFNγ (left panel), IL-2 (middle panel), and IL-2RA (right panel). Shown are normalized expression values for each subject individually to highlight that almost all samples have decreased expression of these genes at day 14 compared to day 3. (b-f) H&E (b) and immunohistochemical analysis of samples for (c) CD3, (d) CD11c, (e) DC-LAMP, and (f) Langerin. For all histological images, left panels show placebo reactions, middle panels show DPCP day 3 reactions, and right panels show DPCP day 14 reactions. Shown is a representative subject (subject 013). For immunohistochemical stains, line graphs indicate subgroup-wide average cell counts for placebo, DPCP day 3, DPCP day 14, and DPCP late samples. Asterisks indicate $p<0.05$ when compared to placebo. Scale bar = 100 μm.

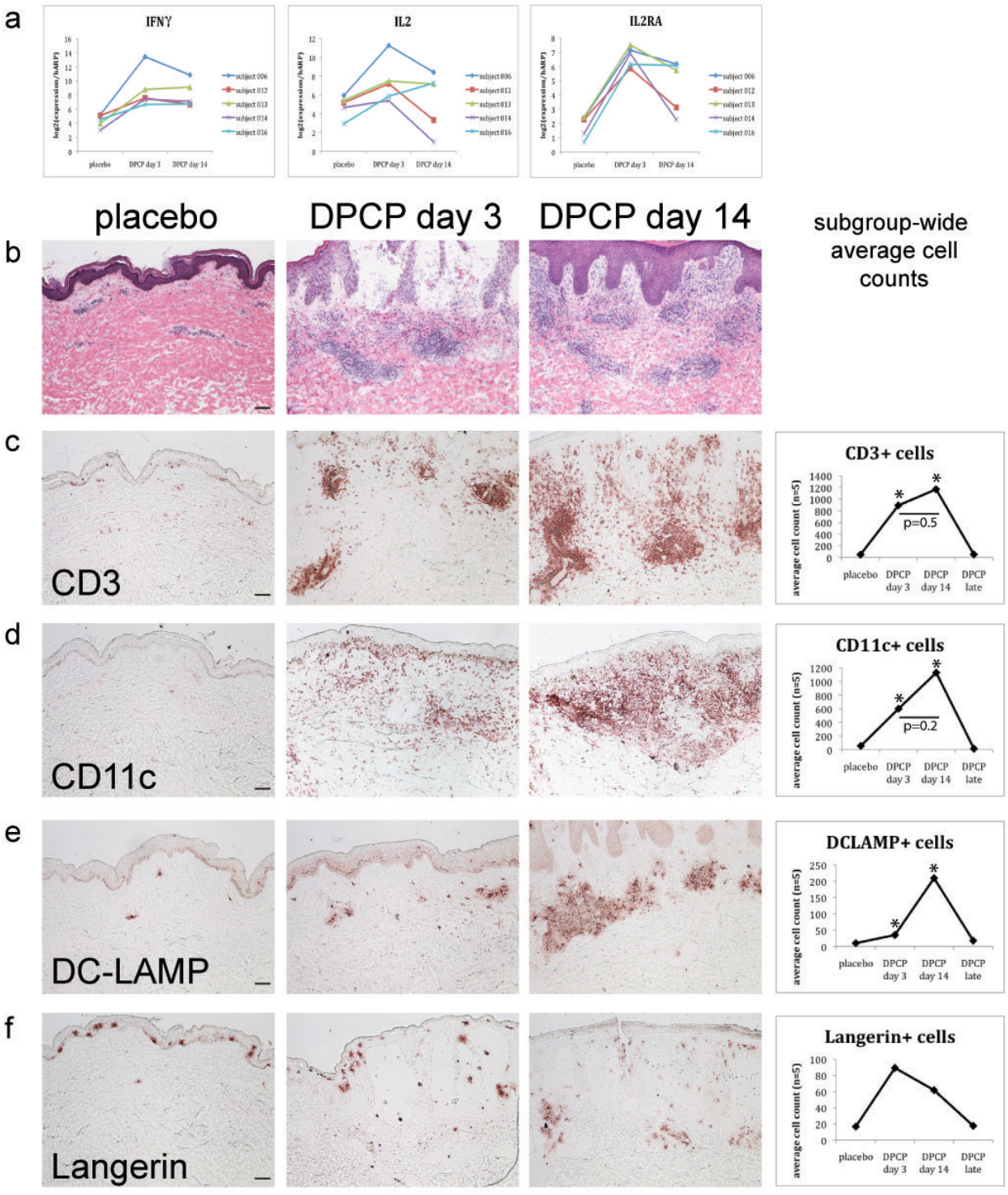
a
IFNγ
IL2
IL2RA
log2(expression/hARP)
placebo
DPCP day 3
DPCP day 14
subject 006
subject 012
subject 013
subject 014
subject 016
placebo
DPCP day 3
DPCP day 14
subgroup-wide average cell counts
b
c
CD3
CD3+ cells
average cell count (n=5)
p=0.5
placebo
DPCP day 3
DPCP day 14
DPCP late
d
CD11c
CD11c+ cells
p=0.2
e
DC-LAMP
DCLAMP+ cells
f
Langerin
Langerin+ cells

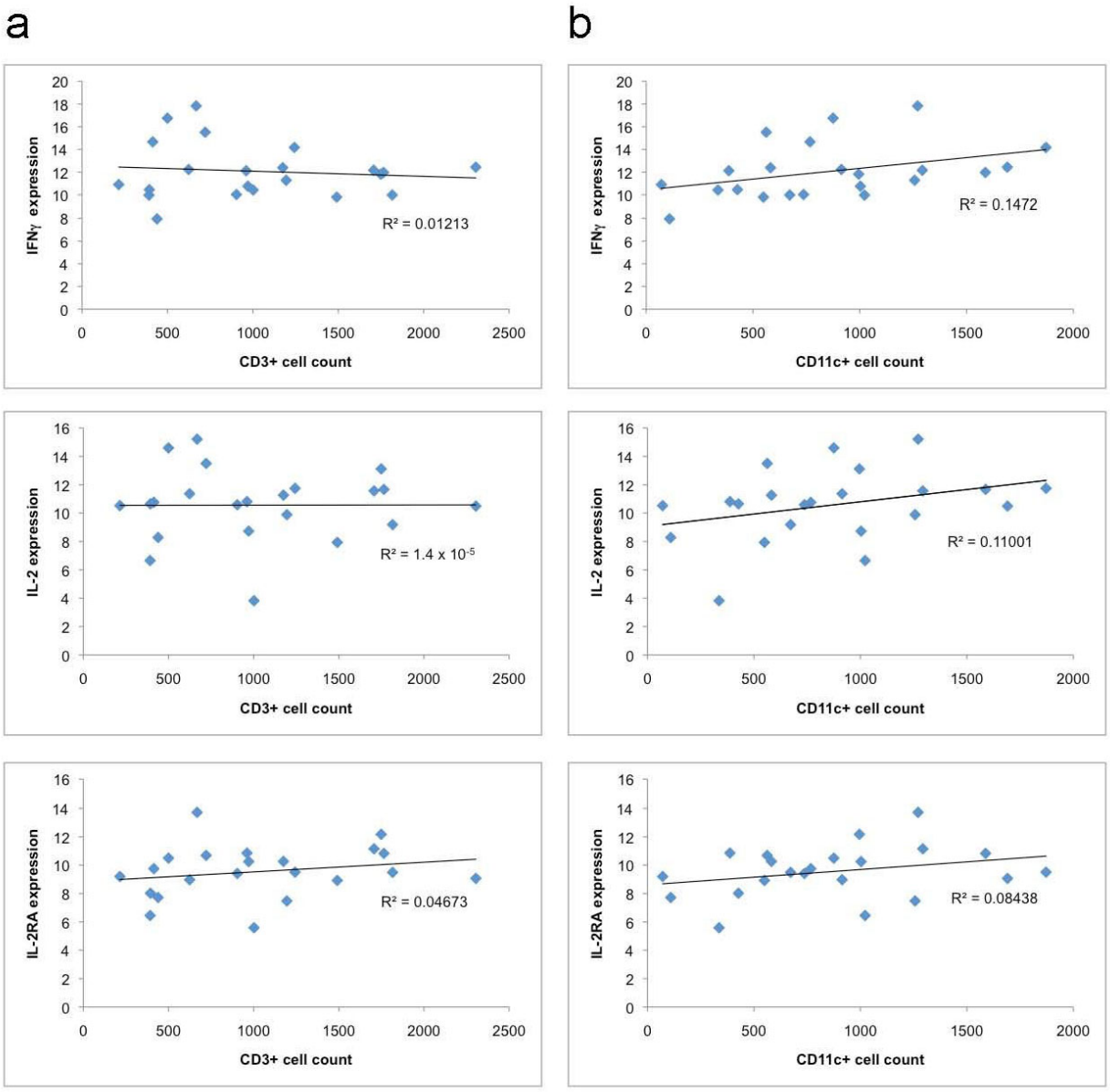

Figure 3.6: Correlations of immunohistochemistry cell counts with immune activation markers by RT-PCR. Shown are scatter plots of (a) CD3+ and (b) CD11c+ cell counts with normalized gene expression measures of IFNγ (top), IL-2 (middle), and IL-2RA (bottom). Only DPCP day 3 and day 14 samples are plotted. *p*-values for all correlations were >0.27 so none reached statistical significance.

Figure 3.7: RT-PCR and histological analysis of subjects whose CD3+ or CD11c+ infiltrates decrease from 3 days to 14 days post-DPCP challenge (subgroup B, n=6). (a) RT-PCR analysis for IFNγ (left panel), IL-2 (middle panel), and IL-2RA (right panel). Shown are normalized expression values for each subject individually to highlight that almost all samples have decreased expression of these genes at day 14 compared to day 3. (b-f) H&E (b) and immunohistochemical analysis of samples for (c) CD3, (d) CD11c, (e) DC-LAMP, and (f) Langerin. For all histological images, left panels show placebo reactions, middle panels show DPCP day 3 reactions, and right panels show DPCP day 14 reactions. Shown is a representative subject (subject 015). For immunohistochemical stains, line graphs indicate subgroup-wide average cell counts for placebo, DPCP day 3, DPCP day 14, and DPCP late samples. Asterisks indicate $p<0.05$ when compared to placebo. Scale bar = 100 μm.

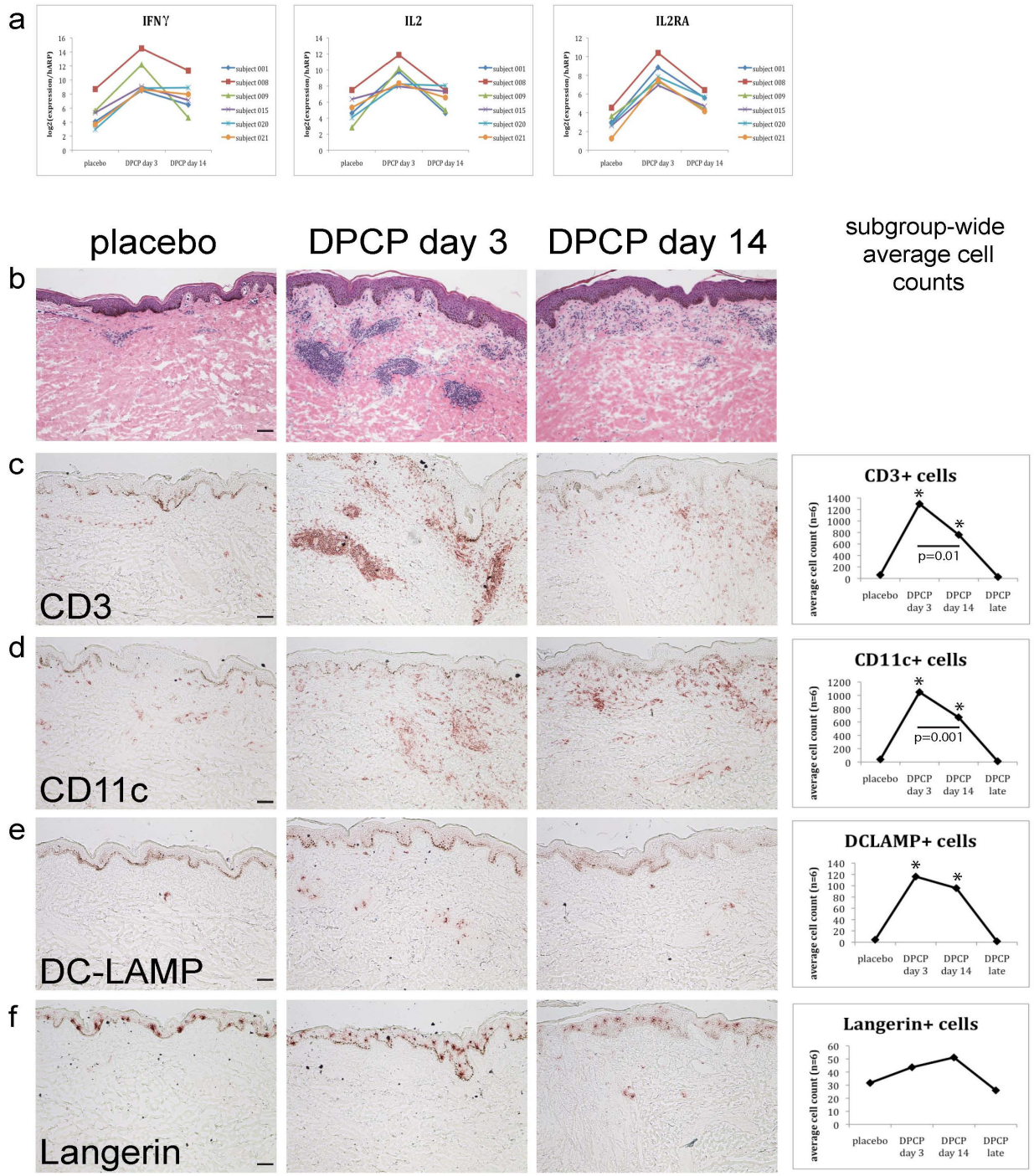
a
IFNγ
IL2
IL2RA
log2(expression/hARP)
subject 001
subject 008
subject 009
subject 015
subject 020
subject 021
placebo
DPCP day 3
DPCP day 14
placebo
DPCP day 3
DPCP day 14
subgroup-wide average cell counts
b
c
CD3
CD3+ cells
p=0.01
d
CD11c
CD11c+ cells
p=0.001
e
DC-LAMP
DCLAMP+ cells
f
Langerin
Langerin+ cells
average cell count (n=6)
placebo
DPCP day 3
DPCP day 14
DPCP late

and were significantly reduced at day 14 (p = 0.01 and 0.001, respectively). As in subgroup A, expression of inflammatory cytokines and activation molecules was decreased in resolution biopsies.

Subjects whose infiltrates decrease from day 3 to day 14 have higher levels of negative regulatory cells and molecules at day 3

We performed immunofluorescence for Foxp3 with CD3 to more specifically identify regulatory T cells, which were then quantified as Foxp3+CD3+ cells. On average, subjects in subgroup B had more Tregs than those in subgroup A at day 3 (21.25 versus 9) (**Figure 3.8a and b)**. We also performed RT-PCR for several known downregulatory molecules. For all molecules tested (IL-10, lymphocyte activation gene 3 (LAG3), programmed cell death 1 (PD1), programmed cell death ligand (PDL) 1, PDL2, indoleamine 2,3-dioxygenase (IDO1), and CTLA4), mRNA levels were higher at day 3 in subgroup B than subgroup A. Also, there were non-significant but consistent trends for subjects in subgroup B to have higher levels of these molecules even in placebo-treated skin, suggesting baseline immunological differences between subjects in the two subgroups (**Figure 3.8c-i**). On a more global level, when looking at a comprehensive list of negative regulator genes (**Table 3.4** has "negative regulator" list, curated through Gene Ontology term 0002683 "negative regulation of immune system process" and literature review, and expression values for DPCP day 3, as well as psoriasis to be discussed in the next section), subjects in subgroup B had higher expression of

Figure 3.8: Negative regulatory immune cells and molecules are increased in DPCP day 3 reactions of subgroup B compared to subgroup A. (a, b) Foxp3 (red)-CD3 (green) immunfluorescence for (a) a representative subgroup A member (subject 012) and (b) a representative subgroup B member (subject 021). Left panels are DPCP day 3 samples and right panels are DPCP day 14 samples. Regulatory T cells were quantified as double-positive for Foxp3 and CD3. Subject 012 had 4 double-positive cells at day 3 (subgroup-wide average of 9) and 24 at day 14 (subgroup wide average of 20.33) while subject 021 had 37 at day 3 (subgroup-wide average of 21.25) and 19 at day 14 (subgroup-wide average of 12). (c-i) RT-PCR analysis for (c) IL-10, (d) CTLA4, (e) PD1, (f) PDL1, (g) PDL2, (h), IDO1, and (i) LAG3. Shown are average normalized expression values of placebo day 3, placebo day 14, DPCP day 3, and DPCP day 14 skin for both subgroups (n=5 for subgroup A (blue bars), n=6 for subgroup B (green bars)). *p*-values are shown to compare subgroup A with subgroup B for each sample type. Scale bar = 100 μm.

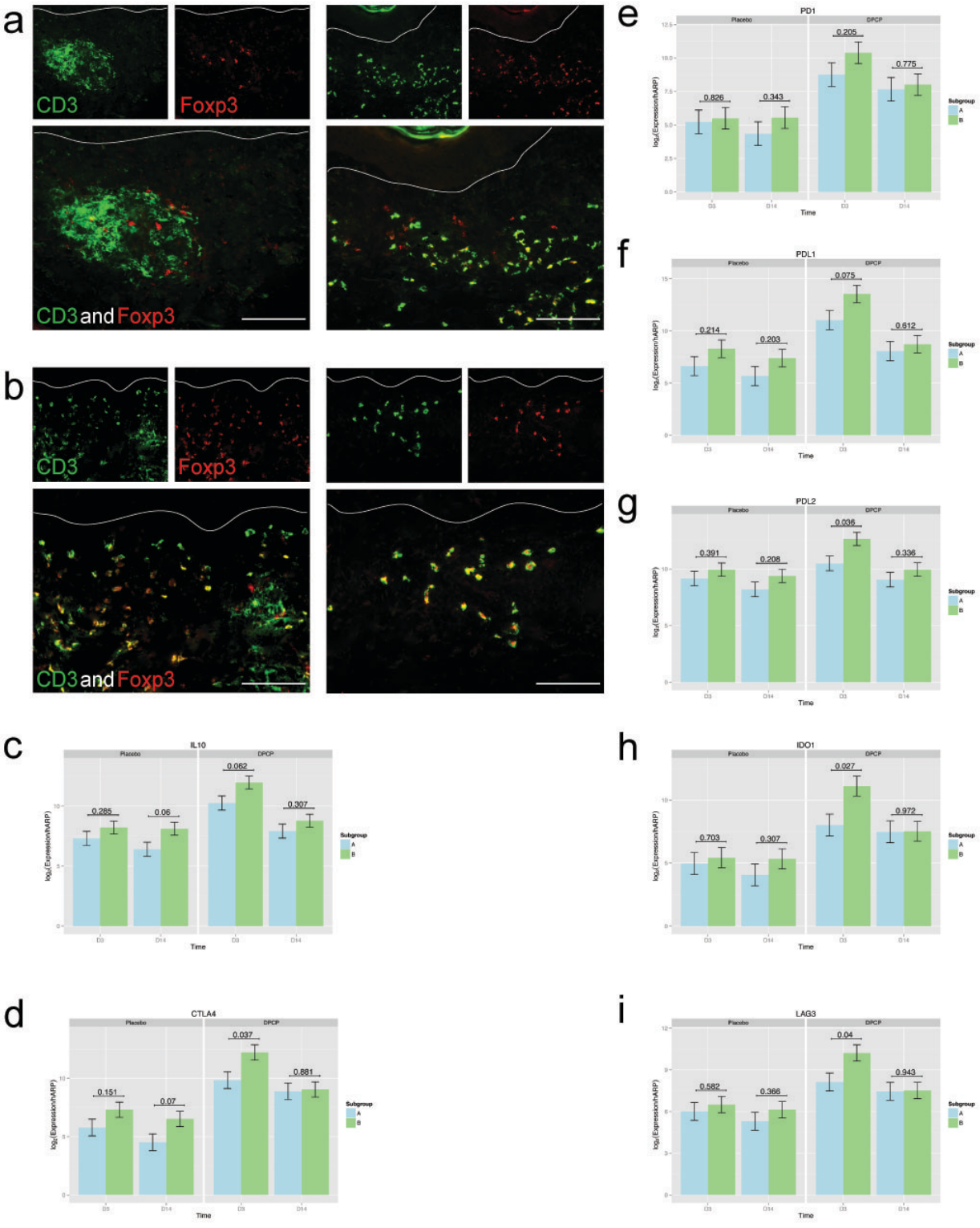
a
CD3
Foxp3
CD3 and Foxp3
b
CD3
Foxp3
CD3 and Foxp3
c
IL10
Placebo
DPCP
0.285
0.06
0.062
0.307
Time
d
CTLA4
Placebo
DPCP
0.151
0.07
0.037
0.881
Time
e
PD1
Placebo
DPCP
0.826
0.343
0.205
0.775
Time
f
PDL1
Placebo
DPCP
0.214
0.203
0.075
0.612
Time
g
PDL2
Placebo
DPCP
0.391
0.208
0.036
0.336
Time
h
IDO1
Placebo
DPCP
0.703
0.307
0.027
0.972
Time
i
LAG3
Placebo
DPCP
0.582
0.366
0.04
0.943
Time

Table 3.4: Expression of negative regulator genes in DPCP day 3 vs. placebo and psoriasis lesional vs. non-lesional skin samples

			DPCP day 3			psoriasis		
Probe	Symbol	Description	FCH	p	FDR	FCH	p	FDR
207526_s_at	IL1RL1	interleukin 1 receptor-like 1	42.8	5.3E-11	2.1E-09	1.1	3.6E-03	1.3E-02
227458_at	CD274	CD274 molecule	34.6	1.9E-12	1.3E-10	23.7	0.0E+00	0.0E+00
236341_at	CTLA4	cytotoxic T-lymphocyte-associated protein 4	21.6	3.7E-11	1.5E-09	3.7	6.0E-02	1.4E-01
207238_s_at	PTPRC	protein tyrosine phosphatase, receptor type, C	18.0	1.6E-12	1.2E-10	2.6	0.0E+00	0.0E+00
206341_at	IL2RA	interleukin 2 receptor, alpha	17.9	4.7E-14	6.3E-12	1.3	1.6E-01	2.9E-01
210146_x_at	LILRB2	leukocyte immunoglobulin-like receptor, subfamily B (with TM and ITIM domains), member 2	12.5	3.6E-08	5.4E-07	2.9	0.0E+00	0.0E+00
222062_at	IL27RA	interleukin 27 receptor, alpha	12.3	9.9E-13	7.6E-11	1.3	1.7E-03	6.7E-03
217192_s_at	PRDM1	PR domain containing 1, with ZNF domain	11.1	8.7E-12	4.6E-10	3.0	0.0E+00	0.0E+00
215719_x_at	FAS	Fas (TNF receptor superfamily, member 6)	9.3	7.8E-07	7.6E-06	1.1	2.8E-02	7.6E-02
205926_at	IL27RA	interleukin 27 receptor, alpha	8.3	5.9E-11	2.3E-09	1.2	1.3E-01	2.4E-01
204780_s_at	FAS	Fas (TNF receptor superfamily, member 6)	8.0	2.6E-05	1.6E-04	1.1	1.3E-01	2.4E-01
242743_at	IL4R	interleukin 4 receptor	8.0	7.6E-13	6.2E-11	1.1	6.0E-02	1.4E-01
242809_at	IL1RL1	interleukin 1 receptor-like 1	6.6	1.5E-06	1.3E-05	1.0	7.6E-01	8.3E-01
207697_x_at	LILRB2	leukocyte immunoglobulin-like receptor, subfamily B (with TM and ITIM domains), member 2	6.6	1.2E-13	1.4E-11	1.5	0.0E+00	0.0E+00
212588_at	PTPRC	protein tyrosine phosphatase, receptor type, C	6.5	2.8E-08	4.3E-07	2.4	0.0E+00	0.0E+00
216252_x_at	FAS	Fas (TNF receptor superfamily, member 6)	6.3	9.4E-08	1.2E-06	1.1	7.0E-04	2.9E-03
230052_s_at	NFKBID	nuclear factor of kappa light polypeptide gene enhancer in B-cells inhibitor, delta	6.2	1.0E-07	1.3E-06	1.4	1.4E-02	4.3E-02
211336_x_at	LILRB1	leukocyte immunoglobulin-like receptor, subfamily B (with TM and ITIM domains), member 1	5.2	4.8E-16	1.5E-13	1.3	2.3E-03	8.7E-03
212587_s_at	PTPRC	protein tyrosine phosphatase, receptor type,	5.1	6.5E-13	5.5E-11	1.8	2.2E-03	8.3E-03

		C						
		leukocyte immunoglobulin-like receptor, subfamily B (with TM and ITIM domains),						
207104_x_at	LILRB1	member 1	5.1	3.0E-17	1.6E-14	1.2	0.0E+00	0.0E+00
211269_s_at	IL2RA	interleukin 2 receptor, alpha	5.1	2.8E-08	4.4E-07	1.1	1.8E-01	3.1E-01
204781_s_at	FAS	Fas (TNF receptor superfamily, member 6)	4.7	3.4E-06	2.7E-05	1.2	3.6E-02	9.3E-02
		protein tyrosine phosphatase, receptor type,						
1552480_s_at	PTPRC	C	4.5	9.0E-08	1.2E-06	1.0	3.3E-01	4.7E-01
203233_at	IL4R	interleukin 4 receptor	4.4	1.2E-10	4.0E-09	3.9	0.0E+00	0.0E+00
		protein tyrosine phosphatase, non-receptor						
206060_s_at	PTPN22	type 22 (lymphoid)	4.3	7.6E-06	5.5E-05	2.3	1.0E-04	4.0E-04
223834_at	CD274	CD274 molecule	3.8	5.7E-09	1.1E-07	1.5	3.6E-03	1.3E-02
235458_at	HAVCR2	hepatitis A virus cellular receptor 2	3.8	6.6E-07	6.6E-06	1.5	1.4E-03	5.5E-03
		cytotoxic T-lymphocyte-associated protein						
231794_at	CTLA4	4	3.4	1.6E-09	3.7E-08	1.2	6.4E-02	1.4E-01
		Cbl proto-oncogene, E3 ubiquitin protein						
227900_at	CBLB	ligase B	3.3	1.8E-04	8.3E-04	0.8	9.6E-03	3.1E-02
		ubiquitin associated and SH3 domain						
220418_at	UBASH3A	containing A	3.3	3.0E-05	1.8E-04	1.1	2.7E-02	7.3E-02
		tumor necrosis factor, alpha-induced						
202643_s_at	TNFAIP3	protein 3	3.2	1.0E-08	1.8E-07	1.2	1.9E-01	3.2E-01
		T cell immunoreceptor with Ig and ITIM						
240070_at	TIGIT	domains	3.0	2.9E-05	1.8E-04	1.3	4.2E-02	1.0E-01
201537_s_at	DUSP3	dual specificity phosphatase 3	3.0	4.8E-11	1.9E-09	1.5	0.0E+00	0.0E+00
228964_at	PRDM1	PR domain containing 1, with ZNF domain	2.9	3.4E-06	2.7E-05	3.0	0.0E+00	0.0E+00
201538_s_at	DUSP3	dual specificity phosphatase 3	2.9	3.6E-10	1.1E-08	1.3	2.5E-01	3.8E-01
203236_s_at	LGALS9	lectin, galactoside-binding, soluble, 9	2.7	3.5E-07	3.8E-06	1.6	0.0E+00	0.0E+00
224399_at	PDCD1LG2	programmed cell death 1 ligand 2	2.7	1.3E-07	1.7E-06	1.0	1.6E-01	2.8E-01
		nuclear factor of kappa light polypeptide						
241889_at	NFKBID	gene enhancer in B-cells inhibitor, delta	2.6	6.5E-06	4.8E-05	1.0	8.8E-02	1.9E-01
223506_at	ZC3H8	zinc finger CCCH-type containing 8	2.6	5.6E-04	2.2E-03	1.6	0.0E+00	0.0E+00
209744_x_at	ITCH	itchy E3 ubiquitin protein ligase	2.6	3.8E-07	4.1E-06	2.8	1.4E-02	4.1E-02
		phosphoprotein associated with						
225622_at	PAG1	glycosphingolipid microdomains 1	2.6	3.4E-05	2.0E-04	1.9	0.0E+00	0.0E+00
217094_s_at	ITCH	itchy E3 ubiquitin protein ligase	2.4	1.1E-05	7.8E-05	2.4	6.9E-02	1.5E-01
224211_at	FOXP3	forkhead box P3	2.4	1.2E-05	7.9E-05	1.0	0.0E+00	1.0E-04
243196_s_at	TRAFD1	TRAF-type zinc finger domain containing 1	2.3	4.0E-05	2.3E-04	0.9	4.8E-01	6.1E-01
228996_at	RC3H1	ring finger and CCCH-type domains 1	2.3	5.5E-05	3.0E-04	1.8	2.5E-01	3.9E-01
		DEXH (Asp-Glu-X-His) box polypeptide						
219364_at	DHX58	58	2.3	5.3E-07	5.4E-06	1.3	0.0E+00	0.0E+00

202763_at	CASP3	caspase 3, apoptosis-related cysteine peptidase	2.2	1.8E-05	1.1E-04	1.1	1.1E-01	2.2E-01
236539_at	PTPN22	protein tyrosine phosphatase, non-receptor type 22 (lymphoid)	2.2	6.9E-05	3.7E-04	2.0	0.0E+00	0.0E+00
202644_s_at	TNFAIP3	tumor necrosis factor, alpha-induced protein 3	2.2	1.4E-06	1.3E-05	1.1	2.8E-01	4.2E-01
205298_s_at	BTN2A2	butyrophilin, subfamily 2, member A2	2.2	3.7E-04	1.6E-03	1.1	1.9E-01	3.2E-01
217513_at	MILR1	mast cell immunoglobulin-like receptor 1	2.1	6.0E-06	4.4E-05	1.2	5.9E-02	1.4E-01
205299_s_at	BTN2A2	butyrophilin, subfamily 2, member A2	2.0	3.9E-05	2.2E-04	1.1	1.1E-01	2.2E-01
242497_at	TRAFD1	TRAF-type zinc finger domain containing 1	1.8	4.1E-04	1.7E-03	1.0	6.3E-01	7.4E-01
234066_at	IL1RL1	interleukin 1 receptor-like 1	1.8	7.5E-03	2.0E-02	1.0	3.6E-01	5.1E-01
235668_at	PRDM1	PR domain containing 1, with ZNF domain	1.8	3.0E-06	2.4E-05	2.2	0.0E+00	0.0E+00
1555628_a_at	HAVCR2	hepatitis A virus cellular receptor 2	1.8	6.7E-04	2.6E-03	1.0	4.3E-01	5.6E-01
209682_at	CBLB	Cbl proto-oncogene, E3 ubiquitin protein ligase B	1.8	6.1E-05	3.3E-04	0.8	0.0E+00	0.0E+00
209354_at	TNFRSF14	tumor necrosis factor receptor superfamily, member 14	1.8	3.2E-06	2.6E-05	1.0	7.1E-01	8.0E-01
227354_at	PAG1	phosphoprotein associated with glycosphingolipid microdomains 1	1.7	7.0E-02	1.3E-01	1.3	3.7E-02	9.4E-02
209743_s_at	ITCH	itchy E3 ubiquitin protein ligase	1.7	4.4E-03	1.3E-02	1.2	0.0E+00	0.0E+00
35254_at	TRAFD1	TRAF-type zinc finger domain containing 1	1.7	1.7E-05	1.1E-04	0.9	2.8E-01	4.1E-01
1555629_at	HAVCR2	hepatitis A virus cellular receptor 2	1.7	2.4E-04	1.1E-03	1.0	7.6E-01	8.4E-01
202837_at	TRAFD1	TRAF-type zinc finger domain containing 1	1.6	5.5E-05	3.0E-04	1.0	9.1E-01	9.4E-01
235057_at	ITCH	itchy E3 ubiquitin protein ligase	1.6	2.7E-02	6.0E-02	0.9	2.0E-01	3.3E-01
1554285_at	HAVCR2	hepatitis A virus cellular receptor 2	1.6	5.4E-04	2.2E-03	1.0	1.5E-01	2.7E-01
225626_at	PAG1	phosphoprotein associated with glycosphingolipid microdomains 1	1.5	2.3E-02	5.2E-02	1.3	6.0E-04	2.5E-03
201536_at	DUSP3	dual specificity phosphatase 3	1.5	3.2E-04	1.4E-03	0.8	0.0E+00	1.0E-04
1553042_a_at	NFKBID	nuclear factor of kappa light polypeptide gene enhancer in B-cells inhibitor, delta	1.5	3.0E-03	9.4E-03	1.1	2.6E-02	7.1E-02
220049_s_at	PDCD1LG2	programmed cell death 1 ligand 2	1.4	5.4E-03	1.5E-02	1.0	4.3E-01	5.7E-01
221331_x_at	CTLA4	cytotoxic T-lymphocyte-associated protein 4	1.3	4.8E-04	2.0E-03	1.1	4.7E-02	1.1E-01
234362_s_at	CTLA4	cytotoxic T-lymphocyte-associated protein 4	1.3	4.6E-03	1.3E-02	1.1	1.2E-01	2.4E-01
208010_s_at	PTPN22	protein tyrosine phosphatase, non-receptor type 22 (lymphoid)	1.3	2.4E-03	7.8E-03	1.1	4.0E-04	1.7E-03
234895_at	CTLA4	cytotoxic T-lymphocyte-associated protein 4	1.1	4.9E-02	9.7E-02	1.0	2.0E-04	8.0E-04
225893_at	RC3H1	ring finger and CCCH-type domains 1	1.1	7.0E-01	7.8E-01	1.0	3.6E-01	5.0E-01

224859_at	CD276	CD276 molecule	0.9	4.4E-01	5.6E-01	0.9	2.0E-04	9.0E-04
236235_at	ITCH	itchy E3 ubiquitin protein ligase	0.8	2.6E-01	3.7E-01	0.7	3.6E-03	1.3E-02
239101_at	ITCH	itchy E3 ubiquitin protein ligase	0.7	1.5E-02	3.6E-02	0.7	0.0E+00	0.0E+00
1559583_at	CD276	CD276 molecule	0.6	8.5E-02	1.5E-01	1.0	3.2E-01	4.6E-01
219768_at	VTCN1	V-set domain containing T cell activation inhibitor 1	0.3	8.1E-05	4.2E-04	0.6	2.2E-03	8.6E-03
204472_at	GEM	GTP binding protein overexpressed in skeletal muscle	0.3	1.1E-05	7.6E-05	1.0	3.0E-01	4.4E-01

FCH, fold change; FDR, false discovery rate.

many of these molecules at day 3 (**Figure 3.9**). These data may help explain why subgroup B had decreased cellular infiltrates at day 14, and suggest that different individuals resolve their inflammatory responses to DPCP with different kinetics (inflammation resolution was faster in subgroup B, based on ultrasound measures at days 7 and 14, **Figure 3.10**).

Psoriasis is characterized by deficient negative immune regulation compared to transient DTH reactions induced by DPCP

Since DTH reactions naturally resolve, we sought to compare our DPCP biopsies to those taken from patients with psoriasis vulgaris (Tian et al. 2012), a chronic T cell-mediated inflammatory disease that does not resolve and which, in many ways, represents amplifications of background immune circuits that exist in normal human skin (Lowes et al. 2014). To globally assess the balance of positive vs. negative immune regulators in both DPCP reactions and psoriasis using our microarray data, we developed a comprehensive gene list for positive regulatory or inflammatory genes and used our previously described negative regulatory or immunosuppressive gene list (**Table 3.4** has the "negative regulator" list and fold change values for DPCP day 3 and psoriasis transcriptomes, "positive regulator" list is derived from Gene Ontology term 0002684 "positive regulation of immune system process" but with genes removed that are in common with Gene Ontology term 0002683 "negative regulation of immune system process"). Our microarray data showed increased fold changes of many negative regulators in DPCP day 3 biopsies vs placebo-treated skin (DPCP

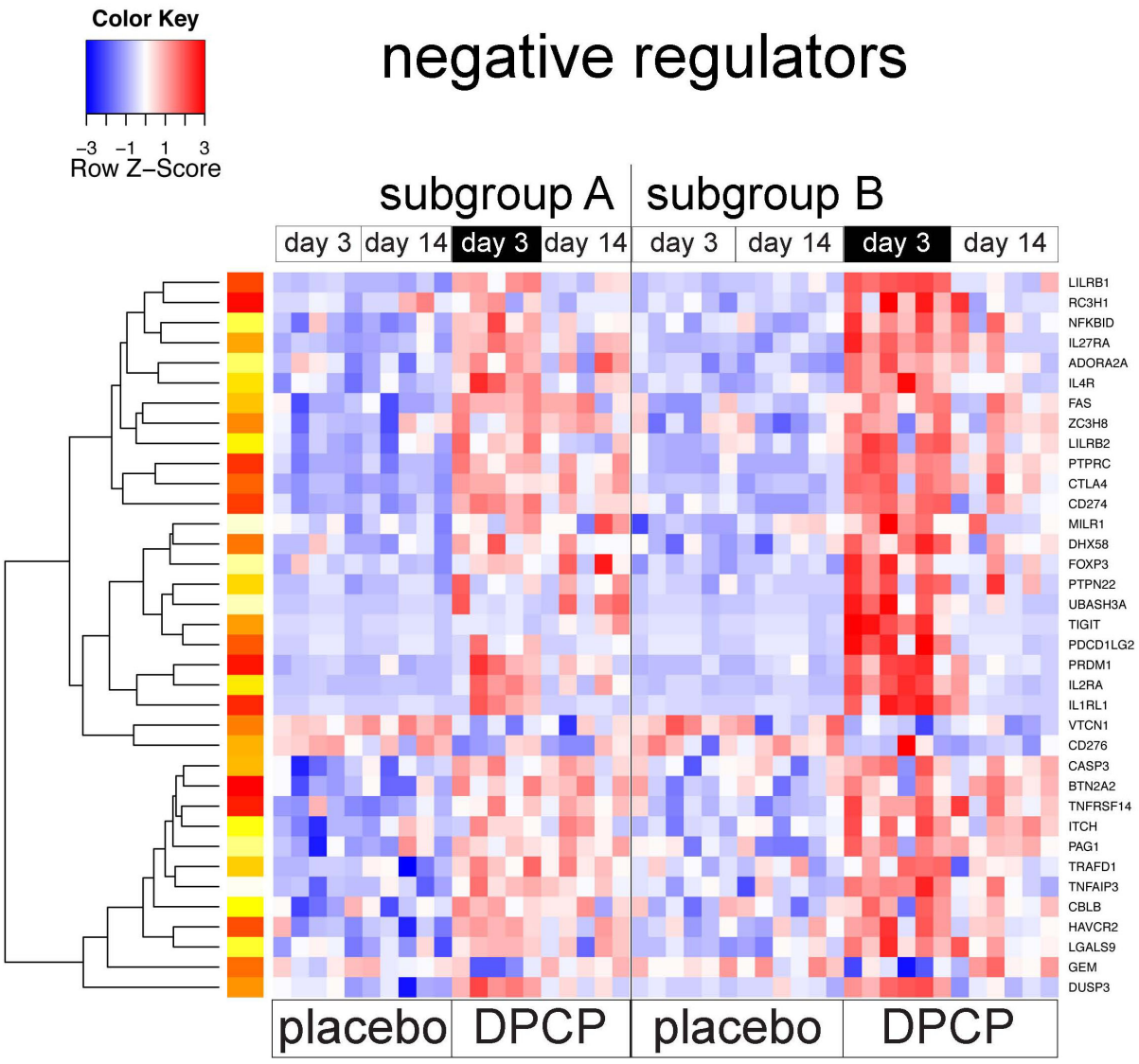

Figure 3.9: Subjects in subgroup B globally have more negative regulatory genes at day 3 than subjects in subgroup A. Heat map of negative regulatory genes for all DPCP samples. Each column represents one sample arranged first by subgroup then by sample type with there being 5 subjects in subgroup A and 6 in subgroup B. DPCP day 3 samples are highlighted as underneath the black bars.

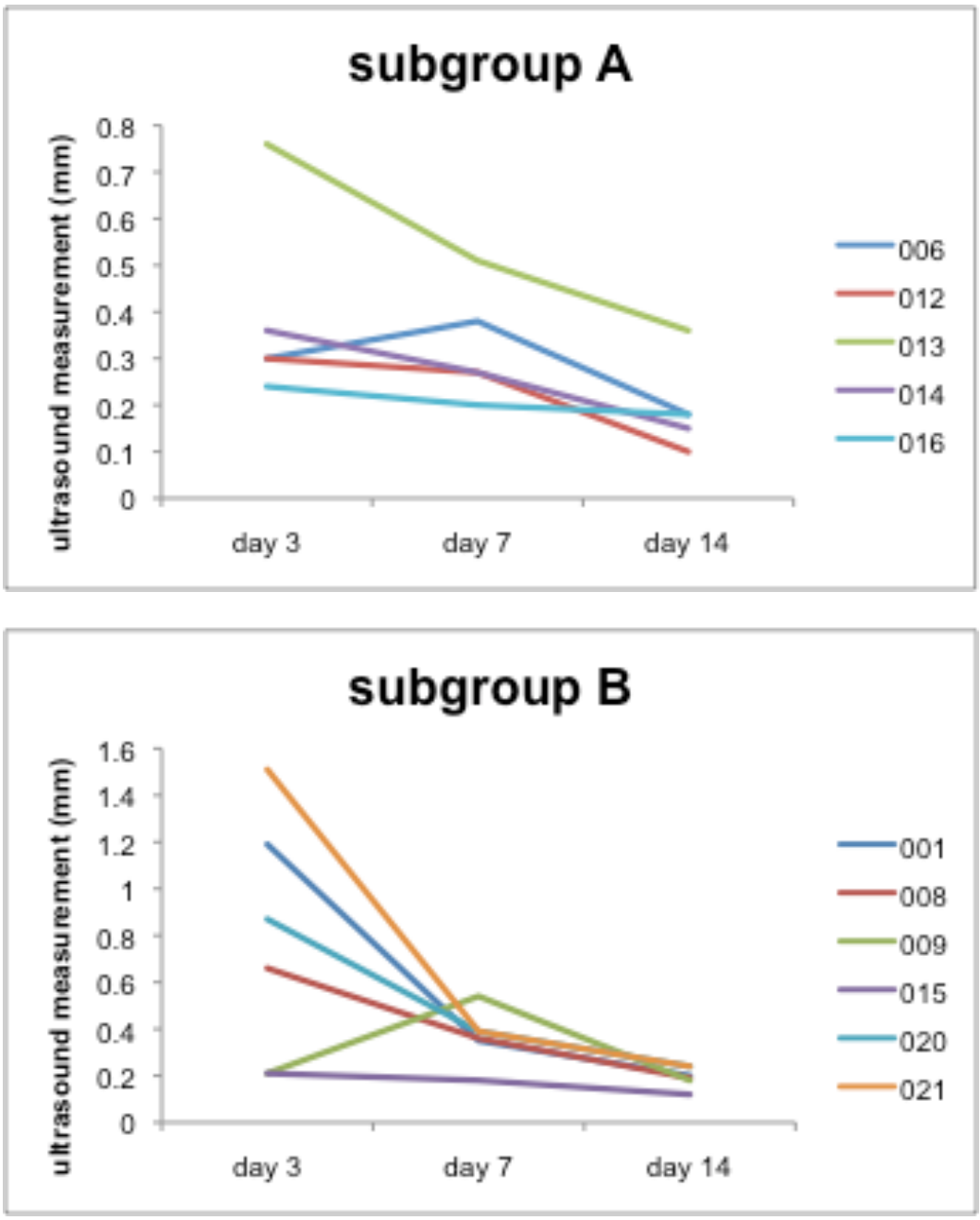

Figure 3.10: Subjects in subgroup B show resolution of clinical inflammation more quickly than subjects in subgroup A. Plots of ultrasound measurements of extents of inflammatory reactions as reflected by dermal thickness (see **Figure 3.1**) versus time for subjects in subgroup A (top) and subjects in subgroup B (bottom). Each subject is shown as an individual line.

day 3 transcriptome) compared to psoriasis lesional vs non-lesional skin (psoriasis transcriptome). For instance, CTLA4 expression was significantly increased 21.6-fold in the DPCP day 3 transcriptome, but non-significantly increased 3.7-fold in the psoriasis transcriptome. Venn diagrams show that the psoriasis transcriptome only has seven genes from the negative regulator list, while the DPCP day 3 transcriptome has 52 (**Figure 3.11a**). Although the DPCP day 3 transcriptome also has more genes from the positive regulator list than psoriasis, the odds ratio for the positive regulator list was not significantly different between these two transcriptomes. The odds ratio for the negative regulator list, however, was significantly different (**Figure 3.11b**). The altered balance between positive vs. negative regulatory transcripts in psoriasis compared to DPCP reactions can also be seen in **Figure 3.11c** which shows that DPCP transcriptomes at all time points (days 3, 14, and 120) have higher ratios of negative to positive regulator genes than the psoriasis transcriptome in terms of expression levels for each gene set as a whole (as opposed to number of genes as indicated in the Venn diagrams). This is despite the fact that the DPCP day 3 transcriptome has comparable expression levels of the MAD3 psoriasis transcriptome genes to actual psoriasis samples, and therefore highlights the negative regulator expression that is unique to DPCP reactions.

To confirm some of our microarray findings, we performed qRT-PCR and found that psoriasis lesional skin biopsies have significantly lower expression of many

Figure 3.11: Psoriasis lesional skin has an altered global balance of positive vs. negative regulatory gene transcripts compared to DPCP reactions. (a) Venn diagrams showing overlap of MAD3 psoriasis transcriptome (left) and DPCP day 3 transcriptome (right) with both positive regulatory (Pos) and negative regulatory (Neg) gene lists (common gene lists applied to both transcriptomes). The percentages of the MAD3 and DPCP day 3 transcriptomes comprised of the positive regulatory gene list are 5.7% and 7.3%, respectively. On the other hand, the percentages comprised of the negative regulatory gene list are 0.7% and 1.5%, respectively. (b) Odds ratios (OR) of negative regulatory (red bars) and positive regulatory (blue bars) gene lists in DPCP day 3 and psoriasis transcriptomes. (c) Black bars represent negative regulator genes, gray bars represent positive regulator genes, and white bars represent all MAD3 psoriasis transcriptome genes. The y-axis shows $\log_2$ (fold change) of all genes in the given gene set. DPCP day 3 and MAD3 samples have comparable MAD3 transcriptome expression levels but there is a substantial difference between all DPCP time points (days 3, 14, and 120 or "late") and MAD3 samples in terms of the relative levels of negative and positive regulator gene list expression. This is quantified as the "ratio of negative to positive regulator genes."

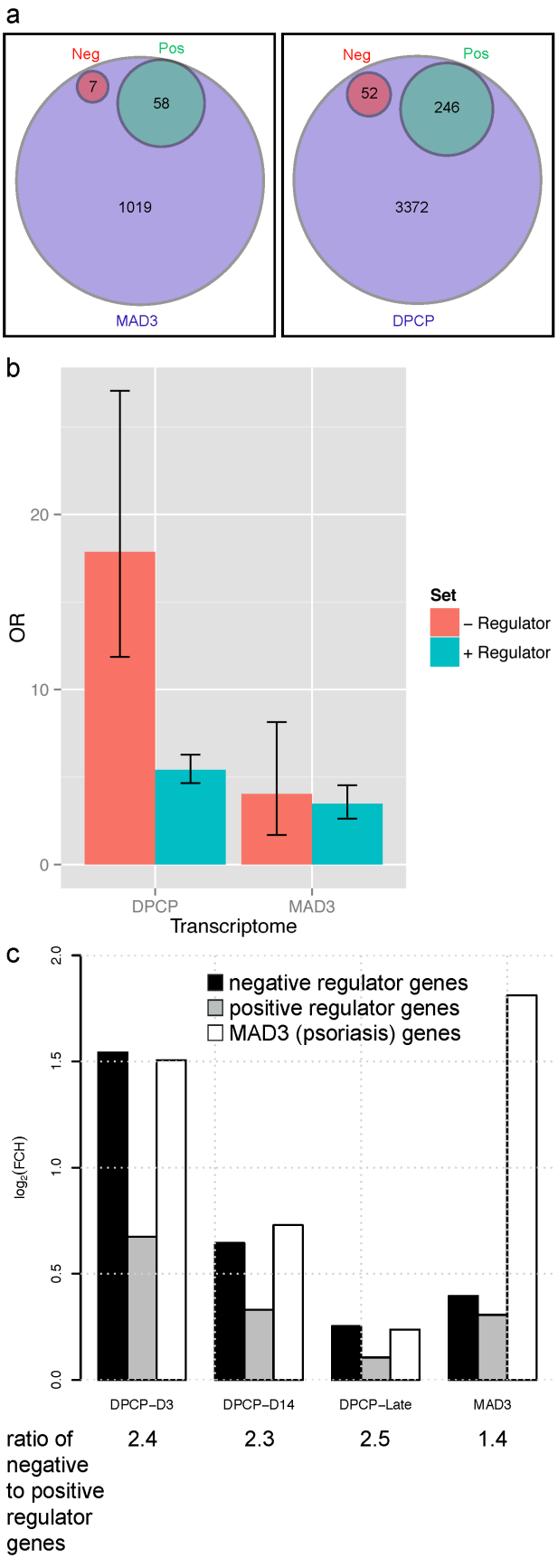
a
Neg
Pos
7
58
1019
MAD3
Neg
Pos
52
246
3372
DPCP
b
OR
20
10
0
DPCP
MAD3
Transcriptome
Set
– Regulator
+ Regulator
c
negative regulator genes
positive regulator genes
MAD3 (psoriasis) genes
log2(FCH)
2.0
1.5
1.0
0.5
0.0
DPCP–D3
DPCP–D14
DPCP–Late
MAD3
ratio of negative to positive regulator genes
2.4
2.3
2.5
1.4

negative immune regulators compared to peak DPCP biopsies. These regulators include LAG3, CTLA4, IDO1, PD1, PDL1, PDL2, and IL-10 (**Figure 3.12a**). We confirmed the decreased expression of these and FAS (which by gene expression had 9.3- and 1.1-fold changes in the DPCP day 3 and psoriasis transcriptomes, respectively) at the protein level by immunohistochemistry (**Figure 3.12b**).

Discussion

This study with DPCP provides, to our knowledge, the first detailed cellular and molecular phenotype of a DTH response at both peak and resolution stages. The strong clinical response at day 3 was accompanied by large increases in infiltrating T cells and myeloid DCs, as well as by differential regulation (>2 fold change) of 7,555 gene transcripts. The resolution phase was characterized by variable changes in infiltrating leukocytes, overall increased in subgroup A and decreased in subgroup B compared to the peak reaction. In molecular terms, the resolution phase showed decreased expression of T cell effector cytokines and molecules associated with the activation phase of immune responses, but relatively higher levels of transcripts associated with negative regulation of immune responses. Also, the resolution phase included expression of certain genes including ARG1, XCR1, and FLT3 that were not present during the peak response. ARG1 has been shown to lead to reversible blocks in T cell proliferation (Bronte *et al*., 2003), XCR1 contributes to regulatory T cell development (Lei *et al*., 2011), and FLT3 is involved in maintaining the balance

Figure 3.12: Psoriasis lesional skin has lower expression of various negative immune regulators than DPCP day 3 reactions by both qRT-PCR and immunohistochemical approaches. (a) qRT-PCR analysis for negative regulators LAG3, CTLA4, IDO1, PD1, PDL1, PDL2, and IL10. Shown are average normalized expression values for DPCP day 3 samples (n=11, purple bars) and psoriasis lesional skin (LS) samples (n=11, brown bars). All except PDL1 are $p<0.05$ by unpaired two-tailed *t*-test assuming equal variance. Error bars represent standard errors of the mean. (b) Immunohistochemistry showing increased protein expression of negative regulators in DPCP day 3 samples compared to psoriasis LS. Shown are stains with antibodies specific to the indicated targets. Scale bar = 100 μm.

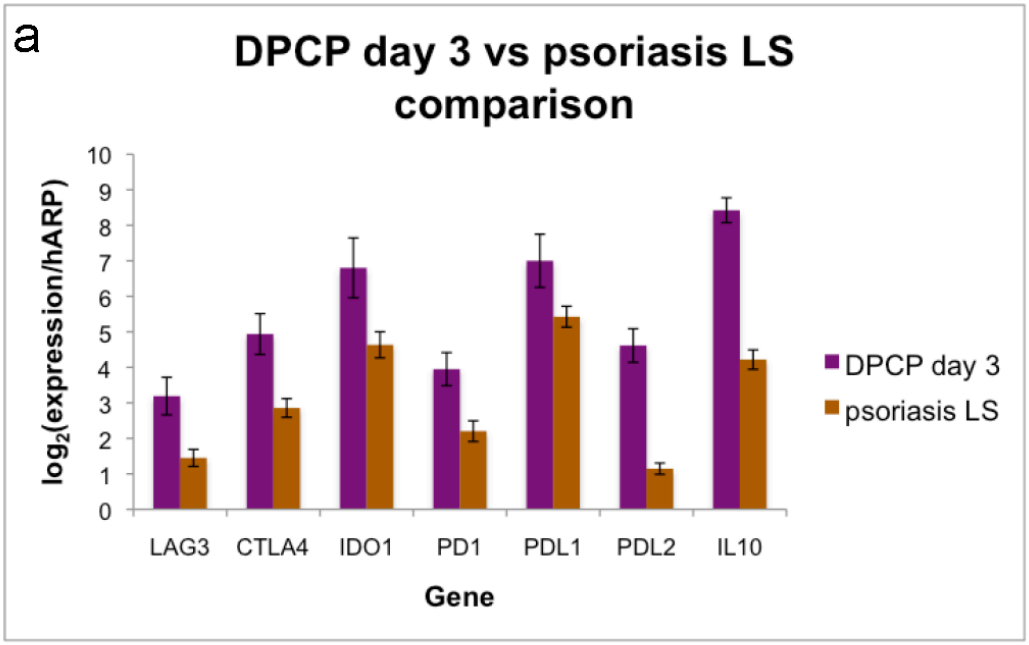
a
DPCP day 3 vs psoriasis LS comparison
log2(expression/hARP)
10
9
8
7
6
5
4
3
2
1
0
LAG3
CTLA4
IDO1
PD1
PDL1
PDL2
IL10
Gene
DPCP day 3
psoriasis LS

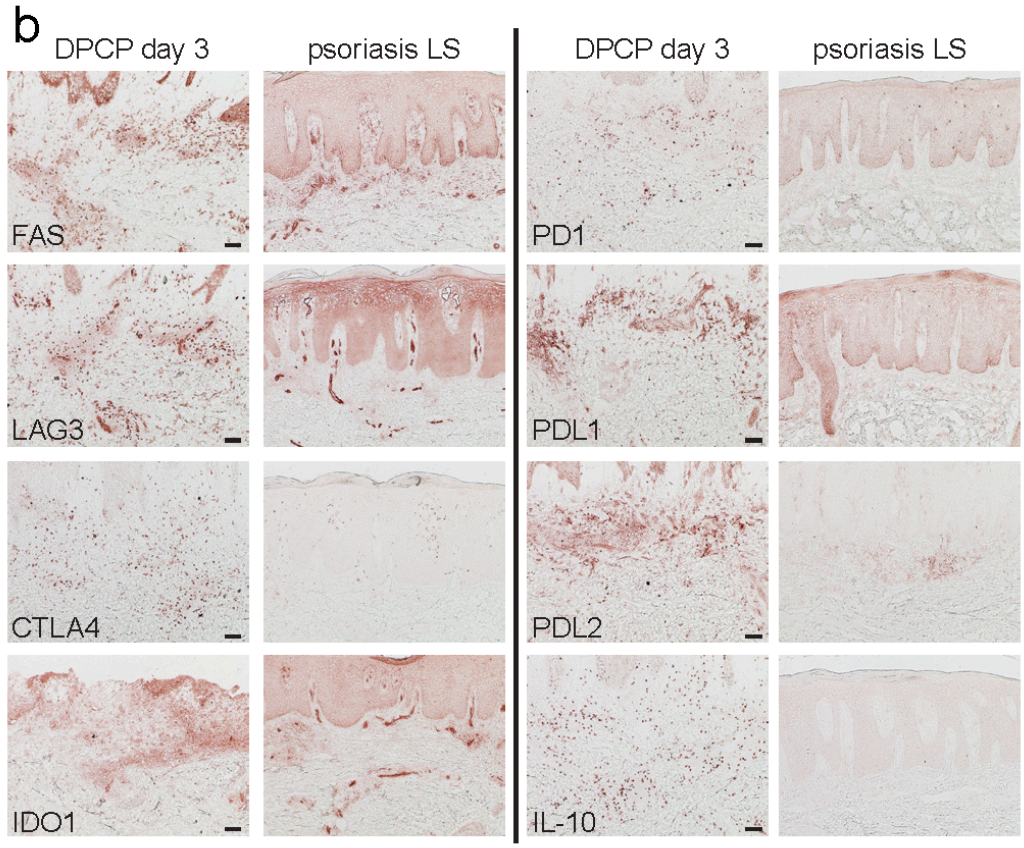
b
DPCP day 3
psoriasis LS
DPCP day 3
psoriasis LS
FAS
PD1
LAG3
PDL1
CTLA4
PDL2
IDO1
IL-10

between DC and regulatory T cell numbers (Liu and Nussenzweig, 2010). Although we chose to characterize the immune response to DPCP in normal human skin, our results identify immune mechanisms that may relate to the use of DPCP as an immune modulator in treatment of melanoma or alopecia areata.

In a recent report, 50 patients with cutaneous metastases of melanoma were treated with repeated application of DPCP. Forty-six percent of patients had complete regression of their lesions and a further 38 percent had partial responses, but corresponding study of the immune response to DPCP was not conducted (Damian *et al*., 2014). The potential of DPCP as an adjuvant to improve immunotherapy has been demonstrated in mice (Moos et al. 2012). Several immune pathways that we found to be induced by DPCP in normal skin might mediate this anti-melanoma response. First, we identified significant up-regulation of IL-24 mRNA, which is a cytokine with established anti-melanoma activity (Jiang *et al*., 1995). Since this cytokine was up-regulated only transiently (peak at day 3, but resolved at day 14), it could indicate the need for chronic/repeated application of DPCP to maintain effector cytokines for tumor responses. Furthermore, we observed strong increases in IFNγ expression and this cytokine enhances antigen presentation potential, is anti-proliferative for many cell types (Braumüller *et al*., 2013), and its induced molecule CXCL10 has anti-melanoma activity (Antonicelli *et al*., 2011). Another cytokine we found to be upregulated by DPCP, IL-9, has recently been linked to melanoma regression (Purwar *et al*., 2012). In addition to these cytokines with potential anti-neoplastic

effects, DPCP use resulted in many infiltrating CD8+ cells, along with increased granzyme B and granulysin expression, and these would be probable cytotoxic effectors. Granulysin has been shown to promote chemotaxis of CD4+ T cells in addition to its cytolytic properties (Deng *et al*., 2005), and both of these functions may contribute to the peak DTH response considering we observed granulysin expression on both CD8+ and CD8- T cells. We also noted a marked increase in DCs and especially DC-LAMP+ mature DCs, that could provide a local environment to increase antigen presentation of tumor antigens (immature DCs, in the absence of appropriate co-stimulation, present antigens in a tolerogenic fashion), as well as XCR1+ DCs, which have a role in antigen cross-presentation (Kroczek and Henn, 2012). Overall, this work forms a basis for investigating specific immune elements that may be induced in melanoma lesions that are treated with DPCP as well as the baseline immune competence of cancer patients.

Many different reports have shown that 50-60% of patients with patchy alopecia areata have meaningful hair regrowth when treated with chronic application of DPCP (Freyschmidt-Paul *et al*., 2003)(Ohlmeier *et al*., 2012). A smaller number of studies have been conducted to investigate immune alterations induced in the scalp that is associated with hair regrowth. Identified effects of DPCP include decreasing CD4+ T cell but increasing CD8+ T cell infiltrates (Simonetti *et al*., 2004). Also, MHC class II expression has been shown to be altered by DPCP treatment in different studies, with both increases (Hunter *et al*., 2011) and decreases (Bröcker *et al*., 1987) having been demonstrated. Furthermore, DPCP

alters the cytokine profile in treated alopecic scalp, in particular increasing IL-2 and IL-10 expression (Hoffmann et al. 1994b). This increased IL-10 expression has been hypothesized to inhibit the lesional T cells of alopecia areata, and our data confirm an upregulation of IL-10 expression, as well as increases in CD8+ T cells, in normal human skin treated with DPCP. Our data also suggested roles for various other regulatory molecules in the response to DPCP whose potential relevance to alopecia areata treatment have not yet been elucidated. However, our data do not directly inform on the potential effects of DPCP on scalp tissue, as well as alterations which may arise from repeated applications.

We compared our findings on DPCP with those published on a DTH reaction to purified protein derivative (PPD) (Tomlinson *et al*., 2011). The reaction to DPCP at 3 days compared to placebo-treated skin largely encompasses genes that are induced by a specific antigen (PPD in this case, 48 hours after exposure compared to 6 hours) (**Figure 3.13**). Of genes that were upregulated in the reactions, 780 were common to PPD and DPCP, but each agent also had unique upregulated genes. Overall there was significant correlation with differentially expressed genes ($r=0.61$, $p<10^{-16}$) and a gene set enrichment analysis for genes regulated in the PPD reaction had a normalized enrichment score of >4.0, indicating highly similar modulation of gene sets. The analysis of the PPD data by Tomlinson *et al*. emphasized the polar Th1 nature of immune reactions, which is supported by measured increases in IFNγ mRNA, STAT1, and many other interferon-regulated

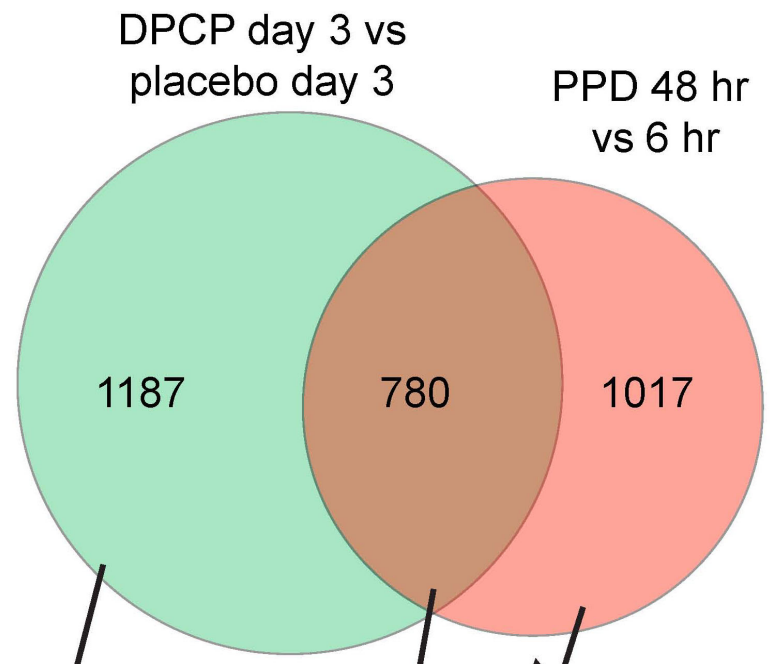

Gene	logFCH
IL24	6.74
IL19	6.49
IL8	4.06
CCL18	3.90
NFKB2	2.56
IL9	2.44
CXCL17	2.37
IL36G	1.77
STAT5B	1.77
IL20	1.57

Gene	logFCH
IFNG	3.82
CCR2	3.54
HLA-DOA	3.04
HLA-DRB4	2.41
HLA-DMB	2.24
CCL20	1.03

Gene	logFCH (DPCP)	logFCH (PPD)
CXCL10	6.70	8.51
OAS2	3.40	3.79
STAT1	2.65	4.49
OAS3	1.85	4.05
CIITA	1.82	3.31
HLA-DRA	1.07	2.02

Figure 3.13: Comparison of DPCP day 3 vs placebo day 3 reactions to PPD 48 hr vs 6 hr reactions (data from (Tomlinson *et al*., 2011)). Venn diagram shows 1,187, 780, and 1,017 upregulated genes uniquely in DPCP, in both DPCP and PPD, and uniquely in PPD, respectively (downregulated gene numbers are 1,690, 24, and 112). Tables underneath Venn diagram show selected genes from each section of the Venn diagram.

gene products. Without measurement of cytokine production by more sensitive techniques, it is a bit uncertain if other "polar" T-cell subsets are significantly activated by PPD. However, the DPCP response clearly showed activation of all defined "polar" T-cell subsets, i.e., Th1, Th2, Th9, Th17, and Th22, based on cytokine mRNA measures by RT-PCR. Ingenuity Pathway Analysis significantly linked the canonical pathways of "IL-10 Signaling," "Interferon Signaling," "IL-6 Signaling," and "IL-17 Signaling" to the set of genes upregulated in both DPCP and PPD reactions. All of these pathways except for "Interferon Signaling" were also significantly linked to the set of genes uniquely upregulated in DPCP reactions. We feel the system provided here provides a valuable human model for studying DTH reactions, particularly as one does not need to select a subset of antigen-reactive individuals from a larger subset of non-immunized or non-reactive individuals. Also, our system with DPCP controls sensitization and therefore fixes the amount of time between initial antigen exposure and challenge reaction, unlike many alternative antigens.

In contrast to soluble protein antigens, haptens derivatize with proteins that are present in the skin and may thus be present for longer time periods. Hence, different response kinetics might be expected for hapten-induced DTH reactions than PPD reactions. In this study, we did identify an expected inflammatory reaction in the skin that was strong at 3 days after DPCP exposure and T cell activation, as judged by specific markers (IFNγ, IL-2, and IL-2RA) as well as other activation-associated molecules, was highest at this time point. However,

much to our surprise, T cell infiltrates persisted for much longer than expected based on the PPD model, and 5/11 patients showed increased numbers of T cells or DCs at day 14 compared to day 3. Also, the number of mature (DC-LAMP+) DCs peaked at day 14 in 7/11 patients. Certainly these data establish a disassociation between T cell activation/cytokine production and the magnitude of the cellular immune response defined by the number of T cells and DCs in the skin. Therefore, the possibility of active negative regulatory mechanisms to suppress T cell activation to a potentially long-lived cutaneous antigen is suggested by these data.

Overall, understanding the active mechanisms present during the resolution of responses to DPCP could have implications not only for cell-mediated immunity in general, but also for other skin pathologies of either chronic immune activation or ineffective immune responses. Most importantly, this system could provide a tractable human antigen-specific model system for primary discovery of new pathways that may be involved specifically in immune regulation in peripheral tissues. Since all T cell subsets become activated by *in vivo* DPCP, this system might also have utility to test mechanism/pharmacodynamic actions of new immune modulators designed to selectively inhibit "polar" T-cell subsets or activated T cells. For example, there has recently been great interest in selective blockade of IL-17 for the treatment of psoriasis and IL-4 for the treatment of atopic dermatitis. As these and many other key cytokines are activated by DPCP,

this system can be used to test a variety of pharmacologic agents targeted against pathogenic immune molecules.

Our data comparing DPCP reactions to psoriasis suggest that disease chronicity in psoriasis could be related to absence of several negative immune regulatory pathways, and have the implication that strategies to obtain stable clearance/restore tolerance in skin lesions may need to focus on increasing these negative pathways. These negative immune mechanisms may be of more general importance for maintaining skin homeostasis as non-inflammatory in the presence of a large population of effector memory T cells that normally reside in skin (Clark et al. 2006). In addition, these negative immune regulators are likely involved in the therapeutic applications of DPCP, particularly alopecia areata where IL-10 has already been implicated (Hoffmann et al. 1994b). Further study of these regulatory mechanisms that are present in DPCP reactions, but not in psoriasis, could reveal novel factors in the pathogenesis of chronic inflammation.

CHAPTER 4: miRNA PROFILING OF HEALTHY VOLUNTEER SKIN REACTIONS TO DIPHENCYPRONE

We expanded our previous histological and gene expression profiling of healthy volunteer DPCP reactions to microRNA (miRNA) profiling. miRNAs are short (19-24 nucleotide) endogenous, non-protein coding RNAs that negatively regulate gene expression at the post-transcriptional level. They do this by sequence-specific base pairing, typically within the 3'-untranslated region of the target mRNA, resulting in transcript cleavage or translational repression. By current estimates, more than 60% of human protein-coding genes contain miRNA target sites (Friedman et al. 2009), and are therefore potentially regulated by miRNAs either physiologically or in disease. Since individual miRNAs target multiple, functionally related (as opposed to single) genes, they are of great interest from a therapeutic perspective (Sayed and Abdellatif 2011). The potential of modulating miRNA activity in a dermatological disease was recently demonstrated by Guinea-Viniegra *et al*., who showed that inhibition of miR-21 leads to amelioration of psoriasis pathology (Guinea-Viniegra et al. 2014). However, the roles of most miRNAs in skin biology and immunology are only recently being characterized (Baltimore et al. 2008).

Despite a number of studies on the involvement of miRNAs in inflammatory skin diseases such as psoriasis, previous work on the role of miRNAs in DTH inflammatory reactions is limited. Vennegaard *et al*. have previously shown by microarray and PCR approaches that miRs-21, -142-3p, -142-5p, and -223 are

significantly upregulated in DPCP-challenged human skin as well as mouse skin challenged with a similar hapten, dinitrofluorobenzene (Vennegaard et al. 2012). However, this study only examined peak reactions and therefore does not inform on potential immunoregulatory mechanims during a resolving DTH reaction. We obtained comprehensive miRNA expression profiles of DPCP challenge reactions at three different time points via deep sequencing to better understand mRNA regulation in DPCP responses over time, and how they may be involved in potential anti-melanoma effects.

To define miRNA expression profiles of DPCP reactions, we used the same RNA samples from which mRNA expression data were obtained. Comprehensive miRNA expression profiles were generated through barcoded small RNA sequencing. By unsupervised principal component analysis (PCA), there was no miRNA separation due to gender, age, or race (volunteer demographics and clinical scoring of DPCP-induced inflammation provided in **Table 3.1**). DPCP challenge biopsies, both at 3 days and 14 days, were clearly separated from placebo-treated skin, with the day 3 samples having a more distinct miRNA expression profile. The DPCP challenge biopsies taken at day 120 clustered with placebo-treated samples. Both of these sample types also clustered with normal skin samples taken from a separate study, therefore confirming that placebo-treated skin and DPCP challenge biopsies taken at 120 days (both of which clinically appear normal) are similar to normal skin (**Figure 4.1a**). This was further supported by a sample correlation matrix analysis, which showed a strong

Figure 4.1: Unique miRNA expression profiles in DPCP reactions at different times. (a) Principal component analysis (PCA) of global miRNA data for DPCP-treated skin at times indicated, placebo-treated skin, and normal skin. Heat maps of day 3 (b) and day 14 (c) samples. Ordinate shows individual volunteers treated with placebo or DPCP and abscissa displays individual miRNA expression levels. (d) Venn diagrams showing overlaps of significantly upregulated (left) and downregulated (right) miRNAs at the three time points post-challenge: 3 days, 14 days, and 120 days.

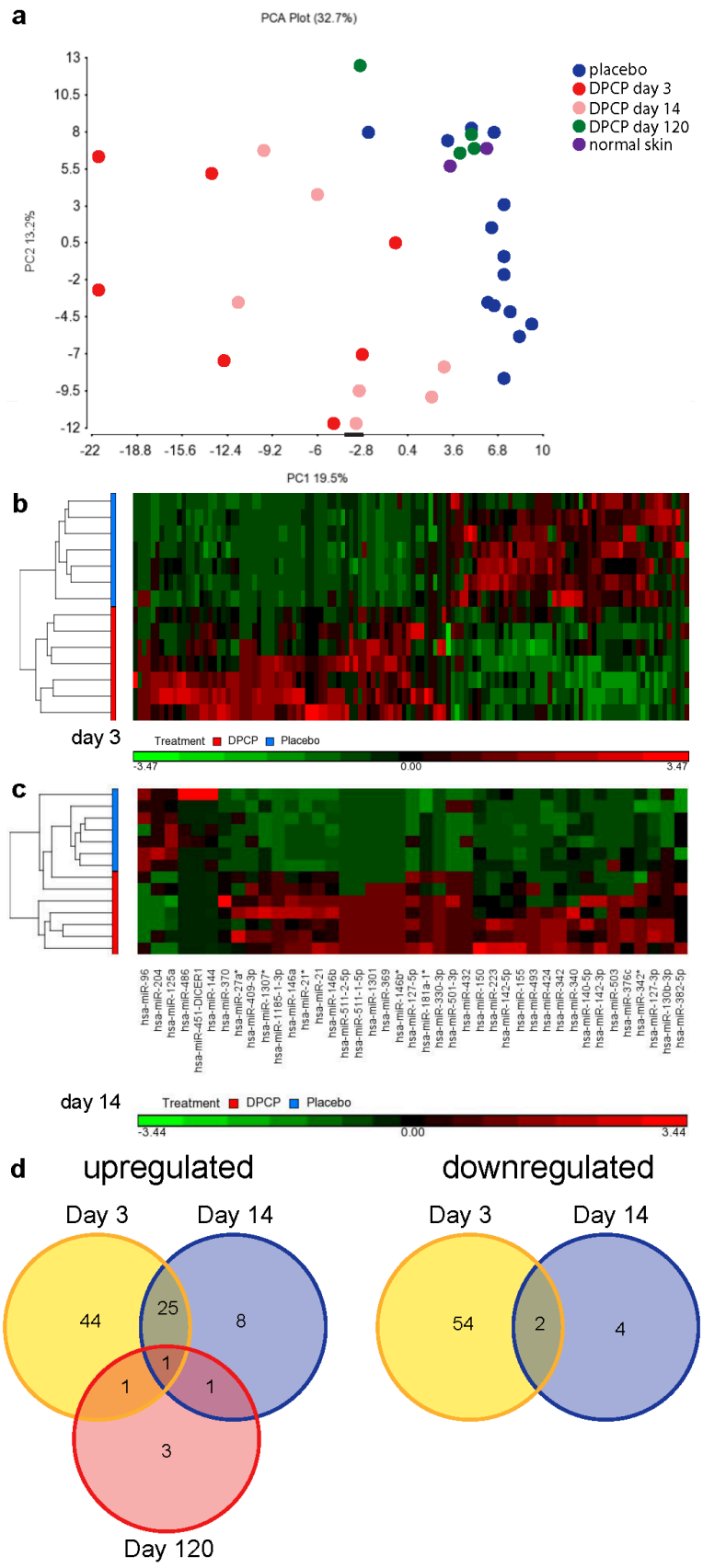
a
PCA Plot (32.7%)
placebo
DPCP day 3
DPCP day 14
DPCP day 120
normal skin
PC2 13.2%
PC1 19.5%
b
day 3
Treatment DPCP Placebo
-3.47
0.00
3.47
c
day 14
Treatment DPCP Placebo
-3.44
0.00
3.44
d
upregulated
downregulated
Day 3
Day 14
Day 120
44
25
8
1
1
1
3
54
2
4

correlation across the normal appearing skin samples compared with DPCP days 3 and 14 samples (**Figure 4.2**). In fact, there were no significantly deregulated miRNAs between normal skin samples and placebo-treated skin. Compared to placebo-treated skin, we found 127 significantly deregulated miRNAs at day 3 after DPCP challenge and 43 at day 14 after challenge (**Figure 4.1b and c**). **Table 4.1** lists the top 10 upregulated miRNAs at days 3 and 14. There were 6 significantly deregulated miRNAs at day 120 (all upregulated, fold changes in parentheses): miR-193a-3p (4.01), -136-5p (3.79), -377 (2.67), -140-5p (2.29), -376c (2.19), -17 (2.12).

Although the lists of top upregulated miRNAs at days 3 and 14 have several miRNAs in common, each of the three time points studied has a unique miRNA profile. For instance, of the 69 upregulated miRNAs at day 3, only 25 are also upregulated at day 14. **Figure 4.1d** provides Venn diagrams showing overlaps of significantly deregulated miRNAs at the three time points. One miRNA in particular, miR-140-5p, increased in expression over time, with fold changes increasing from 1.92 to 2.25 to 2.29 from day 3 to 14 to 120. We used qRT-PCR analysis to corroborate selected miRNA expression changes found by deep sequencing. miRNA-21, one of the top upregulated miRNAs at both days 3 and 14, as well as a novel potential therapeutic target in psoriasis (Guinea-Viniegra et al. 2014), was also found to be upregulated at both of these time points by qRT-PCR analysis (fold changes of 1.9 and 5.4, respectively; $P<0.005$ for both). miR-7 and miR-503, both among the top 10 upregulated miRNAs at day 3, were also

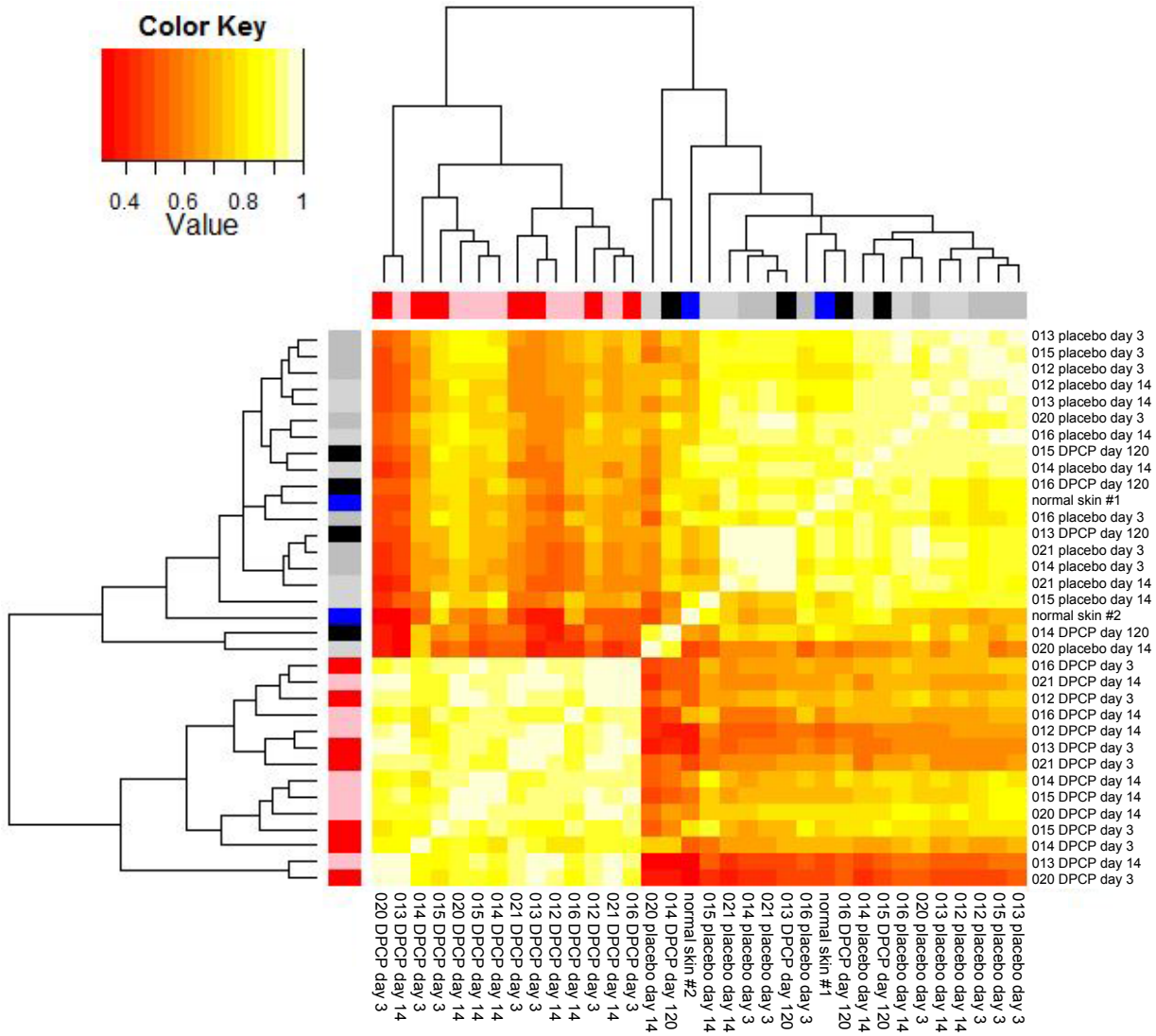

Figure 4.2: Correlation matrix analysis showing all samples. Three-digit numbers indicate subject IDs (see **Table 3.1**) except for the two normal skin samples, which came from a separate study.

Table 4.1: Top 10 upregulated miRNAs in DPCP day 3 and DPCP day 14 samples vs placebo-treated skin

microRNA	fold change	p-value	FDR	Total RF
(a) top upregulated miRNAs at day 3				
hsa-miR-223	20.87	0.00	0.00	252065
hsa-miR-150	15.71	0.00	0.00	519815
hsa-miR-21*	15.20	0.00	0.00	25877
hsa-miR-142-5p	14.45	0.00	0.00	224392
hsa-miR-142-3p	14.26	0.00	0.00	153335
hsa-miR-7-2	12.79	0.00	0.00	5941
hsa-miR-7-1	12.69	0.00	0.00	6128
hsa-miR-7-3	12.69	0.00	0.00	5839
hsa-miR-503	9.37	0.00	0.00	6563
hsa-miR-150*	8.55	0.00	0.00	3935
(b) top upregulated miRNAs at day 14				
hsa-miR-21*	8.08	0.00	0.00	10890
hsa-miR-146b	5.89	0.00	0.00	195770
hsa-miR-21	5.49	0.00	0.00	5895379
hsa-miR-155	5.25	0.00	0.00	33337
hsa-miR-142-3p	4.82	0.00	0.00	99152
hsa-miR-1185-1-3p	4.68	0.00	0.00	3420
hsa-miR-146b*	4.04	0.00	0.00	2868
hsa-miR-369	3.96	0.00	0.00	2836
hsa-miR-223	3.93	0.00	0.00	76363
hsa-miR-142-5p	3.70	0.00	0.00	134138

Abbreviations: FDR, false discovery rate; RF, read frequencies.

validated by qRT-PCR (fold changes of 4.3 and 5.2, respectively; $P<0.001$ for both), and these miRNAs have not been previously studied in skin inflammation. We also confirmed the top downregulated miRNA at day 3, miR-383 (fold change 0.26; $P<0.005$), another previously understudied miRNA (**Table 4.2**).

Discussion

Among the top 10 miRNAs we found upregulated at both days 3 and 14, miR-21, miR-142-3p, miR-142-5p, and miR-223 have all previously been found to be significantly upregulated in both human and mouse DTH reactions (Vennegaard et al. 2012). However, our current study had substantially higher fold changes for the same miRNAs than the study previously published, perhaps in part due to methodological differences (deep sequencing in the current vs microarray in the previous). Deep sequencing not only allows for studies of differential expression, but also facilitates determination of nucleotide variation and discovery of novel miRNAs. These four miRNAs have been shown to be related to T cells and T cell activation, in line with the fact that DTH reactions are mediated by T cells. Furthermore, upregulation of miR-223, miR-142-3p, and miR-142-5p has been reported in atopic dermatitis (Sonkoly et al. 2010) and in psoriasis (Zibert et al. 2010). miR-21 has been shown to be increased in psoriatic lesional skin, with evidence suggesting a causal role for this miRNA in the disease's epidermal hyperplasia (Guinea-Viniegra et al. 2014). Despite this, many of the top deregulated miRNAs found in our study have not previously been studied in the

Table 4.2: qRT-PCR confirmation of selected miRNAs in DPCP day 3 samples vs placebo-treated skin

microRNA	fold change	p-value[1]
hsa-miR-503	5.2	0.0009
hsa-miR-7	4.3	0.0006
hsa-miR-21	1.9	0.004
hsa-miR-383	0.26	0.001

[1]paired two-tailed Student's *t*-test

context of skin biology or immunology, highlighting the emerging nature of miRNA research. Our qRT-PCR data validated sequencing results both for miRNAs previously examined in the skin, such as miR-21, as well as for miRNAs that, to our knowledge, have never been described in the skin.

Since our study captured miRNA profiles at three different time points representing distinct phases of a DTH reaction (peak, actively resolving, fully resolved), and because these profiles proved to be unique and not simply subsets of one another, they may inform on positive vs negative immune regulation in this human model of a DTH reaction over time. For instance, miR-150, one of the top 10 upregulated miRNAs at day 3 (15.71-fold), was only slightly upregulated at day 14 (2.96-fold). This preferential expression of miR-150 during the peak reaction complements the fact that this miRNA inhibits DTH reactions in mice (Bryniarski et al. 2013), and therefore may need to be upregulated early on in a DTH reaction to promote resolution of inflammation. Of the 8 miRNAs uniquely upregulated at day 14, little is known about their roles in immunology, but all have been implicated in decreasing cell proliferation by cancer studies (Jiang et al. 2014)(Uppal et al. 2015)(Liu et al. 2015)(Chen et al. 2014)(Li et al. 2013)(Li et al. 2012)(Jiang et al. 2015)(Gu et al. 2014). As the day 14 reactions are characterized by active resolution and reduced expression of IL-2, it is possible that these miRNAs are related to inhibition of cell proliferation in this context as well. In addition, the unique miRNA expression profiles at different time points may shed light on the paradoxical ability of DPCP to treat conditions of both

autoimmunity (alopecia areata) and ineffective immunity (melanoma and warts). These unique miRNA profiles are paralleled by the unique mRNA profiles we found at days 3 and 14 in our previous study. Interestingly, the day 120 DPCP challenge biopsies, which resemble placebo-treated skin by clinical, histological, and gene expression criteria, do still have some miRNAs significantly upregulated compared to placebo-treated skin. This may reflect persistent changes long after clinical resolution of induced inflammation in this DTH reaction.

Certain miRNAs could account for previously identified mRNA expression changes, via sequence complementarity between the miRNA and mRNA. Nevertheless, because miRNAs can exert their effects by repressing translation (Fabian et al. 2010), one may not necessarily expect to see lower target mRNA levels for a given upregulated miRNA. Also, the miRNA changes could be due to immune cell infiltration bringing in the miRNAs, and not actual deregulation within a given cell type. It has been previously demonstrated that interactions between miRNAs and gene expression are confounded by leukocyte infiltration (Zhu et al. 2012), which our immunohistochemistry work has shown to be abundant in our samples. One way to address this is by the technique of laser capture microdissection, which allows for study of specific regions or cell populations under microscopic visualization, and which has recently has been applied to psoriasis in conjunction with deep sequencing (Løvendorf et al. 2014). This prior study demonstrated that the top 2 upregulated miRNAs at both days 3 and 14 (miR-223, miR-150, miR-21, and miR-146b) are all significantly

upregulated in reticular dermis compared to epidermis, therefore suggesting an immune as opposed to keratinocyte source for these miRNAs. Although laser capture microdissection limits the amount of cell types being examined in a sample, there is still the concern that observed miRNA changes are simply due to infiltrating leukocytes.

Since our study included inflamed biopsies at different time points, we were more directly able to investigate how miRNAs are modulated in leukocytes over time. We have shown that DPCP-challenged skin, at both days 3 and 14, contains many infiltrating leukocytes (including CD11c+ dendritic cells and CD3+ T cells), but that markers of all major defined T cell subsets including Th1 cells decrease from day 3 to 14. miRNA-21, which was significantly upregulated at both days 3 and 14, but more so at day 14 (by both sequencing and qRT-PCR), is known to regulate IL-12p35 expression (Lu et al. 2009) in dendritic cells (Lu et al. 2011), and this molecule is key to Th1 cell polarization. Therefore, in our samples, the increase in miR-21 at day 3 compared to placebo-treated skin could simply be due to the influx of many dendritic cells expressing this miRNA. On the other hand, we speculate that the increase in miR-21 expression from day 3 to 14 is due to actual upregulation in the infiltrating cells, and could explain the decrease in Th1 polarization that we previously demonstrated, via decreasing IL-12p35 expression (**Figure 4.3**). This effect may also be relevant to the therapeutic potential of this miRNA in psoriasis (Guinea-Viniegra et al. 2014), a disease where Th1 cells play an important pathogenic role. Although previous work, including laser capture

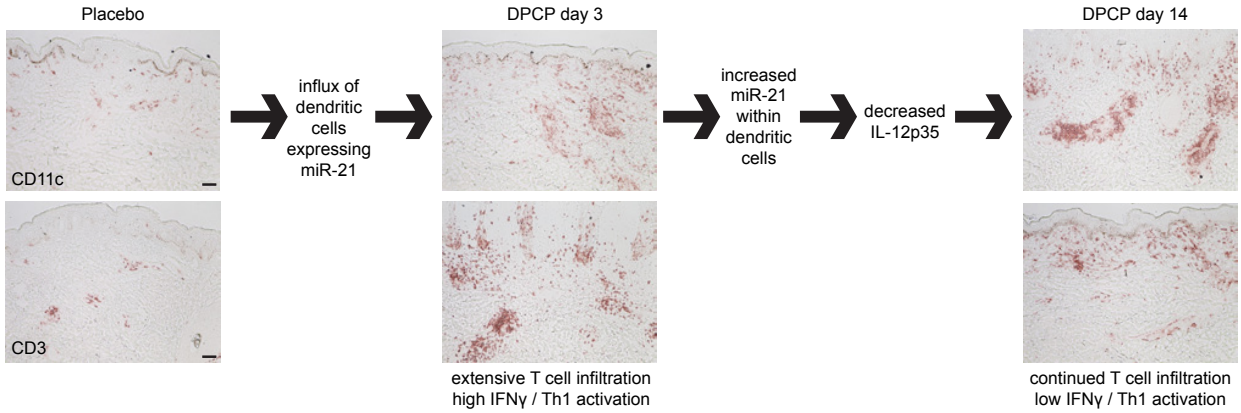

Figure 4.3: Schematic of proposed role of miR-21 in decreasing Th1 activation during resolution of DTH reaction. In placebo-treated skin, there are few CD11c+ dendritic cells and CD3+ T cells. Three days after challenge with DPCP, many cells of both types infiltrate the skin, along with high expression of IFNγ suggestive of Th1 activation. The observed increase in miR-21 expression at day 3 is likely due to influx of cells expressing this miRNA. However, from day 3 to day 14, cellular infiltration persists and therefore the increase in miRNA expression between these time points may in fact be due to upregulation within the infiltrating dendritic cells. miR-21 is known to decrease IL-12p35, and may therefore contribute to the reduced IFNγ and Th1 activation seen at day 14 relative to day 3, as this DTH reaction clinically resolves. Scale bar = 100 μm.

microdissection, has implicated an immune source for the primary miRNAs we found to be deregulated in this DTH reaction, future studies with in situ hybridization will be required to determine the exact cellular sources of the different miRNAs. Overall, here we provide a human antigen-specific model system to study miRNA regulation of a prototypic cell-mediated immune reaction over time, thus providing a useful starting point for the determination of roles of different miRNAs in positive vs negative immune regulation.

CHAPTER 5: T CELL RECEPTOR SEQUENCING OF HEALTHY VOLUNTEER SKIN REACTIONS TO DIPHENCYPRONE

Adaptive immune responses including DTH reactions rely on the generation of antigen-specific T cells, each of which has a unique rearranged T cell receptor (TCR). DPCP is thought to induce DTH reactions by conjugating with endogenous proteins, leading to the formation of antigens that are targeted by T cells. However, the specific antigen(s) involved in this process, and therefore the T cell clone(s) that accumulate in skin during this DTH response, are not known. We performed high-throughput sequencing of the entire T cell repertoire in DTH reactions to DPCP at different time points, in order to better understand the adaptive immune response that leads to the clinically observed inflammation.

From 3 of the healthy volunteers' skin biopsies which were used for mRNA and miRNA expression profiling, we extracted genomic DNA. High-throughput sequencing of the complementarity determining region 3 (CDR3) region of the TCRB locus allowed for comprehensive evaluation of the T cell repertoire present in these human skin reactions to DPCP over time. By looking at numbers of productive gene rearrangements (a strong estimate of the actual number of T cells sequenced in the sample), the DPCP day 3 and day 14 samples had on average 5812 and 5056, respectively, both significantly more than the placebo (557) and DPCP day 120 (568) samples. This is in agreement with CD3+ T cell counts

performed on these same samples by immunohistochemistry. In parallel, numbers of productive unique sequences were on average highest for DPCP day 3 and day 14 samples. However, all samples, despite these differences in T cell counts, were quite diverse (low clonality values) in that they were composed of many different T cell clones (**Table 5.1**). This suggests that DPCP is not leading to the formation of a single antigen to which a single unique T cell clone reacts.

In addition to suggesting the presence of multiple antigens in DPCP reactions within individual volunteers, our data indicate that different volunteers expand different T cell clones. This is supported by the fact that very few clones were shared among different volunteers (**Figure 5.1**), and that the number of clones expanded (as represented by numbers of productive unique sequences) varied among different volunteers. This finding may have therapeutic relevance to the clinical efficacy of DPCP in treating cutaneous melanoma metastases, as each patient treated with DPCP could expand a unique repertoire of T cells targeted against his or her specific tumor-associated antigens.

Our data also have implications for adaptive immune responses in general, particularly in regards to the accumulation of resident memory T cells (T_{RM}) in human skin that is known to occur over time (Clark 2015). In our study, we demonstrated that certain clones expand early (day 3) in skin reactions to DPCP, and persist over time even until day 120 when the inflammation has clinically

Table 5.1: **Summary of TCR sequencing data.** Clonality values range from 0 (each clone appears only once) to 1 (only one clone found).

sample type	subject ID	clonality	productive unique sequences	gene rearrangements
placebo	006	0.2104	247	514
placebo	013	0.0748	499	800
placebo	015	0.1482	182	358
placebo	**AVERAGE**	**0.1445**	**309**	**557**
DPCP day 3	006	0.0617	3975	5834
DPCP day 3	013	0.0577	5300	7703
DPCP day 3	015	0.0936	2569	3900
DPCP day 3	**AVERAGE**	**0.0710**	**3948**	**5812**
DPCP day 14	006	0.1099	3231	6181
DPCP day 14	013	0.0882	4484	8029
DPCP day 14	015	0.0914	548	958
DPCP day 14	**AVERAGE**	**0.0965**	**2754**	**5056**
DPCP day 120	006	0.0946	430	716
DPCP day 120	013	0.0521	91	177
DPCP day 120	015	0.2096	385	811
DPCP day 120	**AVERAGE**	**0.1188**	**302**	**568**

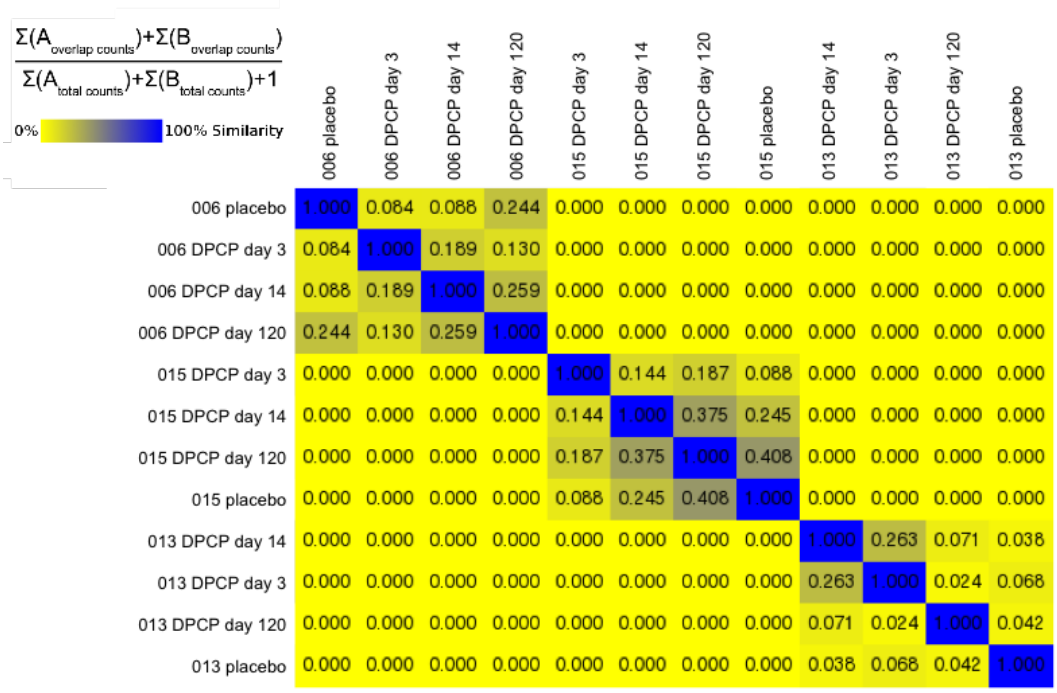

Figure 5.1: Heat map showing similarity of sample profiles. Similarity values are calculated as sum of overlapping sequences divided by sum of all sequences, and range from 0 (no overlap) to 1 (nearly identical sample).

Figure 5.2: DPCP reactions induce resident memory T cells (T_{RM}) in human skin. (a) Schematic of DPCP sensitization and sample recovery. (b) Clinical photos, H&E histology, and CD3+ T cell staining of the skin of healthy volunteers at day 3 (both placebo- and DPCP-treated), 14 (DPCP-treated), and 120 (DPCP-treated). Data representative of a total of 11 volunteers entered in the study. (c,d) Dot plots of the frequency (number of a given sequence divided by the total number of sequences observed in a given sample) of TCRB CDR3 sequences shared in placebo- or DPCP-treated skin from a representative individual. (c) Clones in DPCP day 3 reactions (green, vertical axis) vs. those in placebo-treated skin at the same time point (red, horizontal axis). Clones present in both sites are shown as blue dots. Five clones are identified (1-5) for subsequent reference. (d) Clones present in DPCP day 14 reactions (green, vertical axis) vs. DPCP day 120 (4 months) reactions (red, horizontal axis). The same five clones (labeled and enclosed in boxes) are identified as being present in both samples. (e) Quantification of the T cell clone size observed in (c) and (d) over time. Each line represents one clone of five representative clones mentioned in (c) and (d). From (Gaide et al. 2015).

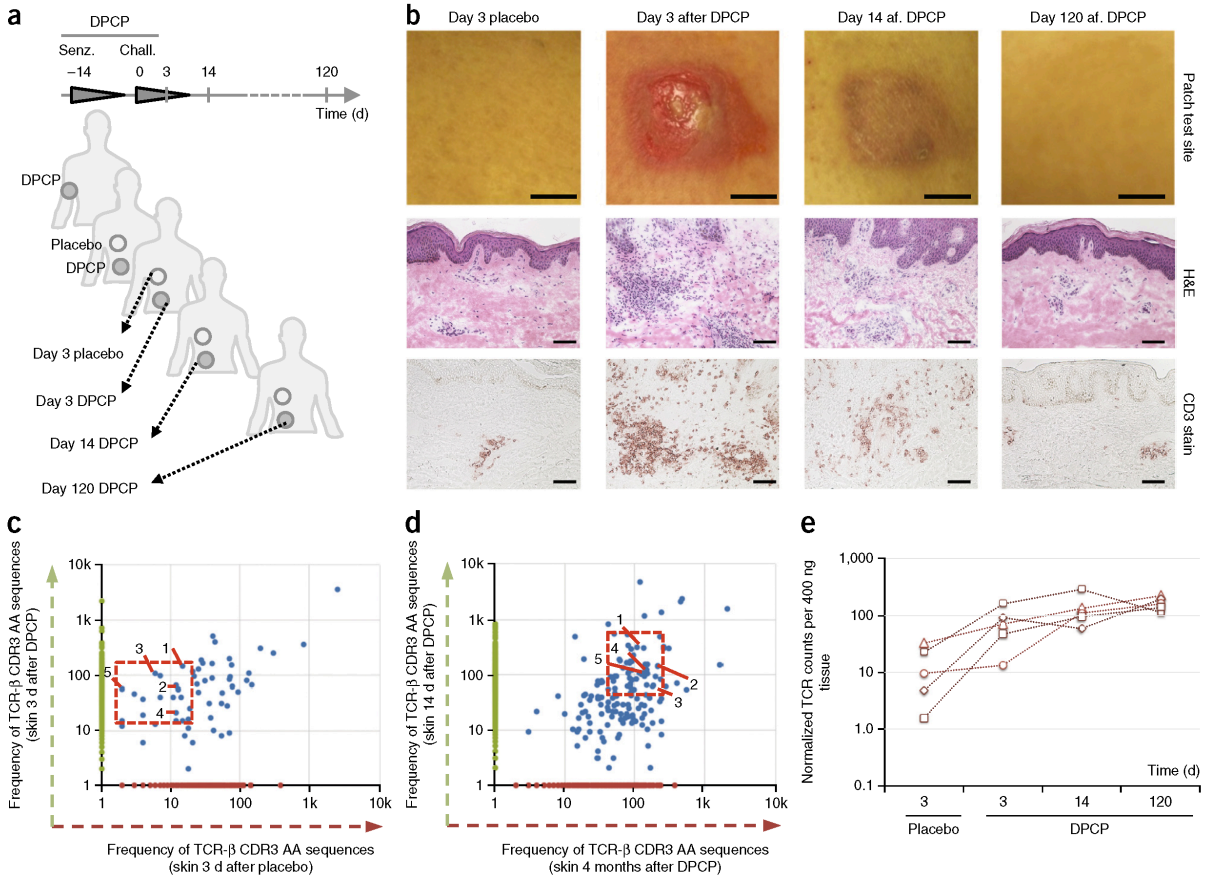
a
DPCP
Senz.
Chall.
−14
0
3
14
120
Time (d)
DPCP
Placebo
DPCP
Day 3 placebo
Day 3 DPCP
Day 14 DPCP
Day 120 DPCP
b
Day 3 placebo
Day 3 after DPCP
Day 14 af. DPCP
Day 120 af. DPCP
Patch test site
H&E
CD3 stain
c
Frequency of TCR-β CDR3 AA sequences (skin 3 d after DPCP)
Frequency of TCR-β CDR3 AA sequences (skin 3 d after placebo)
d
Frequency of TCR-β CDR3 AA sequences (skin 14 d after DPCP)
Frequency of TCR-β CDR3 AA sequences (skin 4 months after DPCP)
e
Normalized TCR counts per 400 ng tissue
Time (d)
Placebo
DPCP

Figure 5.3: TCR clone profiling during DPCP reactions over time. (a) Skin samples from two different volunteers share absolutely no CDR3 sequences (left panel). Within the same patient, the middle panel shows placebo-treated skin (red, horizontal axis), DPCP day 3 reactions (green, vertical axis), and shared clones (blue dots). The right panel shows similar data, with placebo-treated skin again on the horizontal axis (red), DPCP day 120 (4 months) reactions on the vertical axis (green), and shared clones (blue). As this technique will yield false negatives but not false positives, the true number of shared TCR sequences is likely to be higher than what is shown. (b) Dot plots of the TCRB CDR3 sequences shared (or not) in placebo- or DPCP-treated skin. Several clones are present at high levels in all samples (blue box, a-c), whether placebo- or DPCP-treated and irrespective of time point. Since they are present at the four month time point in the skin, at high abundance, these T cells are likely to be T_{RM} cells specific for an environmental antigen encountered before the trial (not DPCP). Several clones (green box) are undetectable in placebo-treated skin and DPCP day 3 reaction, but present at high frequency at days 14 and 120. These cells likely correspond to newly activated T cells recruited to the skin in response to DPCP. (c) Graphic representation of unrelated T_{RM} clones (a-c, blue lines) and newly recruited clones (1-4, green lines); TCR counts are shown on the y axis, log scale. Clones 1-4 at day 120 also represent new T_{RM}. From (Gaide et al. 2015).

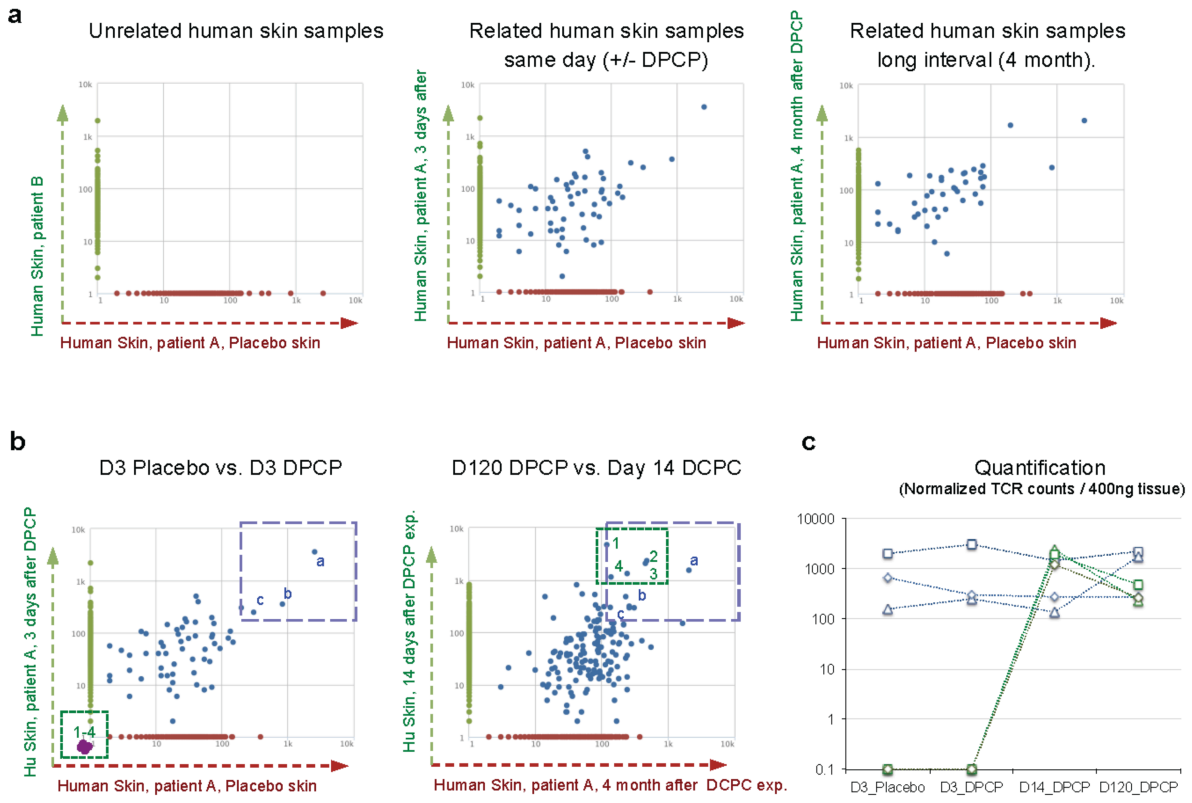
a
Unrelated human skin samples
Related human skin samples same day (+/- DPCP)
Related human skin samples long interval (4 month).
Human Skin, patient B
Human Skin, patient A, 3 days after
Human Skin, patient A, 4 month after DPCP
Human Skin, patient A, Placebo skin
b
D3 Placebo vs. D3 DPCP
D120 DPCP vs. Day 14 DCPC
Hu Skin, patient A, 3 days after DPCP
Hu Skin, 14 days after DPCP exp.
Human Skin, patient A, 4 month after DCPC exp.
1-4
a
b
c
1
2
3
4
c
Quantification
(Normalized TCR counts / 400ng tissue)
10000
1000
100
10
1
0.1
D3_Placebo
D3_DPCP
D14_DPCP
D120_DPCP

fully resolved (**Figure 5.2**). Therefore, we provide the first human data following putative antigen-specific T_{RM} clones over time in skin. Other T cell clones were present in placebo reactions but either did not change or decreased in number over time, and still others did not appear until day 14 reactions after which their abundance decreased (**Figure 5.3**). These clones do not fit the criteria of T_{RM} cells, and are consistent with recent findings that only a subset of T cells in human skin are authentic T_{RM} cells (Watanabe et al. 2015). Our data were synthesized with work from another group using mouse models of T_{RM} cell formation, and were recently published together (Gaide et al. 2015).

CHAPTER 6: CLINICAL AND HISTOLOGICAL RESPONSES OF MELANOMA PATIENTS TO TOPICAL DIPHENCYPRONE TREATMENT

We enrolled 6 patients in our trial using topical DPCP to treat cutaneous melanoma metastases. Each patient had unique treatment histories prior to entering our trial, but all were successfully sensitized to DPCP, and received at least 3 weeks of twice weekly DPCP treatment applications to their cutaneous metastases.

Patient 001 was a 52-year-old female who, 23 months prior to beginning DPCP treatment, was diagnosed with a 1.5 mm high-risk (mitotic rate of 4) melanoma of the right temple with associated lymphovascular invasion, which was treated with wide local excision and negative sentinel node biopsy. 3 months later, she developed multiple satellite metastases, and 2 months after that, underwent radiation therapy. This was followed by ipilimumab and topical imiquimod the next month. 4 months after that, the patient received systemic IL-2 therapy (16 doses), with an additional course of IL-2 2 months later (8 doses). She underwent an additional course of ipilimumab, which was complicated by colitis requiring the use of infliximab. Her cutaneous lesions were controlled with the use of repeated cryotherapy and sustained topical imiquimod. She began temozolomide therapy 2 months before enrolling in our trial. Despite her multiple therapies, the patient continued to have advanced unresectable cutaneous melanoma that was

distributed in her right ear and right cheek and scalp area, and thus her oncologist referred her to our trial at The Rockefeller University.

After completing screening for our trial, the patient had 2 biopsies: one at the site of one of her cutaneous metastases, and one at a site of normal skin. Sensitization was mildly successful, with only 1 of 3 sensitization sites (the right upper arm) having a response, and that response was weak (erythema and induration both scored as 1, size 2 x 1.5 mm). DPCP, at the concentration (0.04%) that elicited robust inflammation in our healthy volunteers, was applied to her cutaneous metastases twice weekly for 3 weeks, but the induced inflammation continued to be weak with only mild erythema observed. A biopsy was taken of a melanoma metastasis 3 weeks into the course of treatment. By CD3 immunohistochemistry of biopsy tissue, the melanoma lesion biopsied before commencing DPCP treatment had more CD3+ T cells than the lesion biopsied 3 weeks into treatment (**Figure 6.1**). Repeat skin biopsy the month after entering our trial revealed the presence of a BRAF mutation (her original BRAF typing was done on her primary tumor, with no mutation found), and so the patient started vemurafenib therapy the following month, thus discontinuing DPCP therapy after 3 weeks of treatment. This patient left our study before definitive assessment of clinical response (tumor regression) to DPCP could be ascertained, but our experience with her prompted us to add flexibility to our protocol in terms of the concentration of DPCP that could be used for future patients. It is likely that

Figure 6.1: Patient 001 only exhibited mild inflammation in response to the concentration of DPCP that led to robust inflammation in our healthy volunteers. Clinical photography and CD3 immunohistochemistry below of patient 001 before topical DPCP applications (left) and 3 weeks into topical DPCP applications (right). Scale bar = 100 μm.

melanoma patients such as this have systemic immunosuppression that may diminish their immune responses generated by DPCP applications.

Patient 002 was a 98-year-old male who, 4 years prior to beginning DPCP treatment, was diagnosed with a melanoma lesion of the chest, which was treated with surgical excision. Two more recurrences occurred in the following years, both also treated with surgical excision. Then a further recurrence occurred, now with many melanoma lesions on the chest. This was treated with 2 months of topical imiquimod without response, and so the patient was referred to our trial at The Rockefeller University.

After completing screening for our trial, the patient had 2 biopsies: one at the site of one of his cutaneous metastases, and one at a site of normal skin. Sensitization was successful, and applications of DPCP to cutaneous metastases continued twice weekly for 7 weeks. A biopsy was taken of a melanoma metastasis both 3 weeks and 7 weeks into the course of treatment. Unlike patient 001, this patient exhibited robust clinical inflammation in response to DPCP, and immunohistochemistry of biopsy tissue for CD3 showed increased T cells upon DPCP treatment. Patient 002 also demonstrated partial tumor regression, as evidenced by immunohistochemistry for the melanoma marker MLANA, within 7 weeks of starting treatment (**Figure 6.2**). Sadly, after 7 weeks on treatment, the patient passed away from what we believe are natural causes/medical problems unrelated to his melanoma or its treatment.

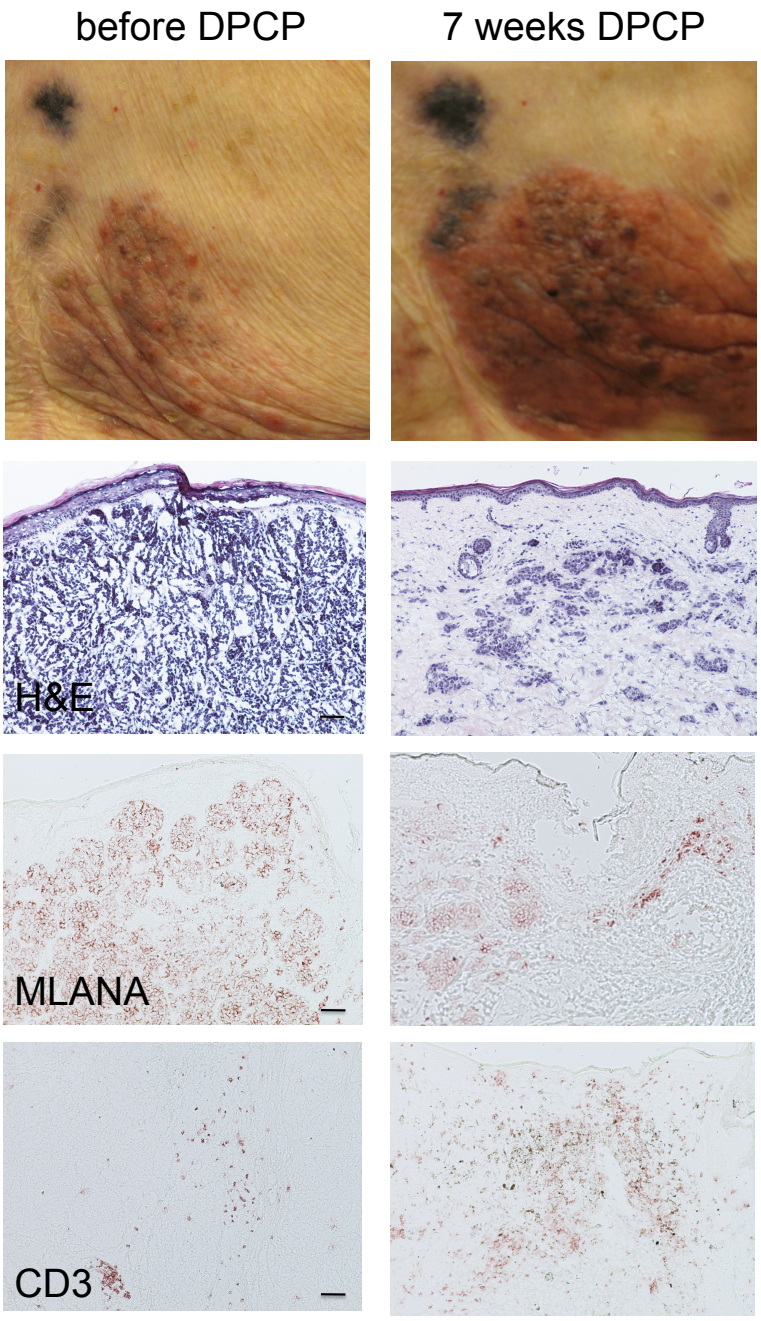

Figure 6.2: Patient 002 exhibited robust inflammation and partial melanoma regression in response to DPCP. Clinical photography as well as specified histological stains below of patient 002 before topical DPCP applications (left) and 7 weeks into topical DPCP applications (right). Scale bar = 100 μm.

Patient 003 was a 91-year-old female who, 59 months prior to beginning DPCP treatment, was diagnosed with a 1.8 mm non-ulcerated melanoma of the pretibial region, which was treated with wide excision/split thickness skin graft. 11 months later, a small focus of local recurrence appeared at the edge of the split thickness skin graft, which was treated with wide excision. 24 months after that, a further area of local recurrence appeared that initially responded well to imiquimod. However, 22 months later (2 months before beginning DPCP treatment), the patient developed progressive low-volume local recurrence (two pigmented metastasis lesions, each about 5 mm in diameter, **Figure 6.3**), which was unresponsive to imiquimod and the patient declined surgery due to previous difficulty with healing. At the recommendation of her oncologist, the patient entered our trial at The Rockefeller University.

After completing screening, the patient had 2 biopsies: one at the site of one of her cutaneous metastases, and one at a site of normal skin. After successful sensitization, applications of DPCP to cutaneous metastases occurred twice weekly for 14 weeks (98 days, the full course of DPCP treatment specified in our clinical protocol), at which point the patient's left lower leg was very inflamed and therefore it was impossible to see whether melanoma lesions were present or not (**Figure 6.4**). One biopsy was taken at this time (day 98) of an inflamed skin site that was not previously involved with melanoma. We then examined the patient at day 128 (with no DPCP being applied since day 98), and the inflammation largely subsided, thus allowing us to see that the melanoma

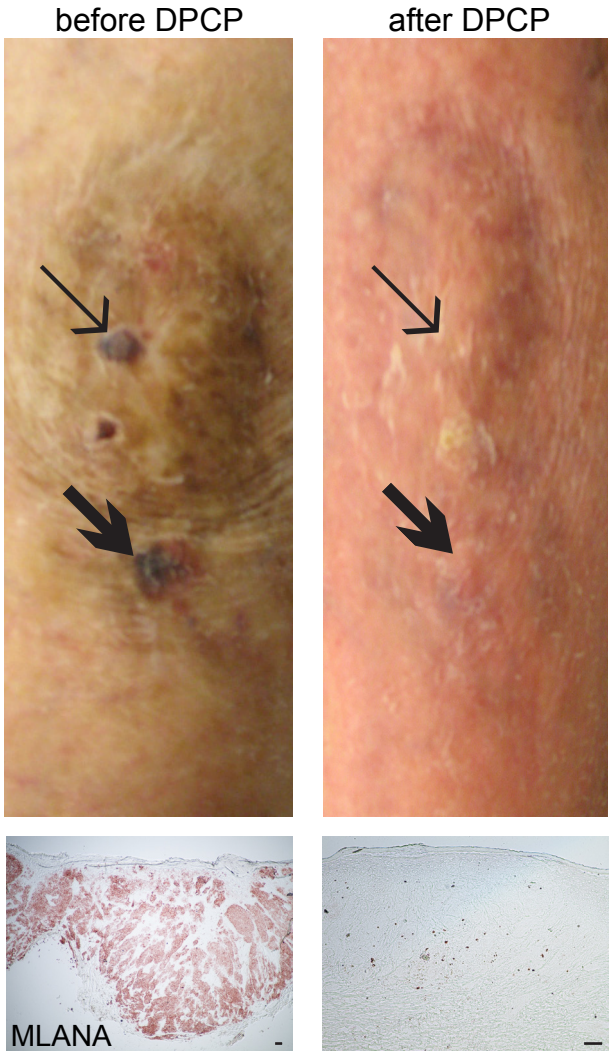

Figure 6.3: Patient 003 exhibited full clinical and histological melanoma metastasis regression upon DPCP treatment. Skin photography, with immunohistochemistry for melanocyte marker MLANA below, of the patient's left lower leg before DPCP application (left) and after 14 weeks of twice weekly DPCP applications (right). Brown staining in histological image at right likely represents melanophages. There were two melanoma metastases visible before DPCP application, and their locations are indicated by arrows (the thick arrow shows the site that was biopsied). Scale bar = 100 μm.

Figure 6.4: Skin photography of patient 003's left lower leg at end of DPCP applications (day 98, after 14 weeks of twice weekly applications). The skin was inflamed to the point that it was not possible to determine whether the patient's melanoma lesions were still present. Therefore, the patient discontinued DPCP treatment at this time and returned 30 days later (day 128) for the photograph shown in **Figure 6.3**.

metastases were clinically resolved (**Figure 6.3**). One biopsy was performed of a resolved lesion (at a site previously involved with melanoma). We confirmed the absence of melanoma cells by immunohistochemistry for MLANA (**Figure 6.3**). The patient was seen for follow-up visits 1 month after and 4 months after the day 128 visit, and appeared well both times with no cutaneous metastases visible.

Patient 004 was a 93-year-old male who, 10 years prior to beginning DPCP treatment, was diagnosed with a melanoma on his right foot, which was treated surgically. 5 years later, after spread had occurred, the patient received imatinib (4 injections every 3 weeks for 9 weeks), which resulted in complete remission lasting 3 years. After those 3 years, another round of imatinib was received with complete remission once again, but this time only lasting for 6 months. 1 year prior to beginning DPCP treatment, the patient completed a course of ipilimumab (4 doses spaced 3 weeks apart), which did not result in any response. The patient then began a third round of imatinib, which also did not result in any response. At this point the patient had many cutaneous melanoma metastases on his right anterior thigh, along the shin, and behind the knee, and this is when he was referred to our trial at The Rockefeller University.

This patient followed a unique clinical course that allowed us to evaluate melanoma regression in response to DPCP, PD-1 checkpoint inhibitor therapy (now considered the standard of care treatment for metastatic melanoma; see (Ribas et al. 2015)), and a combination of the two. After completing screening,

the patient had 2 biopsies: one at the site of one of his cutaneous metastases, and one at a site of normal skin. After successful sensitization, applications of DPCP to cutaneous metastases occurred twice weekly for 9 weeks. During this time period, strong inflammation was induced by DPCP as expected, and some lesions disappeared or shrank, but some new ones also appeared (**Figure 6.5**). Therefore, the efficacy of DPCP alone to regress melanoma was difficult to assess. A biopsy was taken of a melanoma metastasis both 3 weeks and 9 weeks into the course of treatment. After these 9 weeks, the patient left our trial because his oncologist wanted to prescribe the (at the time not FDA approved) PD-1 checkpoint inhibitor nivolumab, of which he began receiving infusions every 3 weeks. 3 months later, since the patient was not responding to nivolumab (which at that time became FDA approved), his oncologist recommended he restart DPCP treatment (twice weekly) in conjunction with nivolumab, which the patient continued to receive every 3 weeks. Since we were unsure of how these two immunomodulatory agents would interact with each other (i.e. there was concern for too robust an immune reaction), we started by only treating a select area of skin with topical DPCP. After 1 month of this, the patient tolerated the dual treatment well and showed tumor regression in the select DPCP-treated area. Therefore, we expanded the DPCP treatment field to include all of the patient's cutaneous metastases, and this expanded the regression response to a wider region (**Figure 6.6**). The patient received this dual therapy for 7 months, with a biopsy taken of a cutaneous metastasis at 1 month, as well as biopsies of both a cutaneous metastasis and nearby uninvolved (but inflamed due to treatment) skin taken at 7

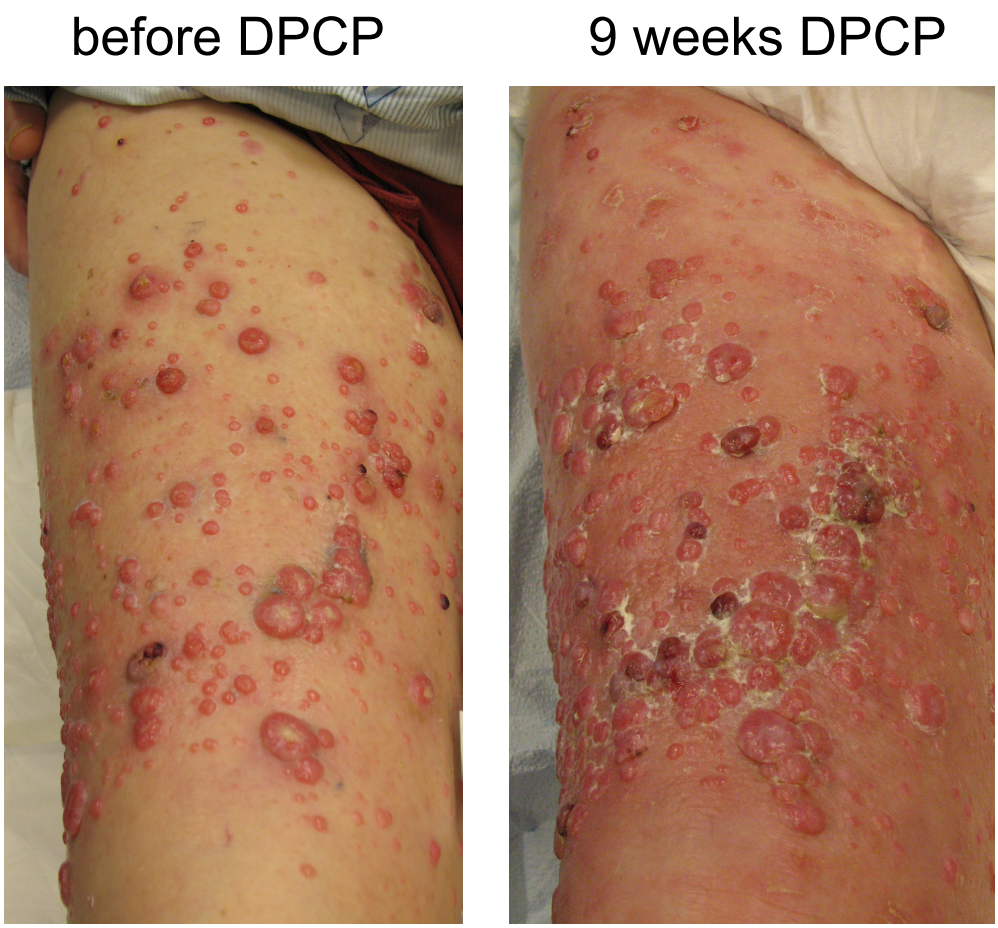

Figure 6.5: Patient 004 exhibited melanoma metastasis regression upon DPCP treatment alone, but new lesions also developed. Skin photography of the patient's right anterior thigh before topical DPCP applications (left) and 9 weeks into topical DPCP applications (right).

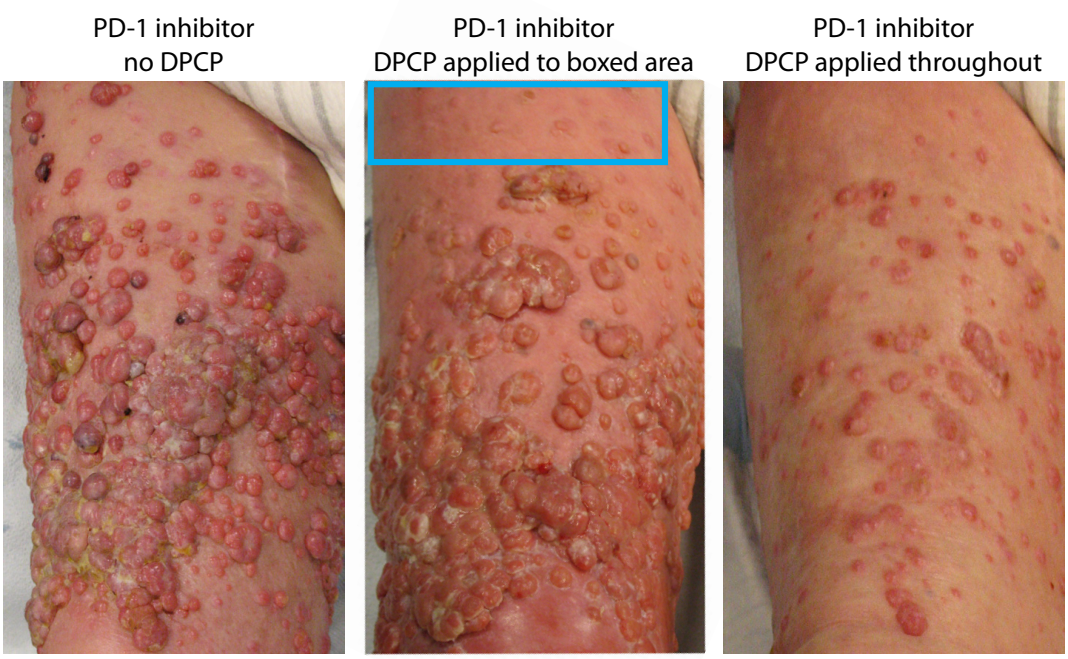

Figure 6.6: Patient 004 exhibited widespread melanoma metastasis regression upon combined DPCP and PD-1 checkpoint inhibitor therapy. Skin photography of the patient's right anterior thigh before restarting topical DPCP applications but having been on PD-1 checkpoint inhibitor nivolumab for 3 months (left), 1 month into combined nivolumab and topical DPCP therapy (only to boxed area) (middle), and 4 months into combined nivolumab and topical DPCP therapy (applied throughout) (right).

months. After these 7 months, although many of the patient's lesions regressed, it became more difficult for him to tolerate DPCP applications to the large areas of skin (with resultant extensive inflammation) that were involved with melanoma, and so he elected to discontinue DPCP treatment (but still continued nivolumab treatment). During this patient's dual treatment, we observed patches of skin on the leg not involved with melanoma to be affected with vitiligo (**Figure 6.7**), suggesting a loss of pigment-producing cells distant from the site of DPCP application, that presumably are targeted by the immune system along with melanoma cells. This is in line with previous reports showing that DPCP leads to vitiligo (Pires et al. 2010).

Patient 005 was a 66-year-old male who, 16 months prior to beginning DPCP treatment, was diagnosed with a 2.1 mm melanoma on the left forehead, which was treated surgically. He was diagnosed with a new focus of melanoma medial to the scalp scar 7 months later, and received 3600 centiGray of adjuvant radiation in 6 doses. In the following months, he developed multiple foci of cutaneous metastases in the scalp, and was treated with both cryotherapy and topical imiquimod. The patient was applying imiquimod daily to only part of his scalp, and this began 2 months prior to entering our trial, with resultant mild erythema. However, many cutaneous metastases persisted, and so the patient was referred to our trial at The Rockefeller University, while still receiving topical imiquimod applications.

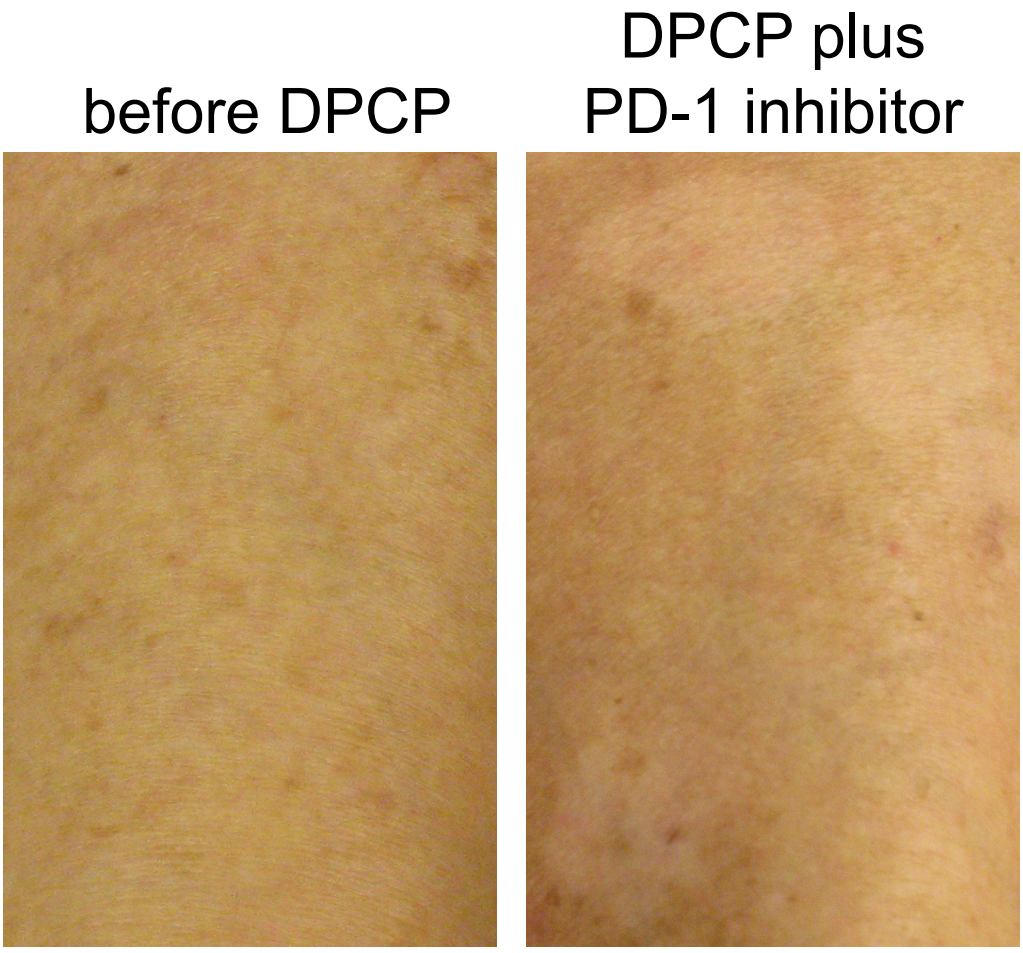

Figure 6.7: Patient 004 exhibited vitiligo at skin sites distant from DPCP applications. Skin photography of the patient's left anterior thigh (as opposed to right anterior thigh which was involved with melanoma) before starting topical DPCP applications (left) and 3 months into combined nivolumab and topical DPCP therapy (right).

After completing screening, the patient had 3 biopsies: one at the site of one of his cutaneous metastases, one at a site of normal skin, and one at an area of skin treated with topical imiquimod (treatment had been ongoing for 2 months). After successful sensitization, applications of DPCP to cutaneous metastases occurred twice weekly for 7 weeks, only to the metastases not already being treated with imiquimod (which continued). A biopsy was taken of a DPCP-treated melanoma metastasis both 3 weeks and 7 weeks into the course of treatment. As imiquimod, like DPCP, acts through the immune system, we elected to perform a biopsy of imiquimod-treated skin, so that we could compare it to a biopsy of DPCP-treated skin from the same patient. This revealed increases in various immune cell types in DPCP-treated compared to imiquimod-treated skin, including: CD3+ T cells, CD8+ cytotoxic T cells, CD11c+ myeloid dendritic cells, and CD163+ macrophages (**Figure 6.8**). Furthermore, by qRT-PCR analysis, DPCP induced stronger upregulation of IFNγ (3-fold) and IL-9 (5-fold) than imiquimod. During the 7 weeks of DPCP treatment, many of the patient's cutaneous metastases became lighter and/or smaller, with histological evidence of melanoma regression along with inflammation (**Figure 6.9**). However, the patient unfortunately developed internal metastases at this point, and so elected to leave our trial and begin ipilimumab treatment.

Patient 006 was an 81-year-old female who, 18 months prior to beginning DPCP treatment, was diagnosed with a melanoma on the right lower calf, which was treated surgically. Then the patient developed many small metastatic melanoma

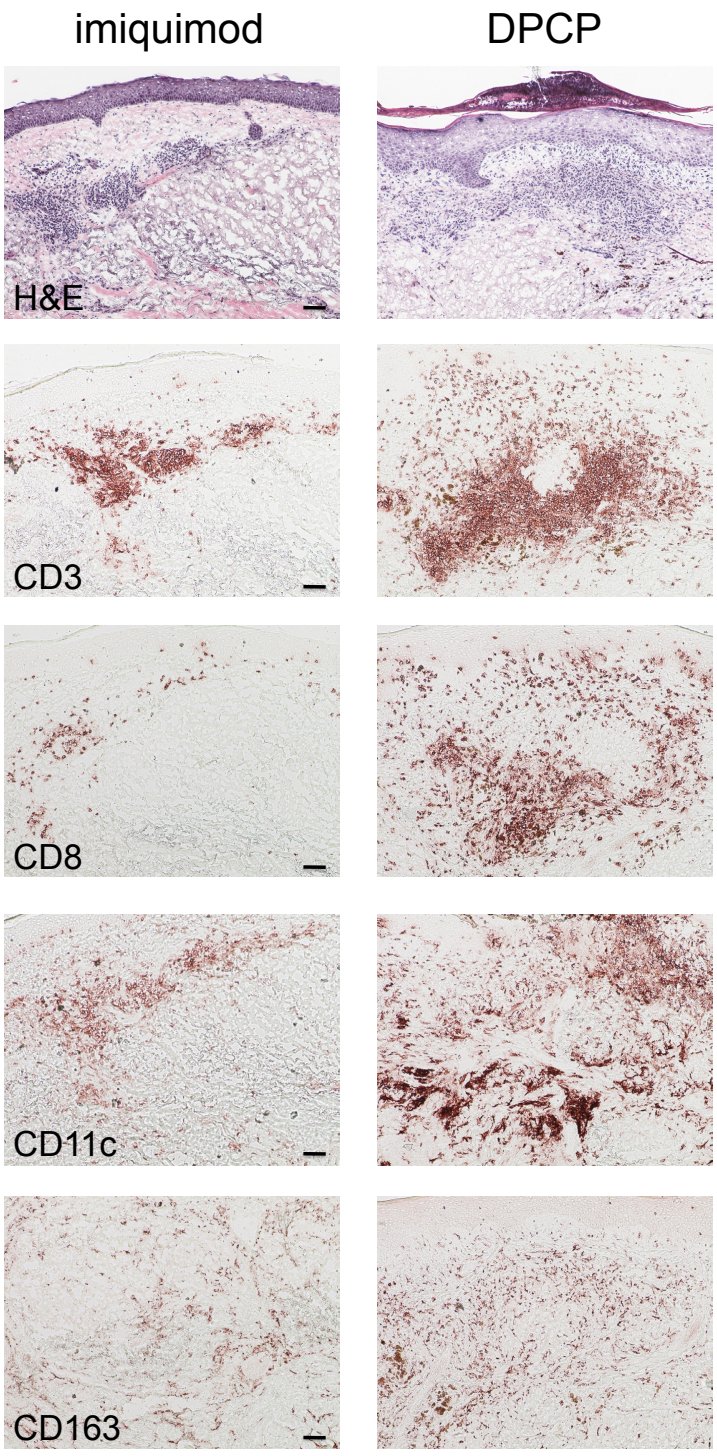

Figure 6.8: In patient 005, DPCP induced stronger histological inflammation than imiquimod. Specified histological stains of biopsies from patient 005 of skin treated with imiquimod (left) and DPCP (right).

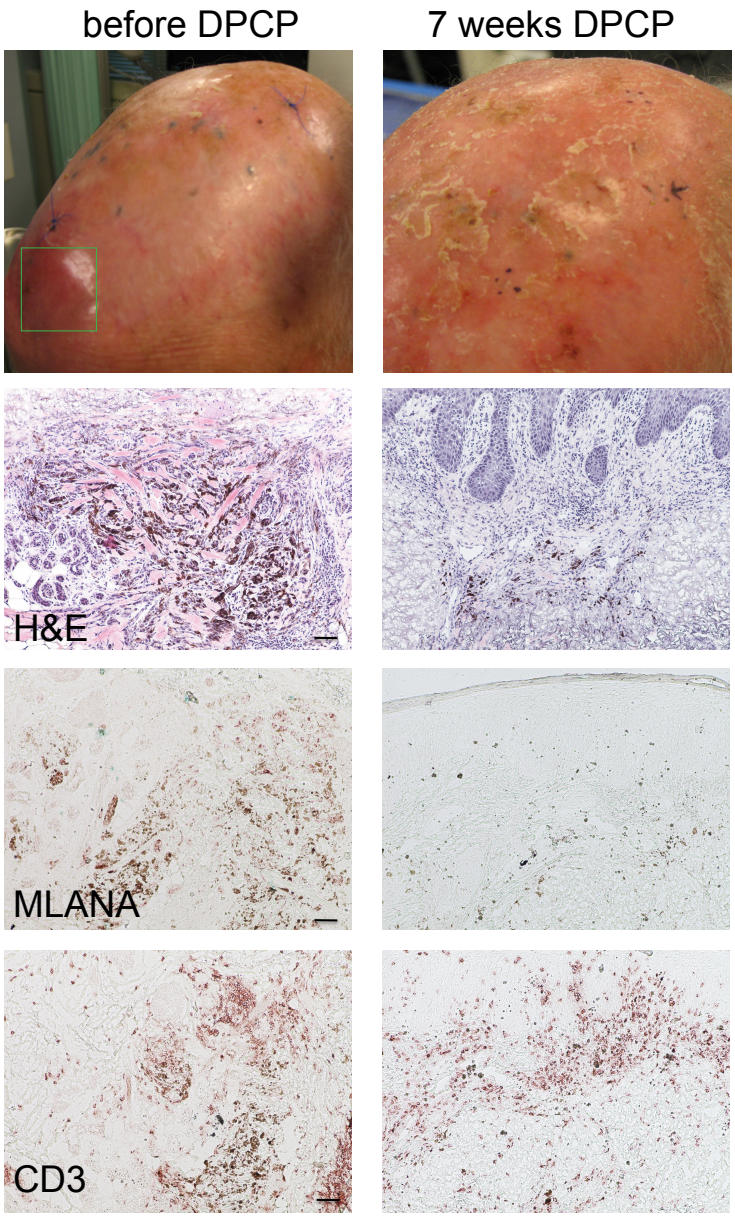

Figure 6.9: Patient 005 exhibited robust inflammation and partial melanoma regression in response to DPCP. Clinical photography as well as specified histological stains below of patient 005 before topical DPCP applications (left) and 7 weeks into topical DPCP applications (right). Green box indicates area of imiquimod application (commenced 2 months prior to DPCP applications). Scale bar = 100 μm.

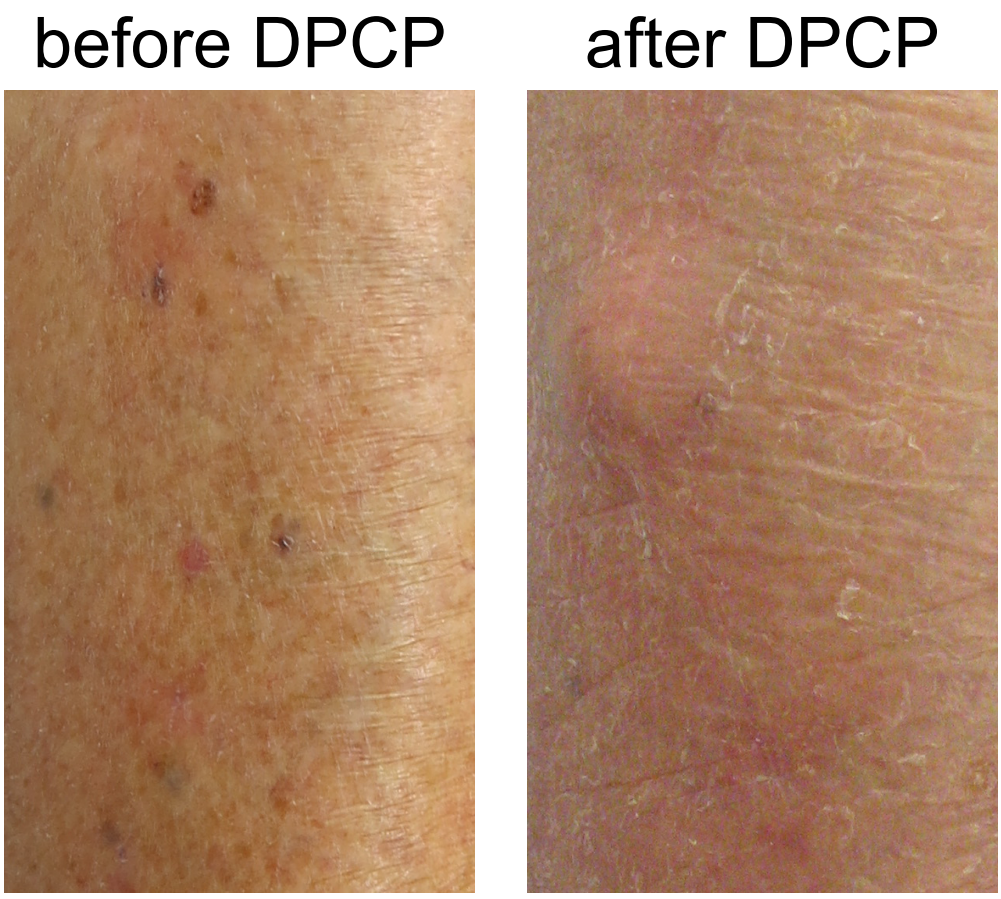

Figure 6.10: Patient 006 exhibited nearly complete clinical melanoma metastasis regression upon DPCP treatment. Skin photography of the patient's right lower calf before DPCP application (left) and after 14 weeks of twice weekly DPCP applications (right).

lesions on her right lower calf, and so was referred to our trial at The Rockefeller University.

After completing screening, the patient had 2 biopsies: one at the site of one of her cutaneous metastases, and one at a site of normal skin. After successful sensitization, applications of DPCP to cutaneous metastases occurred twice weekly for 14 weeks (98 days, the full course of DPCP treatment specified in our clinical protocol), at which point the patient's right lower calf was very inflamed and therefore it was impossible to see whether melanoma lesions were present or not. A biopsy was taken of a melanoma metastasis both 3 weeks and 9 weeks into the course of treatment. We then examined the patient at day 128 (with no DPCP being applied since day 98), and the inflammation largely subsided, thus allowing us to see that, while most metastases regressed, two small lightly pigmented lesions remained in the treated area (**Figure 6.10**). One biopsy was performed of each of these lesions, with site #1 referring to the superior and site #2 referring to the inferior. The results from these biopsies will be discussed in the following chapter, wherein mechanistic studies on the biopsy specimens from all 6 patients are presented.

CHAPTER 7: MECHANISTIC STUDIES OF IMMUNE-MEDIATED MELANOMA METASTASIS REGRESSION INDUCED BY DIPHENCYPRONE

To better ascertain the mechanisms involved in immune-mediated tumor regression induced by DPCP, we studied biopsy tissues from our 6 patients at various time points. In line with our healthy volunteer data, DPCP applications in melanoma patients led to extensive immune cell infiltrates, including CD3+ T cells, CD11c+ myeloid dendritic cells, and CD163+ macrophages, both after a single and repeated applications. These infiltrates persisted in follow-up biopsies performed 30 days after cessation of DPCP treatment (**Figure 7.1**). In addition to these cells, which are presumably integral to immune-mediated anti-melanoma responses, we found that DPCP application led to increases in granulysin. By two-color immunofluorescence, granulysin co-localized with NKp46+ natural killer cells more than CD8+ cytotoxic T cells (**Figure 7.2**).

In an effort to obtain a more specific understanding of the kind of immune response that may lead to tumor regression, we determined the evolving T cell polarization in this repeated DPCP application scenario. Our work with healthy volunteers demonstrated that gene expression markers of all major T cells subsets (Th1, Th2, Th9, Th17, Th22, and regulatory T cells) all significantly increase at 3 days following a single application of DPCP. With our melanoma patients, we similarly obtained biopsies of a normal skin site 3 days following a single application of DPCP. However, with these patients, we also obtained biopsies of

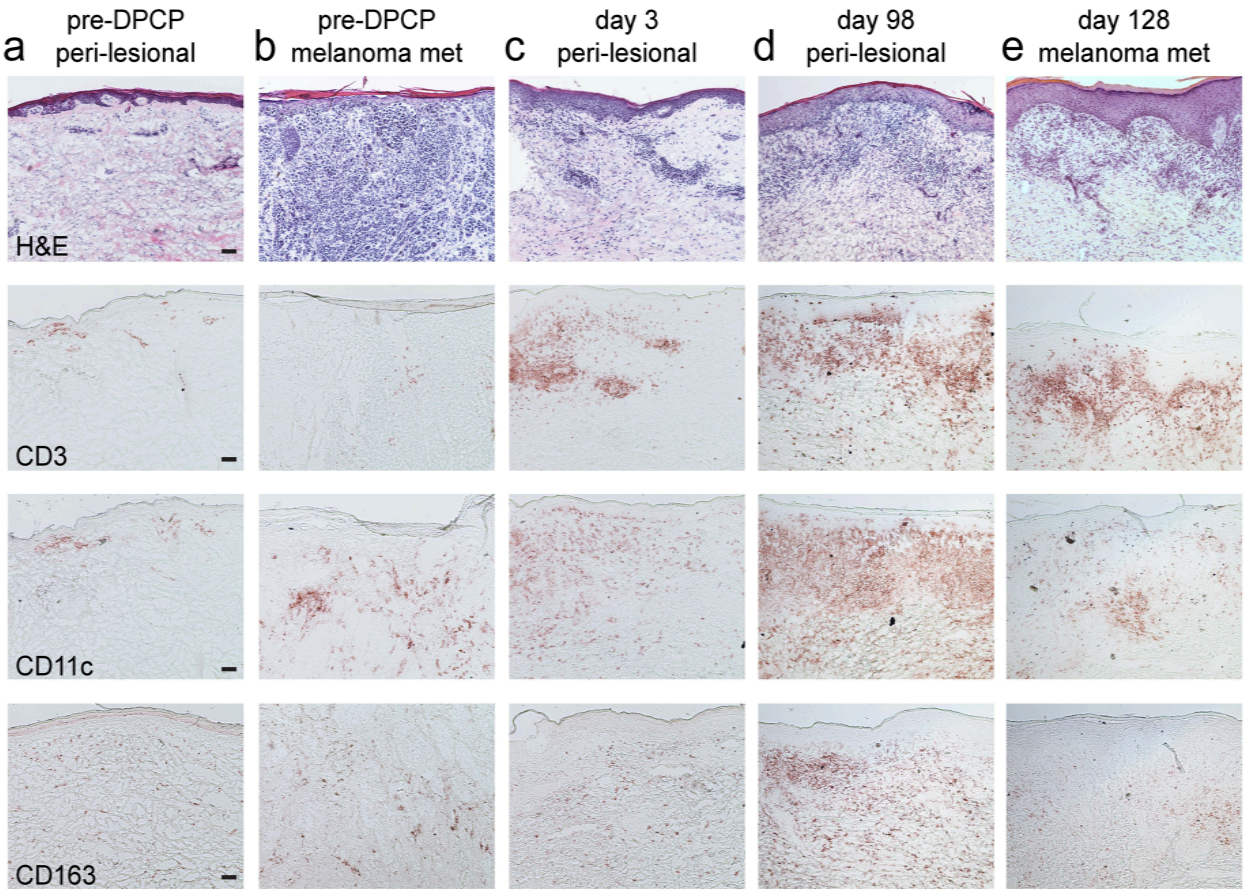

Figure 7.1: Histological analysis of biopsy samples indicates that DPCP leads to extensive immune cell infiltrates both after a single and repeated applications, and that these infiltrates persist for at least 30 days following cessation of DPCP application. Shown are H&E staining and immunohistochemistry for T cell marker CD3, myeloid dendritic cell marker CD11c, and macrophage marker CD163, on: (a) peri-lesional skin before DPCP treatment, (b) melanoma metastasis before DPCP treatment, (c) peri-lesional skin 3 days after first DPCP application, (d) peri-lesional skin at end of DPCP applications (day 98, after 14 weeks of twice weekly applications), and (e) melanoma metastasis 30 days after DPCP applications concluded (day 128). Biopsies from patient 003 are shown. Scale bar = 100 μm.

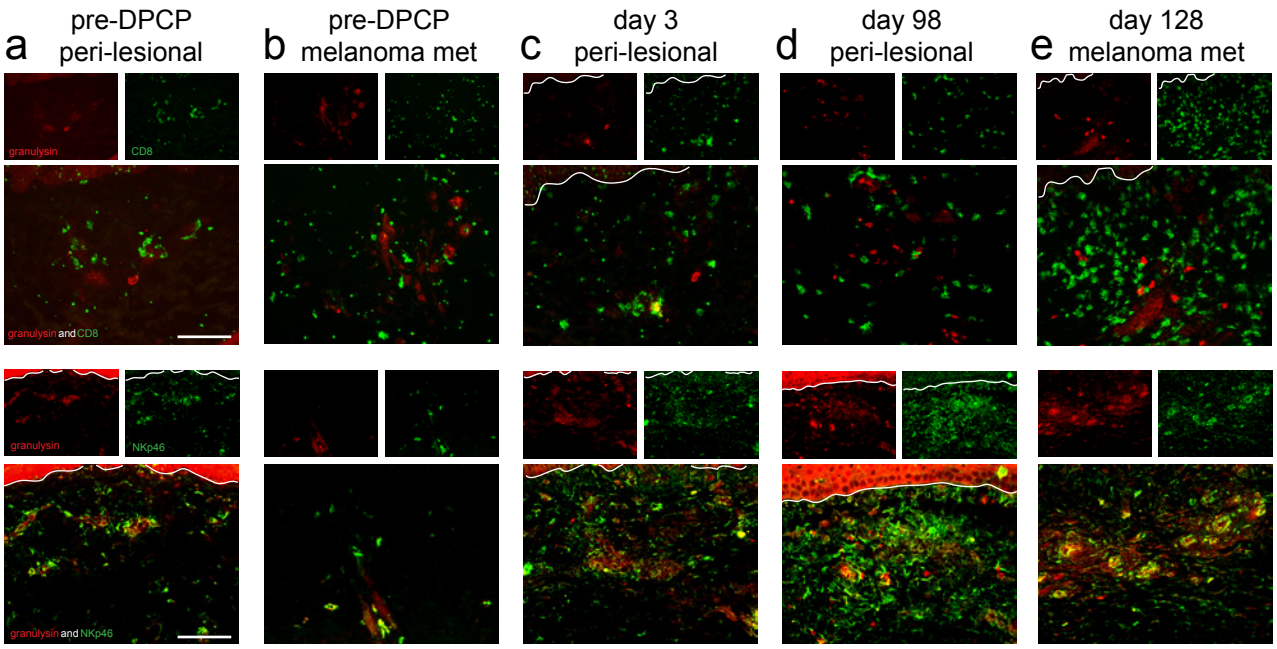

Figure 7.2: Two-color immunofluorescence demonstrates co-localization of granulysin with natural killer cells more than cytotoxic T cells during and following DPCP treatment. Shown are granulysin (red)/CD8 (green) (top) and granulysin (red)/NKp46 (green) (bottom) immunofluorescence on: (a) peri-lesional skin before DPCP treatment, (b) melanoma metastasis before DPCP treatment, (c) peri-lesional skin 3 days after first DPCP application, (d) peri-lesional skin at end of DPCP applications (day 98, after 14 weeks of twice weekly applications), and (e) melanoma metastasis 30 days after DPCP applications concluded (day 128). Biopsies from patient 003 are shown. Scale bar = 100 μm.

skin sites after repeated (twice weekly) DPCP applications (the number of applications varied among patients, as discussed in Chapter 6). The study of repeated DPCP applications is clinically relevant as this is what is traditionally required when DPCP is used as a treatment, whether for cutaneous melanoma metastases (Damian et al. 2014), alopecia areata (Ohlmeier et al. 2012), or warts (Buckley et al. 1999). By qRT-PCR analysis of paired single and repeated DPCP application biopsy sites from the 6 melanoma patients, we found that expression of Th1-related genes (IFNG, CXCL9, CXCL10, and CXCL11) generally increased with repeated applications, while markers of all other major T cell subsets (Foxp3, IL4, IL13, IL9, IL17A, and IL22) decreased (**Figure 7.3**). IL9 expression was significantly increased in single compared to repeated DPCP applications, and this may be necessary for production of other pro-inflammatory cytokines including IFNG (Schlapbach et al. 2014). Th1-related genes IFNG and CXCL9 were, on the other hand, significantly increased in repeated compared to single DPCP applications, and this overall shift towards Th1 polarization would be expected to promote anti-neoplastic effects (Braumüller et al. 2013). These findings, along with the increasing numbers of natural killer cells (**Figure 7.2**), reaffirm the utility of repeated DPCP applications in melanoma treatment.

As described in Chapter 6, patient 006 had two small lightly pigmented lesions remaining on her skin following DPCP treatment. Both of these lesions were

Figure 7.3: Repeated DPCP applications leads to shift towards Th1 polarization. Each chart shows normalized gene expression values measured by qRT-PCR, and each line represents 1 of the 6 melanoma patients. IFNG, CXCL9, Foxp3, IL4, IL13, and IL9 were all significantly different ($p<0.05$) between single and repeated DPCP applications by paired Student's *t*-test.

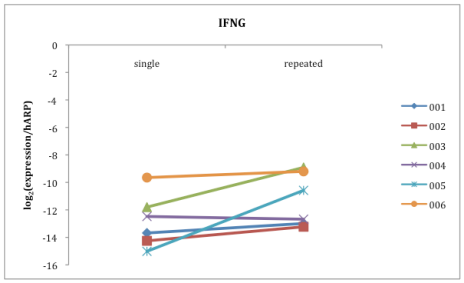
IFNG
single
repeated
log2(expression/hARP)
001
002
003
004
005
006

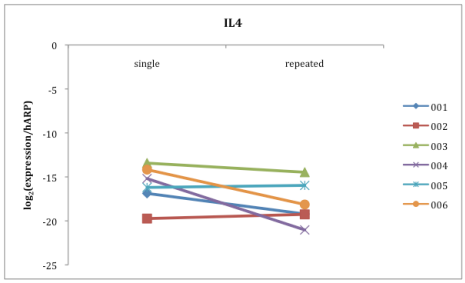
IL4
single
repeated
log2(expression/hARP)
001
002
003
004
005
006

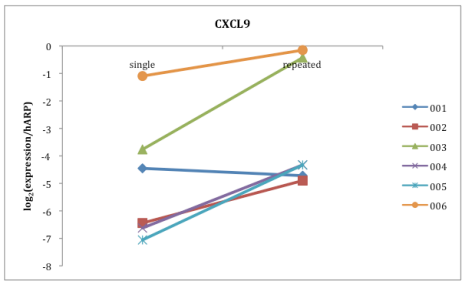
CXCL9
single
repeated
log2(expression/hARP)
001
002
003
004
005
006

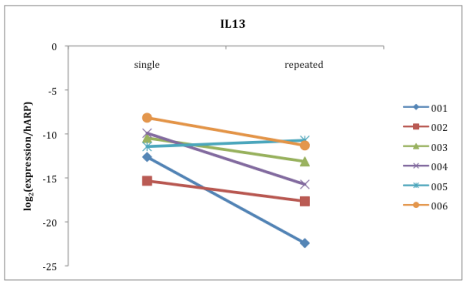
IL13
single
repeated
log2(expression/hARP)
001
002
003
004
005
006

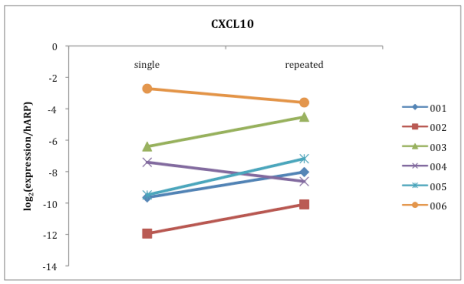
CXCL10
single
repeated
log2(expression/hARP)
001
002
003
004
005
006

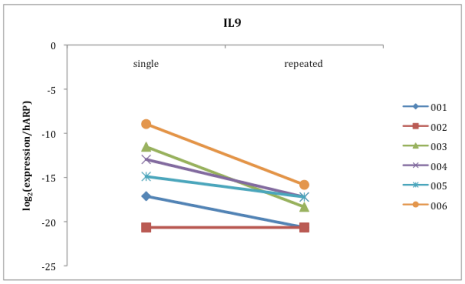
IL9
single
repeated
log2(expression/hARP)
001
002
003
004
005
006

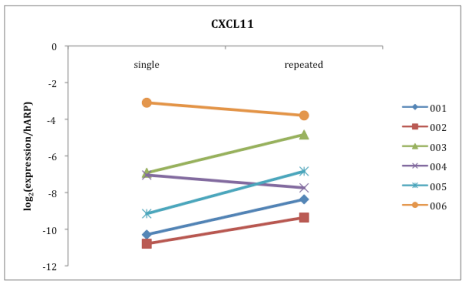
CXCL11
single
repeated
log2(expression/hARP)
001
002
003
004
005
006

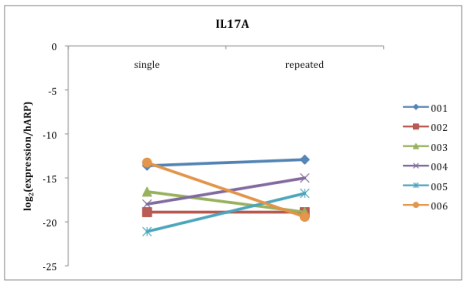
IL17A
single
repeated
log2(expression/hARP)
001
002
003
004
005
006

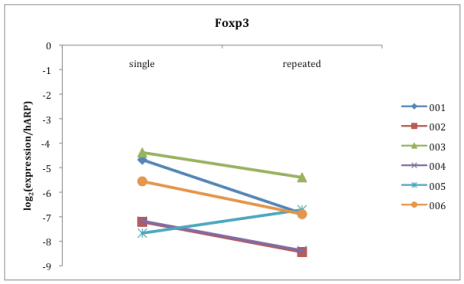
Foxp3
single
repeated
log2(expression/hARP)
001
002
003
004
005
006

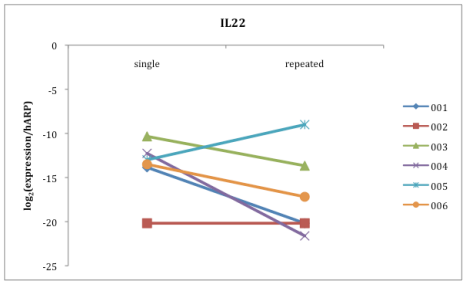
IL22
single
repeated
log2(expression/hARP)
001
002
003
004
005
006

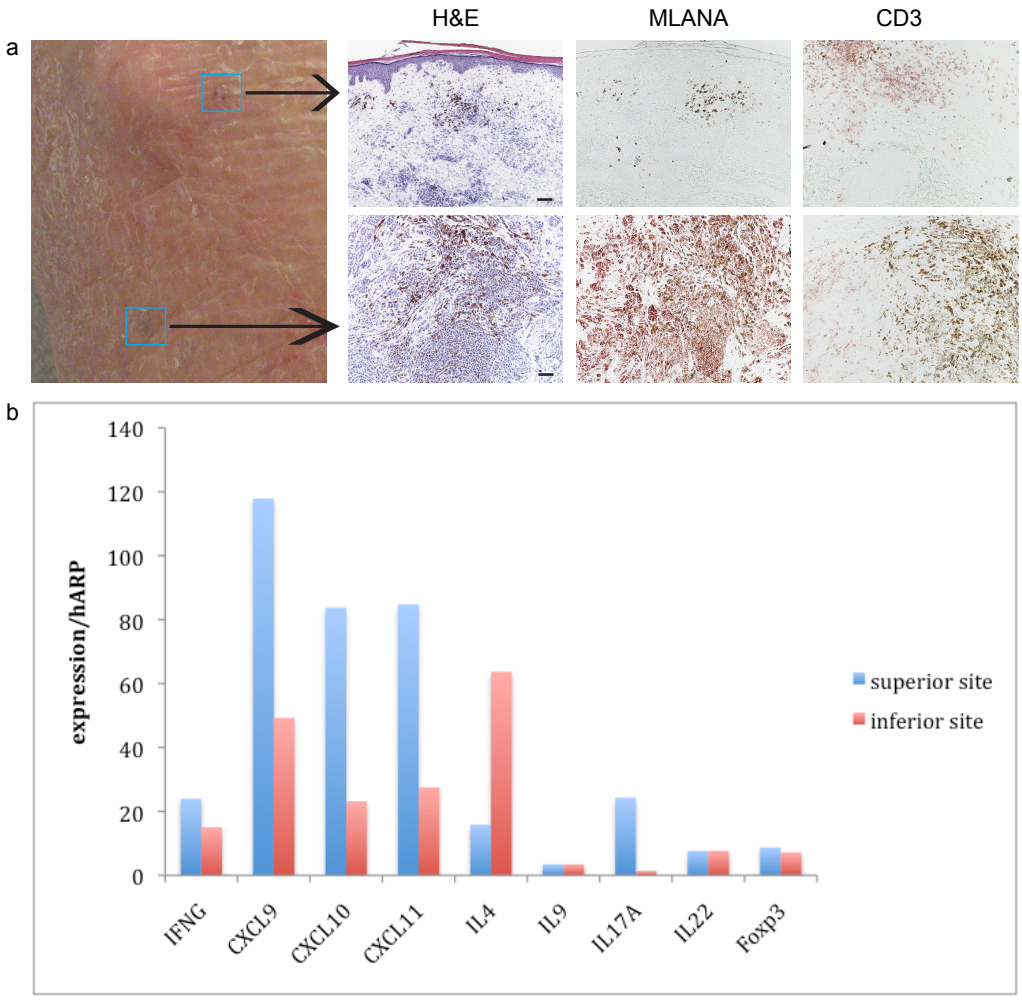

Figure 7.4: Successfully regressed melanoma metastasis compared to one that did not from the same patient shows increased Th1 polarization. (a) Skin photography showing both lightly pigmented lesions that remained on patient 006's skin following DPCP treatment, with arrows pointing to corresponding histology images taken from biopsy tissue. (b) Normalized qRT-PCR gene expression measures for various molecules defining different T cell subsets.

biopsied, and only one of the two had MLANA+ melanoma cells. Therefore, the other lesion was likely pigmented in appearance due to the presence of melanophages which had ingested melanin pigment, and was therefore an example of successful immune-mediated metastasis regression. Although this is only a single case, we examined both of these biopsies in an attempt to ascertain the differences between a successfully regressed melanoma metastasis and one that did not from the same patient. More CD3+ T cells were observed in the successfully regressed metastasis, along with stronger Th1 polarization (**Figure 7.4**), in agreement with our hypothesis that Th1 polarization promotes melanoma regression. Future study of additional patients (both responders and non-responders to DPCP) will likely provide valuable insight into the roles played by different immune cell subsets in promoting tumor regression.

CHAPTER 8: GENERAL DISCUSSION

Spontaneous regression of metastatic melanoma occasionally occurs, therefore suggesting a role for immune mechanisms in the control of this disease (McGovern 1975), and the clinical condition vitiligo provides evidence for the potential of immune attack against melanocytes. We have previously demonstrated the presence and potential functional role of dendritic cells in pigmented lesion pathogenesis (Gulati et al. 2015), thus further highlighting the role of immunosurveillance in melanoma. The FDA has recently approved antibodies that act by inhibiting two different immune checkpoints: cytotoxic T lymphocyte-associated antigen 4 (CTLA-4) and programmed cell death protein 1 (PD-1) (Postow et al. 2015a).

Another emerging therapeutic approach in melanoma (but not currently approved by the FDA), also in the realm of immunotherapy, is the contact sensitizer diphencyprone (DPCP). Compared to immune checkpoint inhibitors, DPCP has the advantages of lower price (being an easily produced hapten as opposed to an antibody) and favorable safety profile (the main toxicity being the expected inflammatory reaction). DPCP has recently been used in a 50-patient case series of cutaneously metastatic melanoma, with 46% of patients having complete clearance of their disease, and a further 38% having partial clearance (Damian et al. 2014), but corresponding study of the immune response to DPCP was not

conducted. We studied immune reactions to DPCP, first in healthy volunteers and then in melanoma patients, to better understand the immune mechanisms underlying this anti-tumor response.

Several immune pathways that we found to be induced by DPCP in healthy volunteer normal skin might mediate this anti-melanoma response. First, we identified significant up-regulation of IL-24 mRNA, which is a cytokine with established anti-melanoma activity (Jiang *et al*., 1995). Since this cytokine was up-regulated only transiently (peak at day 3, but resolved at day 14), it could indicate the need for chronic/repeated application of DPCP to maintain effector cytokines for tumor responses. Furthermore, we observed strong increases in IFNγ expression and this cytokine enhances antigen presentation potential, is anti-proliferative for many cell types (Braumüller *et al*., 2013), and its induced molecule CXCL10 has anti-melanoma activity (Antonicelli *et al*., 2011). Another cytokine we found to be upregulated by DPCP, IL-9, has recently been linked to melanoma regression (Purwar *et al*., 2012). In addition to these cytokines with potential anti-neoplastic effects, DPCP use resulted in many infiltrating CD8+ cells, along with increased granzyme B and granulysin expression, and these would be probable cytotoxic effectors. Granulysin has been shown to promote chemotaxis of CD4+ T cells in addition to its cytolytic properties (Deng *et al*., 2005), and both of these functions may contribute to the peak DTH response considering we observed granulysin expression on both CD8+ and CD8- T cells. We also noted a marked increase in DCs and especially DC-LAMP+ mature DCs,

that could provide a local environment to increase antigen presentation of tumor antigens (immature DCs, in the absence of appropriate co-stimulation, present antigens in a tolerogenic fashion), as well as XCR1+ DCs, which have a role in antigen cross-presentation (Kroczek and Henn, 2012).

We also examined the potential roles of miRNAs in healthy volunteer skin reactions to DPCP, as they may be involved in its therapeutic applications. Among the top 10 miRNAs we found upregulated at both days 3 and 14, miR-21, miR-142-3p, miR-142-5p, and miR-223 have all previously been found to be significantly upregulated in both human and mouse DTH reactions (Vennegaard et al. 2012). These four miRNAs have been shown to be related to T cells and T cell activation, in line with the fact that DTH reactions are mediated by T cells. Despite this, many of the top deregulated miRNAs found in our study have not previously been studied in the context of skin biology or immunology, highlighting the emerging nature of miRNA research. Our qRT-PCR data validated sequencing results both for miRNAs previously examined in the skin, such as miR-21, as well as for miRNAs that, to our knowledge, have never been described in the skin. The unique miRNA expression profiles at different time points may shed light on the paradoxical ability of DPCP to treat conditions of both autoimmunity (alopecia areata) and ineffective immunity (melanoma and warts). These unique miRNA profiles are paralleled by the unique mRNA profiles we found at days 3 and 14 via microarray analysis.

Our TCR sequencing data from the healthy volunteer study demonstrated that these DTH reactions are polyclonal, and therefore suggests that the induced inflammation is not due to a single antigen. Also, different individuals expanded different T cell clones in response to the same application of DPCP, which could mean that DPCP is conjugating with unique proteins in each person. This may have relevance to the action of DPCP in melanoma patients, as each treated patient may expand a unique repertoire of T cells specific to antigens found only in that patient. Another way to interpret these data is that DPCP application leads to the formation of one or few antigens, but then many other T cell clones with various antigen specifities are non-specifically recruited to the site, due to release of chemokines and other inflammatory mediators. It is known that the tissue damage and inflammation that occur during an immune response can lead to the release of epitopes from injured tissue which act as antigens, in a process known as antigen or epitope spreading (Vanderlugt and Miller 2002). Our TCR sequencing data demonstrated the appearance of new T cell clones at 14 days (but not 3 days) after DPCP challenge (**Figure 5.3**), and these may represent newly recruited clones which migrated to the skin due to antigen spreading. This phenomenon of antigen spreading has been shown to promote anti-tumor vaccination responses and occurs in melanoma patients (Hu et al. 2014). Vaccination of a melanoma patient with antigenic peptides MAGE-A3 and MAGE-A1 led to the expansion of T cell clones targeting antigens not present in the vaccine, including one clone that was not present in the patient's blood or cutaneous metastases prior to vaccination. This clone, which was able to lyse

autologous tumor cells *in vitro*, targeted the mutated (but not wild-type) form of a protein called caseinolytic protease P (CLPP) present in this particular patient, a mutation not commonly found in other melanoma patients (Corbière et al. 2011). These results provide demonstration of antigen spreading in cancer immunotherapy, and also highlight the potential clinical utility of targeting antigens not classically associated with melanoma, which may occur upon DPCP application.

Overall, this work with healthy volunteers formed a basis for investigating specific immune elements that may be induced in melanoma lesions that are treated with DPCP, as well as the baseline immune competence of cancer patients. It also led to insights regarding the regulation of immune responses, and provides a useful comparison point to inflammatory skin diseases such as psoriasis. Furthermore, due to our inclusion of a late time point (day 120) representing a fully resolved inflammatory reaction, our samples capture the tissue-resident memory T cells that are known to accumulate in skin over time (Clark 2015). Our TCR sequencing data demonstrated that certain T cell clones expand early (day 3) in skin, and persist over time even until day 120. Therefore, we provided the first human data following putative antigen-specific resident memory T cell clones over time in skin (Gaide et al. 2015).

The specific mechanisms of DPCP within melanoma treatment are largely unknown. One study showed (paradoxical) decreases in IL-17 family cytokines

in regressed lesions, possibly because the biopsy may not have been done at a time of active DPCP-induced inflammation. There was an increase in CTLA-4 and CD27 expression, which could indicate T cell activation by DPCP. However, other activation pathways were not explored (Martiniuk et al. 2010). Although our healthy volunteer study generated much data informing on potential anti-neoplastic effects of DPCP, a trial with actual melanoma patients was needed to better understand mechanisms of DPCP-mediated tumor regression, as well as potential toxicity that may be induced in these patients. We utilized the same topical DPCP formulation on both healthy volunteers and melanoma patients, but the latter often required higher concentrations of DPCP in order to achieve the same inflammatory response. This suggests a baseline immunosuppression in these patients. Although our patients' skin metastases often had infiltrating T cells at baseline (before DPCP applications), these may represent exhausted T cells which are known to infiltrate melanoma metastases, but whose functional deficiency is reversible (Baitsch et al. 2011). Future work will characterize how molecules of the exhausted T cell phenotype are modified by DPCP, and how positive vs negative immune regulation changes in tumors upon treatment.

Our clinical trial with metastatic melanoma patients allowed us to more directly study the immunologic mechanisms underlying the efficacy of DPCP to treat skin metastases. Six patients were enrolled in the study, and although each had a unique treatment course, 5 demonstrated at least partial melanoma regression in response to DPCP treatment, with only patient 001 having an indeterminate

outcome (due to her leaving the study after only 3 weeks of treatment). Our study was limited by a small sample size with several confounding factors including varied treatment histories. Recent FDA approval of several agents for metastatic melanoma treatment while we were conducting our clinical trial (**Figure 1.1**) decreased the pool of patients referred to our trial. Despite this, by studying the 6 patients together, several general principles emerged. First, DPCP led to increases in several cell types that are likely integral to immune-mediated tumor regression, including T cells, myeloid DCs, macrophages, and natural killer cells (which co-localized with granulysin). Since we took skin biopsies of DPCP-treated skin both at 3 days after a single challenge (similar to as was done with the healthy volunteers), and after many repeated challenges (as is generally done when DPCP is used clinically), we were able to examine the differences between these two immune reactions. We observed significant increases in Th1-defining molecules in repeated vs. single applications, with parallel decreases in molecules defining other T cell subsets (Th2, Th9, Th17, Th22, and regulatory T cells). This shift towards Th1 polarization is likely relevant to melanoma treatment, as these cells have established roles in anti-melanoma responses. To further support this, our patient with both a regressing and non-regressing metastasis in response to DPCP had increased expression of Th1-defining molecules in the former.

Since one of our patients was receiving topical imiquimod upon entering our trial, we had the opportunity to biopsy a site treated with this immunomodulatory compound, and to compare it to topically applied DPCP. Imiquimod signals to

the innate immune system through toll-like receptor 7, and therefore has a distinct mechanism of action to DPCP, which acts through the adaptive immune system. By gene expression analysis of skin biopsy specimens, immune reactions to these two agents were in fact distinct, with higher IFNγ expression in DPCP-treated skin. Also in the realm of immunotherapy, one of our patients received the PD-1 inhibitor nivolumab, which acts by inhibiting a negative regulator of immune responses. As such, we were able to obtain preliminary data regarding the potential synergy between these two treatments. It has been recently demonstrated that tumor regression with PD-1 inhibition requires pre-existing CD8+ T cells that are negatively regulated by the PD-1/PD-L1 axis (Tumeh et al. 2014). Since our data have shown that DPCP leads to increases in CD8+ T cells as well as PD-1, PD-L1, and PD-L2, DPCP is likely to increase the clinical efficacy of PD-1 inhibition. This may be a therapeutic avenue of interest in the future, as both PD-1 inhibitors and DPCP act on the immune system but in different ways, and PD-1 inhibitors have recently emerged as the standard of care treatment for metastatic melanoma. Our patient was having minimal regression of his bulky cutaneous metastases while solely on nivolumab, but demonstrated dramatic regression when topical DPCP applications were added in conjunction. This supports the hypothesis that these two therapies would complement each other, but a larger trial with more patients is needed.

Overall, the work contained herein provides varied insights into cutaneous immune responses through the use of DPCP, a prototypic cause of DTH reactions,

and examines how they can be successfully employed in the context of melanoma therapy.

REFERENCES

Antonicelli, F, Lorin, J, Kurdykowski, S, *et al.* (2011). CXCL10 reduces melanoma proliferation and invasiveness in vitro and in vivo. *Br J Dermatol* 164: 720–8.

Askenase, PW (2001). Yes T cells, but three different T cells (alphabeta, gammadelta and NK T cells), and also B-1 cells mediate contact sensitivity. *Clin Exp Immunol* 125: 345–50.

Baitsch, L, Baumgaertner, P, Devêvre, E, *et al.* (2011). Exhaustion of tumor-specific $CD8^+$ T cells in metastases from melanoma patients. *J Clin Invest* 121: 2350–60.

Baltimore, D, Boldin, MP, O'Connell, RM, *et al.* (2008). MicroRNAs: new regulators of immune cell development and function. *Nat Immunol* 9: 839–45.

Black, CA (1999). Delayed type hypersensitivity: current theories with an historic perspective. *Dermatol Online J* 5: 7.

Braumüller, H, Wieder, T, Brenner, E, *et al.* (2013). T-helper-1-cell cytokines drive cancer into senescence. *Nature* 494: 361–5.

Breslow, A (1980). Prognosis in cutaneous melanoma: tumor thickness as a guide to treatment. *Pathol Annu* 15: 1–22.

Bröcker, EB, Echternacht-Happle, K, Hamm, H, *et al.* (1987). Abnormal expression of class I and class II major histocompatibility antigens in alopecia areata: modulation by topical immunotherapy. *J Invest Dermatol* 88: 564–8.

Bronte, V, Serafini, P, Mazzoni, A, *et al.* (2003). L-arginine metabolism in myeloid cells controls T-lymphocyte functions. *Trends Immunol* 24: 302–6.

Bryniarski, K, Ptak, W, Jayakumar, A, *et al.* (2013). Antigen-specific, antibody-coated, exosome-like nanovesicles deliver suppressor T-cell microRNA-150 to effector T cells to inhibit contact sensitivity. *J Allergy Clin Immunol* 132: 170–81.

Buckley, DA, Keane, FM, Munn, SE, *et al.* (1999). Recalcitrant viral warts treated by diphencyprone immunotherapy. *Br J Dermatol* 141: 292–6.

Chen, X-P, Chen, Y-G, Lan, J-Y, *et al.* (2014). MicroRNA-370 suppresses proliferation and promotes endometrioid ovarian cancer chemosensitivity to cDDP by negatively regulating ENG. *Cancer Lett* 353: 201–10.

Chudnovsky, Y, Khavari, PA, Adams, AE (2005). Melanoma genetics and the development of rational therapeutics. *J Clin Invest* 115: 813–24.

Clark, RA (2015). Resident memory T cells in human health and disease. *Sci Transl Med* 7: 269rv1.

Clark, RA, Chong, B, Mirchandani, N, *et al.* (2006). The vast majority of CLA+ T cells are resident in normal skin. *J Immunol* 176: 4431–9.

Clemente, CG, Mihm, MC, Bufalino, R, *et al.* (1996). Prognostic value of tumor infiltrating lymphocytes in the vertical growth phase of primary cutaneous melanoma. *Cancer* 77: 1303–10.

Corbière, V, Chapiro, J, Stroobant, V, *et al.* (2011). Antigen spreading contributes to MAGE vaccination-induced regression of melanoma metastases. *Cancer Res* 71: 1253–62.

Damian, DL, Saw, RPM, Thompson, JF (2014). Topical immunotherapy with diphencyprone for in transit and cutaneously metastatic melanoma. *J Surg Oncol* 109: 308–13.

Damian, DL, Shannon, KF, Saw, RP, *et al.* (2009). Topical diphencyprone immunotherapy for cutaneous metastatic melanoma. *Australas J Dermatol* 50: 266–71.

Deng, A, Chen, S, Li, Q, *et al.* (2005). Granulysin, a cytolytic molecule, is also a chemoattractant and proinflammatory activator. *J Immunol* 174: 5243–8.

Dudda, JC, Perdue, N, Bachtanian, E, *et al.* (2008). Foxp3+ regulatory T cells maintain immune homeostasis in the skin. *J Exp Med* 205: 1559–65.

Fabian, MR, Sonenberg, N, Filipowicz, W (2010). Regulation of mRNA translation and stability by microRNAs. *Annu Rev Biochem* 79: 351–79.

Farazi, TA, Brown, M, Morozov, P, *et al.* (2012). Bioinformatic analysis of barcoded cDNA libraries for small RNA profiling by next-generation sequencing. *Methods* 58: 171–87.

Freyschmidt, E-J, Mathias, CB, Diaz, N, *et al.* (2010). Skin inflammation arising from cutaneous regulatory T cell deficiency leads to impaired viral immune responses. *J Immunol* 185: 1295–302.

Freyschmidt-Paul, P, Happle, R, McElwee, KJ, *et al.* (2003). Alopecia areata: treatment of today and tomorrow. *J Investig Dermatol Symp Proc* 8: 12–7.

Friedman, RC, Farh, KK-H, Burge, CB, *et al.* (2009). Most mammalian mRNAs are conserved targets of microRNAs. *Genome Res* 19: 92–105.

Gaide, O, Emerson, RO, Jiang, X, *et al.* (2015). Common clonal origin of central and resident memory T cells following skin immunization. *Nat Med* 21: 647–53.

Gajewski, TF (2006). Identifying and overcoming immune resistance mechanisms in the melanoma tumor microenvironment. *Clin Cancer Res* 12: 2326s – 2330s.

Gray-Schopfer, V, Wellbrock, C, Marais, R (2007). Melanoma biology and new targeted therapy. *Nature* 445: 851–7.

Guinea-Viniegra, J, Jiménez, M, Schonthaler, HB, *et al.* (2014). Targeting miR-21 to treat psoriasis. *Sci Transl Med* 6: 225re1.

Gulati, N, Mitsui, H, Fuentes-Duculan, J, *et al.* (2015). Dendritic cells are contained within melanocytic nevus nests in vivo and can alter gene expression of epidermal melanocytes in vitro. *Pigment Cell Melanoma Res* 28: 110–3.

Gu, Y, Cheng, Y, Song, Y, *et al.* (2014). MicroRNA-493 suppresses tumor growth, invasion and metastasis of lung cancer by regulating E2F1. *PloS One* 9: e102602.

Hafner, M, Landgraf, P, Ludwig, J, *et al.* (2008). Identification of microRNAs and other small regulatory RNAs using cDNA library sequencing. *Methods* 44: 3–12.

Hafner, M, Renwick, N, Farazi, TA, *et al.* (2012). Barcoded cDNA library preparation for small RNA profiling by next-generation sequencing. *Methods* 58: 164–70.

Hoffmann, K, Feldmann, S, Dirschka, T, *et al.* (1994a). Sonographic quantification of the type IV reaction after intradermal application of recall antigens. *Skin Pharmacol* 7: 291–9.

Hoffmann, R, Wenzel, E, Huth, A, *et al.* (1994b). Cytokine mRNA levels in Alopecia areata before and after treatment with the contact allergen diphenylcyclopropenone. *J Invest Dermatol* 103: 530–3.

Hunder, NN, Wallen, H, Cao, J, *et al.* (2008). Treatment of metastatic melanoma with autologous CD4+ T cells against NY-ESO-1. *N Engl J Med* 358: 2698–703.

Hunter, N, Shaker, O, Marei, N (2011). Diphencyprone and topical tacrolimus as two topical immunotherapeutic modalities. Are they effective in the treatment of alopecia areata among Egyptian patients? A study using CD4, CD8 and MHC II as markers. *J Dermatol Treat* 22: 2–10.

Hu, Y, Petroni, GR, Olson, WC, *et al.* (2014). Immunologic hierarchy, class II MHC promiscuity, and epitope spreading of a melanoma helper peptide vaccine. *Cancer Immunol Immunother* 63: 779–86.

Jiang, H, Jin, C, Liu, J, *et al.* (2014). Next generation sequencing analysis of miRNAs: MiR-127-3p inhibits glioblastoma proliferation and activates TGF-β signaling by targeting SKI. *Omics J Integr Biol* 18: 196–206.

Jiang, H, Lin, JJ, Su, ZZ, *et al.* (1995). Subtraction hybridization identifies a novel melanoma differentiation associated gene, mda-7, modulated during human melanoma differentiation, growth and progression. *Oncogene* 11: 2477–86.

Jiang, N, Chen, W-J, Zhang, J-W, *et al.* (2015). Downregulation of miR-432 activates Wnt/β-catenin signaling and promotes human hepatocellular carcinoma proliferation. *Oncotarget* 6: 7866–79.

Johnson, WE, Li, C, Rabinovic, A (2007). Adjusting batch effects in microarray expression data using empirical Bayes methods. *Biostat* 8: 118–27.

Kelly, DA, Walker, SL, McGregor, JM, *et al.* (1998). A single exposure of solar simulated radiation suppresses contact hypersensitivity responses both locally and systemically in humans: quantitative studies with high-frequency ultrasound. *J Photochem Photobiol B* 44: 130–42.

Kroczek, RA, Henn, V (2012). The Role of XCR1 and its Ligand XCL1 in Antigen Cross-Presentation by Murine and Human Dendritic Cells. *Front Immunol* 3: 14.

Lehtimäki, S, Savinko, T, Lahl, K, *et al.* (2012). The Temporal and Spatial Dynamics of Foxp3+ Treg Cell-Mediated Suppression during Contact Hypersensitivity Responses in a Murine Model. *J Invest Dermatol* 132: 2744–51.

Lei, Y, Ripen, AM, Ishimaru, N, *et al.* (2011). Aire-dependent production of XCL1 mediates medullary accumulation of thymic dendritic cells and contributes to regulatory T cell development. *J Exp Med* 208: 383–94.

Levis, WR, Holzer, AM, Leonard, LK (2006). Topical diphenylcyclopropenone as a measure of immune competence in HIV-seropositive subjects. *J Drugs Dermatol* 5: 853–8.

Li, C, Nie, H, Wang, M, *et al.* (2012). MicroRNA-409-3p regulates cell proliferation and apoptosis by targeting PHF10 in gastric cancer. *Cancer Lett* 320: 189–97.

Li, S, Meng, H, Zhou, F, *et al.* (2013). MicroRNA-132 is frequently down-regulated in ductal carcinoma in situ (DCIS) of breast and acts as a tumor suppressor by inhibiting cell proliferation. *Pathol Res Pract* 209: 179–83.

Liu, K, Nussenzweig, MC (2010). Origin and development of dendritic cells. *Immunol Rev* 234: 45–54.

Liu, X, Shi, H, Liu, B, *et al.* (2015). miR-330-3p controls cell proliferation by targeting early growth response 2 in non-small-cell lung cancer. *Acta Biochim Biophys Sin* 47: 431–40.

Løvendorf, MB, Mitsui, H, Zibert, JR, *et al.* (2014). Laser capture microdissection followed by next-generation sequencing identifies disease-related microRNAs in psoriatic skin that reflect systemic microRNA changes in psoriasis. *Exp Dermatol*.

Lowes, MA, Suárez-Fariñas, M, Krueger, JG (2014). Immunology of psoriasis. *Annu Rev Immunol* 32: 227–55.

Lu, TX, Hartner, J, Lim, E-J, *et al.* (2011). MicroRNA-21 limits in vivo immune response-mediated activation of the IL-12/IFN-gamma pathway, Th1 polarization, and the severity of delayed-type hypersensitivity. *J Immunol* 187: 3362–73.

Lu, TX, Munitz, A, Rothenberg, ME (2009). MicroRNA-21 is up-regulated in allergic airway inflammation and regulates IL-12p35 expression. *J Immunol* 182: 4994–5002.

Martiniuk, F, Damian, DL, Thompson, JF, *et al.* (2010). TH17 is involved in the remarkable regression of metastatic malignant melanoma to topical diphencyprone. *J Drugs Dermatol* 9: 1368–72.

McGovern, VJ (1975). Spontaneous regression of melanoma. *Pathology* 7: 91–9.

Moos, S von, Johansen, P, Waeckerle-Men, Y, *et al.* (2012). The contact sensitizer diphenylcyclopropenone has adjuvant properties in mice and potential application in epicutaneous immunotherapy: Experimental Allergy and Immunology. *Allergy*.

Netscher, DT, Leong, M, Orengo, I, *et al.* (2011). Cutaneous malignancies: melanoma and nonmelanoma types. *Plast Reconstr Surg* 127: 37e – 56e.

Ohlmeier, MC, Traupe, H, Luger, TA, *et al.* (2012). Topical immunotherapy with diphenylcyclopropenone of patients with alopecia areata--a large retrospective study on 142 patients with a self-controlled design. *J Eur Acad Dermatol Venereol* 26: 503–7.

Pires, MC, Martins, JM, Montealegre, F, *et al.* (2010). Vitiligo after diphencyprone for alopecia areata. *Dermatol Res Pract* 2010: 171265.

Postow, MA, Callahan, MK, Wolchok, JD (2015a). Immune Checkpoint Blockade in Cancer Therapy. *J Clin Oncol* 33: 1974–82.

Postow, MA, Chesney, J, Pavlick, AC, *et al.* (2015b). Nivolumab and ipilimumab versus ipilimumab in untreated melanoma. *N Engl J Med* 372: 2006–17.

Purwar, R, Schlapbach, C, Xiao, S, *et al.* (2012). Robust tumor immunity to melanoma mediated by interleukin-9-producing T cells. *Nat Med*.

Ribas, A, Puzanov, I, Dummer, R, *et al.* (2015). Pembrolizumab versus investigator-choice chemotherapy for ipilimumab-refractory melanoma (KEYNOTE-002): a randomised, controlled, phase 2 trial. *Lancet Oncol*.

Rigel, DS, Friedman, RJ, Kopf, AW, *et al.* (2005). ABCDE--an evolving concept in the early detection of melanoma. *Arch Dermatol* 141: 1032–4.

Robinson, MD, McCarthy, DJ, Smyth, GK (2010). edgeR: a Bioconductor package for differential expression analysis of digital gene expression data. *Bioinforma* 26: 139–40.

Saint-Mezard, P, Chavagnac, C, Vocanson, M, *et al.* (2005). Deficient contact hypersensitivity reaction in CD4-/- mice is because of impaired hapten-specific CD8+ T cell functions. *J Invest Dermatol* 124: 562–9.

Sayed, D, Abdellatif, M (2011). MicroRNAs in development and disease. *Physiol Rev* 91: 827–87.

Schlapbach, C, Gehad, A, Yang, C, *et al.* (2014). Human TH9 cells are skin-tropic and have autocrine and paracrine proinflammatory capacity. *Sci Transl Med* 6: 219ra8.

Schmittgen, TD, Livak, KJ (2008). Analyzing real-time PCR data by the comparative C(T) method. *Nat Protoc* 3: 1101–8.

Simonetti, O, Lucarini, G, Bernardini, ML, *et al.* (2004). Expression of vascular endothelial growth factor, apoptosis inhibitors (survivin and p16) and CCL27 in alopecia areata before and after diphencyprone treatment: an immunohistochemical study. *Br J Dermatol* 150: 940–8.

Snyder, A, Makarov, V, Merghoub, T, *et al.* (2014). Genetic basis for clinical response to CTLA-4 blockade in melanoma. *N Engl J Med* 371: 2189–99.

Sonkoly, E, Janson, P, Majuri, M-L, *et al.* (2010). MiR-155 is overexpressed in patients with atopic dermatitis and modulates T-cell proliferative

responses by targeting cytotoxic T lymphocyte-associated antigen 4. *J Allergy Clin Immunol* 126: 581–9.e1–20.

Spritz, RA (2012). Six decades of vitiligo genetics: genome-wide studies provide insights into autoimmune pathogenesis. *J Invest Dermatol* 132: 268–73.

Stute, J, Hausen, BM, Schulz, KH (1981). [Diphenylcyclopropenone - a new strong contact sensitizer (author's transl)]. *Dermatosen Beruf Umw Occup Environ* 29: 12–4.

Suárez-Fariñas, M, Pellegrino, M, Wittkowski, KM, *et al.* (2005). Harshlight: a "corrective make-up" program for microarray chips. *BMC Bioinformatics* 6: 294.

Tian, S, Krueger, JG, Li, K, *et al.* (2012). Meta-analysis derived (MAD) transcriptome of psoriasis defines the "core" pathogenesis of disease. *PloS One* 7: e44274.

Tomlinson, GS, Cashmore, TJ, Elkington, PTG, *et al.* (2011). Transcriptional profiling of innate and adaptive human immune responses to mycobacteria in the tuberculin skin test. *Eur J Immunol* 41: 3253–60.

Tumeh, PC, Harview, CL, Yearley, JH, *et al.* (2014). PD-1 blockade induces responses by inhibiting adaptive immune resistance. *Nature* 515: 568–71.

Upitis, JA, Krol, A (2002). The use of diphenylcyclopropenone in the treatment of recalcitrant warts. *J Cutan Med Surg* 6: 214–7.

Uppal, A, Wightman, SC, Mallon, S, *et al.* (2015). 14q32-encoded microRNAs mediate an oligometastatic phenotype. *Oncotarget* 6: 3540–52.

Vanderlugt, CL, Miller, SD (2002). Epitope spreading in immune-mediated diseases: implications for immunotherapy. *Nat Rev Immunol* 2: 85–95.

Vennegaard, MT, Bonefeld, CM, Hagedorn, PH, *et al.* (2012). Allergic contact dermatitis induces upregulation of identical microRNAs in humans and mice. *Contact Dermatitis* 67: 298–305.

Vocanson, M, Hennino, A, Rozières, A, *et al.* (2009). Effector and regulatory mechanisms in allergic contact dermatitis. *Allergy* 64: 1699–714.

Watanabe, R, Gehad, A, Yang, C, *et al.* (2015). Human skin is protected by four functionally and phenotypically discrete populations of resident and recirculating memory T cells. *Sci Transl Med* 7: 279ra39.

Wong, CL, Ghassabian, S, Smith, MT, *et al.* (2015). In vitro methods for hazard assessment of industrial chemicals - opportunities and challenges. *Front Pharmacol* 6: 94.

Zhu, W, Streicher, K, Shen, N, *et al.* (2012). Genomic signatures characterize leukocyte infiltration in myositis muscles. *BMC Med Genomics* 5: 53.

Zibert, JR, Løvendorf, MB, Litman, T, *et al.* (2010). MicroRNAs and potential target interactions in psoriasis. *J Dermatol Sci* 58: 177–85.